UNIVERSITY OF PLYMOUTH

SYNTHESIS AND MANUFACTURE OF HIGH PERFORMANCE FA-GGBS-HMNS BASED GEOPOLYMER CONCRETE

by

AISSA BOUAISSI

A thesis submitted to the University of Plymouth in partial fulfilment for the degree of

DOCTOR OF PHILOSOPHY

School of Engineering, Computing and Mathematics

June 2019

*** وَمَا تَوْفِيقِي إِلَّا بِاللَّهِ ۚ عَلَيْهِ تَوَكَّلْتُ وَإِلَيْهِ أُنِيبُ ***

*** And my success is not but through Allah. Upon him, I have relied, and to Him, I return ***

ABSTRACT

Geopolymer has received great attention in recent years as a new material that could replace Ordinary Portland cement (OPC) for producing concrete. Geopolymer uses the raw materials rich in aluminium and silicon, which are activated by alkaline solutions to formulate the binder. It has been proven that the geopolymer could be a material capable of providing high-quality properties and having less environmental impact.

This research project aims to investigate the capability for producing a geopolymer concrete (GPC) mainly based on the combination of various by-product materials (fly ash, (FA), ground granulated blast-furnace slag (GGBS) and high-magnesium nickel slag (HMNS)) at ambient temperature.

The characteristics of the precursor materials such as the chemical compositions, particle size and shape, unburned carbon content (LOI), and amorphous and crystalline phases were characterized using various technical methods. These included Scanning Electron Microscopy (SEM), Energy Dispersive X-ray Spectroscopy (EDX), X-ray fluorescence spectrometer (XRF), X-Ray Diffraction (XRD) and Fourier Transform Infrared Spectroscopy analysis (FTIR), to identify the different functional groups. In addition, a mix design procedure has been proposed in order to manufacture the FA-GGBS-HMNS-based geopolymer concrete, which is mainly based on the selection of the sodium silicate to sodium hydroxide (alkaline activator solution) ratio and the binder-to-liquid and binder-to-aggregate ratios. The effects of the selected materials and their characteristics on the properties of the fresh GPC at a room temperature of 25±2℃ and a relative humidity of 85-90% were later evaluated by performing workability and setting time tests. The fresh FA-GGBS-HMNS based geopolymer concrete showed excellent workability which maintained for at least 240 minutes, without any sign of setting or stiffness before starting to harden.

The mechanical properties of the hardened FA-GGBS-HMNS based geopolymer concrete, e.g. the compressive strength, the splitting tensile strength and modulus of elasticity, are similar or better when compared to those of OPC concrete. A strong

relationship between the compressive strength and the theoretical modulus of elasticity was shown by a true correlation with an approximate $R^2 \approx 0.997$. The microstructure analysis of the GPC produced exhibits the formation of an aluminosilicate amorphous phase in a three-dimensional network. The SEM images reveal a fully compact and cohesive geopolymer matrix, which explains why the mechanical properties of the FA-GGBS-HMNS based GPC are improved, both with GGBS and with HMNS.

The thermal stability and durability of the designed GPC were investigated by performing both a thermal residual test at elevated temperatures up to 900ºC and a Rapid Chloride Permeability Test (RCPT) respectively. The results confirmed that the manufactured GPC showed great resistance to high temperatures, with residual strength ranged from 48.4 to 20.56 MPa. Moreover, it was found that FA-GGBS-HMNS based GPC could have the capability of resisting the migration of chloride ions and showed good behaviour against the diffusivity of chloride ions at 75 days after casting. It was also observed that, at 210 days after casting, the chloride migration coefficient increased due to the influence of different parameters such as the fineness of precursor materials, the continuation of the geopolymerization process and the pH of the pore solution of the mixture.

To evaluate the dynamic behaviour of the designed FA-GGBS-HMNS GP further, an impact test was implemented using a SHPB system. The results showed that the dynamic compressive strength increased with the strain rates. A linear relationship between the dynamic increase factor (DIF) and the logarithmic strain rates experimentally, demonstrated the strain rate sensitivity of the GP paste–like material. From the aspects of damages, different failure patterns were observed under various strain rates ranging from 24.1 to 176 s^{-1}.

Furthermore, the synthesised GPC achieved good mechanical and microstructure properties at ambient curing temperature, which are sufficient for the quality of concretes, and hence it can provide the construction industry with a feasible technology which could be used for on-site and off-site applications. The main significant findings of this investigative study are:

- A high compressive strength and splitting strength were achieved at 28 days with about 55.6 MPa and 4.57 MPa, respectively, with a high workable mix design.
- The microstructure analysis showed the formation of dense and compact gels such as Quartz, Calcium Beryllium Praseodymium Oxide, and Magnesium Vanadium Molybdenium Oxide.
- A strong relationship between the dynamic compressive strength and strain rate, which increases as the strain rate increase.
- The continuity of the geopolymerization process negatively affects chloride diffusion coefficient.
- The residual compressive strength increased by 3% after exposing the samples to 200 ℃, then it showed different degradation trends with the temperature up to 900 ℃.

KEY WORDS: geopolymer concrete; alkaline activator; fly ash; high magnesium nickel slag; ground granulated blast-furnace slag; mechanical properties; microstructure properties; dynamic behaviour; chloride penetration; chloride migration coefficient; residual compressive strength; thermal stability; capillary tension.

ACKNOWLEDGEMENT

AUTHOR'S DECLARATION

At no time during the registration for the degree of *Doctor of Philosophy* has the author been registered for any other University award without prior agreement of the Doctoral College Quality Sub-Committee.

Work submitted for this research degree at the University of Plymouth has not formed part of any other degree either at the University of Plymouth or any other establishment.

Publications:

Bouaissi, A., Li, L.Y., Abdullah, M.M.A.B. and Bui, Q.B. (2019). Mechanical properties and microstructure analysis of FA-GGBS-HMNS based geopolymer concrete. *Construction and Building Materials*. Vol. 210, pp. 198-209. https://doi.org/10.1016/j.conbuildmat.2019.03.202.

Bouaissi, A., Li, L.Y., Moga, L.M., Sandu, I.G., Abdullah, M.M.A.B. and Sandu, A.V.(2018). A Review on Fly Ash as a Raw Cementitious Material for Geopolymer Concrete. *Revista de Chimie*.Vol. 69(7), pp.1661-1667. https://doi.org/10.37358/RC.18.7.6390.

Dong, Z., Bouaissi, A., Wang, X., Huang, Y., Li, L.Y., Abdullah, M.M.A.B. and Ramasamy, S. (2019). Dynamic Behaviors of Fly Ash-Ground-Granulated Blast-Furnace Slag-High-Magnesium Nickel Slag-Based Geopolymer Paste When Subjected to Impact Compressive Loadings. *Advanced Engineering Materials*. Vol. 32(11), pp.1-8. https://doi.org/10.1002/adem.201900621.

Al-bahrani, M., Bouaissi, A. and Cree, A. (2019). Mechanical and electrical behaviors of self-sensing nanocomposite-based MWCNTs material when subjected to twist

shear load. *Mechanics of Advanced Materials and Structures*. Taylor & Francis, pp. 1–10. https://doi.org/10.1080/15376494.2019.1681038.

Zailan, S.N., Bouaissi, A., Mahmed, N. and Abdullah, M.M.A.B, (2019). Influence of ZnO Nanoparticles on Mechanical Properties and Photocatalytic Activity of Self-cleaning ZnO-Based Geopolymer Paste. *Journal of Inorganic and Organometallic Polymers and Materials*. pp.1-10. https://doi.org/10.1007/s10904-019-01399-3.

Shahedan, N.F., Abdullah, M.M.A.B., Mahmed, N., Kusbiantoro, A. and Bouissi, A. (2018). Characterization of fly ash geopolymer concrete with glass bubble for thermal insulation application. In *AIP Conference Proceedings*, 2030(1), pp. 020294. AIP Publishing. November 12. https://doi.org/10.1063/1.5066935.
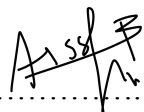
Presentations at conferences:

Invited speaker at the ''International Geopolymer Workshop'', 29 April 2018, Ho Chi Minh City, Vietnam.
Invited speaker at the ''1st International Conference on Green Environmental Engineering and Technology (IConGDM 2019)'', 29-30 April 2019, Bandung, Indonesia.
Poster presentation at the ''5th PRIMaRIE conference'', 5th -6th July 2018, University of Bristol, UK.

Word count of the thesis: **41425** Words

Signed…………………………………………

Date……………30/03/2020…………………

CONTENTS

LIST OF FIGURES

LIST OF TABLES

LIST OF EQUATIONS

NOMENCLATURE

OPC   Ordinary Portland cement

FA   Fly ash

GGBS   Ground granulated blast furnace slag

HMNS   High-magnesium nickel slag

GPC   Geopolymer concrete

SHPB   Split Hopkinson pressure bar test

RCPT   Rapid Chloride Permeability Test

HVFA   High Volume Fly Ash

PC   Portland cement

IEA   International Energy Agency

PFA   Pulverized fly ash

RHA   Rice husk ash

GP   Geopolymer

SS   Sodium silicate

SH   Sodium hydroxide

AA   Alkali activator

AAS   Alkaline activator solution

LOI   Loss on ignition

GOI   Gain on ignition

ACI   American Concrete Institute

ASTM   American Society for Testing and Materials

M   concentration

Mw   Molecule weight in (g/mol)

v   volume

E_c Theoretical Modulus of elasticity

f_c' Compressive strength

f_{ct} Splitting tensile strength

CFRP   Carbon Fibre Reinforced Polymer

GFRP   Glass Fibre reinforced Polymer

MPCM   Micro-encapsulated Phase Change Materials

SEM   Scanning Electron Microscopy

EDX   Energy dispersive X-ray

XRF   X-ray fluorescence spectrometer

XRD   X-Ray diffractometer

FTIR   Fourier Transform infrared

OM   Optical microscopy

σ Stress

A0   Cross-section

ε Strain

E Elastic modulus

u   Displacement

t   Time

ρ Density

C_0 Velocity

ε_i Strain created in incident bar

ε_r Reflected strain

ε_t Strain created in transmitted bar

$\dot{\varepsilon}$ Strain rate

L_s Length of specimen

V velocity of striker bar

W   Strain energy

W_{ab} Energy absorbed

DPCS   Dynamic peak compressive strength

DIF   Dynamic increase factor

D_{nssm} Non-steady-state migration coefficient

TGA   Thermal gravimetric analysis

PSA   Particle size analysis

Chapter 1‖
Introduction‖

1.1. Background of Research - What are Geopolymers?

In recent years, worldwide consumption of cement has increased by 3.2 Mt, due to the huge demand for conventional Ordinary Portland Cement (OPC) (Topçu, Toprak and Uygunoğlu, 2014). World production of this construction material increases by around 7% per annum compared with other materials. Mixing OPC with other aggregates creates a product called concrete. Limestone, and other soils such as clay, are mixed and cured at high temperature to formulate a new chemical composition by a process of chemical reaction (Aliabdo *et al.*, 2016). However, in the near future, the production of OPC could increase the total global warming and greenhouse gas emissions by about 10% (Benhelal *et al.*, 2013). In the last decade, many studies have been carried out to pursue and support the concept of environmentally friendly blending materials (Suwan, 2016). It has been reported that geopolymer technology has been considered as an alternative binder to the conventional cement (Davidovits, 1989). The main process to formulate geopolymers is by the reaction of an aluminosilicate from different geological compounds such as metakaolin and clay or by industrial by-products such as fly ash (FA) and ground granulated blast furnace slag (GGBS) mixing with a chemical solution which is known as an alkaline activator. The aluminosilicate in powder forms reacts with the alkali solution and produces a new composition called alkali aluminosilicate as an amorphous phase between 20 and 90°C, to a semi-

crystalline state at between 150 and 200°C (Topçu, Toprak and Uygunoğlu, 2014; Neupane, 2016). The finally formed mixture possesses a high quality of binding properties and is similar to the paste of calcium silicon hydrate (C-S-H) obtained from OPC concrete (Neupane, 2016).

In general, the mechanical properties and structure of geopolymers can be affected by many factors; the most significant factor is the curing condition. Usually, geopolymers cast and cure under a heating temperature from 40 to 90°C for a period of 6 to 48 hours, which accelerates the geopolymeric reaction and ameliorates its mechanical performances. After that, geopolymer cement is subjected to an ambient temperature for other treatments (Chindaprasirt *et al.*, 2011; Suwan, 2016). Using geopolymer for the construction sector is considered as a development of new products, basically using industrial by-products and wastes. Fly ash (FA) has been widely considered the main source material for producing geopolymers, due to its richness in alumina-silica compounds (Nath and Sarker, 2014; Suwan, 2016).

According to ASTM C618, FA is classified into two classes, namely class F and class C. Based on the main source of mineral coal, both classes can be distinguished from each other by their chemical compositions. The totality of silica (SiO_2), alumina (Al_2O_3), and iron oxide (Fe_2O_3) present in the class F FA should amount to at least 70% of the total mass, with only a low amount (less than10%), of calcium oxide (CaO) present, whereas the class C FA should consist at least 50% of silica (SiO_2), alumina (Al_2O_3), and iron oxide (Fe_2O_3). Generally, class C contains a high portion (from 10% to 30%) of calcium oxide, which is a highly reactive mineral constituent. The physical characteristics of FA improve the performance of the concrete in terms of water demand, porosity, rheology and reactivity with other compounds (Jayant, 2013).

Numerous research works have reported on the combined use of raw materials. For example, the combination of class F FA with slag such as GGBS is a commonly used blend for developing binder material, whose mechanical properties and other parameters have been investigated (Neupane, 2016). Furthermore, using concrete based on slag such as GGBS to interact with the marine environment has become the

main interest of several researchers, due to the significant development in offshore engineering sectors, particularly for marine environment constructions (Das *et al.*, 2015). This research project will study the engineering properties of geopolymer concrete based on class F FA and different types of slag (ground granulated blast furnace slag (GGBS) and high-magnesium nickel slag (HMNS)), which is cured under ambient conditions.

1.2.   Research Aims and Objectives

The main aim of this research project is the formulation of a new mix design of geopolymer concrete (GPC) by identification of the kind of industrial by-products that can meet the requirement of the concrete structures, which will be used in several applications. The project will study and identify the relationship between different mechanical properties, microstructures and the durability of geopolymer concrete by determining the optimum mix design, which leads to producing a new mix of FA-GGBS-HMNS-based geopolymer concrete.

As aforementioned, the purpose of this research project is to produce a new mix of FA-GGBS-HMNS-based geopolymer concrete. The experimental work focuses on two main approaches, (i) the use of class F FA with different proportions of slag and (ii) manufacturing and processing the production of the mix design, and then investigate its mechanical properties, microstructural characteristics and long-term durability. The objectives of this research therefore are:

1. Identify which kinds of raw materials can be selected to optimize the properties of GPC in terms of mechanical properties, microstructures and durability under ambient temperature.
2. Study the mechanical properties of the manufactured GPC subjecting to uniaxial stresses.
3. Investigate the dynamic behaviours of the designed GPC under a high strain rate, using the Split Hopkinson Pressure Bar test (SHPB).

4. Study the resistivity of the new mix GPC to the migration of chloride ions using the Rapid Chloride Permeability Test (RCPT).

5. Evaluate the thermal stability of GP paste at high temperatures (up to 900 $^{\circ}$C).

1.3. Research Scope

This study is an experimental work which focuses on the mechanical properties, morphological and other fundamental tests such as compressive strength, splitting tensile strength, and the Split Hopkinson pressure bar test (SHPB). Durability includes the deterioration of mechanical properties and the resistance to chloride migration. To achieve the aforementioned properties, the proportions of the precursor materials and activator solution used have to be varied, which leads to determining the optimum mix design. Class F FA, GGBS and HMNS are mixed with the activator solution, consisting of sodium hydroxide and sodium silicate. The lab-experimental work comprises:

o Manufacturing procedures: the preparation of raw materials in terms of pre-drying, separation and mixing process, followed by the preparation of the required activator solution.

o Geopolymer system: the preparation of the binder materials, which consist of class F FA, GGBS and HMNS.

o Curing conditions: producing a mix design of GPC cured at room temperature.

o Producing a Geopolymer concrete (GPC): the optimum mix design of the paste has to be calculated, this determining the proportions of geopolymer and aggregates needed.

1.4.   Research Standing and Importance

This research project presents an experimental study in developing a new geopolymer concrete (GPC), which is required for different applications. Achieving more suitable mechanical properties under the diverse mode of stresses and improving resistance to chloride ions are the main factors required.

Class F FA, GGBS and HMNS are the main materials needed for preparing the proposed GPC, this choice of materials being for the following reasons:

- The importance of the amounts of silica (SiO_2), alumina (Al_2O_3), and iron oxide (Fe_2O_3) that need to be present in class F FA.
- The particle size of the slag that helps to achieve great strength and improves resistance to the aggressive environmental aspects such as chloride penetration.
- The huge quantities of FA, GGBS and HMNS materials, which can be obtained from coal-fired power stations and smelting iron plants. These materials are considered industrial by-products or waste, which can cause environmental problems due to the landfill storage issues.
- Geopolymer cement can be considered eco-friendly due to the use as main ingredients in its production of what would otherwise be waste by-products. This circumvents many problems such as landfill storage, soil contamination and wasting energy.
- The use of the abovementioned raw materials during the fabrication process reduces the emission of CO_2 into the atmosphere.
- The significance of this research project can be summarised in the points listed below:
- GPC based on the appropriate combination of raw materials and chemical activators to obtain High Volume Fly Ash (HVFA) concrete is suitable for marine and certain other applications.

- The production of the proposed GPC is mainly based on the use of waste materials, so reducing their negative impact on the environment, such as degradation and soil contamination.
- The main problem which faces marine constructions is the performance of concrete in terms of its mechanical properties and long-term durability. This project focuses on the production of a GPC which, when compared to OPC, offers greater strength, improved thermal stability and high resistance to chloride penetration.
- The produced GPC shows a significant mechanical behaviour, which in turn extends the areas of its application. In addition, most research has been done on GP was focused on the static behaviours. Form this aspect, the author found it to be worthy to investigate how GP acts under dynamical behaviours, where many structures, such as bridges and high constructions in unstable areas faced numerous structural problems, such as explosive loading and earthquakes zones.

In respect to the above-listed reasons, the author has focused on the implementation of the main significant tests to optimise the mix design proportion by referring to the compressive strength test as a key-control index. In addition, to explore the excellent behaviours of the produced material dynamical impact, thermal and durability tests were adopted.

1.5. Organization of Thesis

This thesis is organised into eight chapters. **Chapter one** describes the main motivation and enthusiasm towards alkali-activated geopolymer concrete, which is considered an alternative cementitious material to Ordinary Portland cement.

Chapter two provides a general literature review of Ordinary Portland cement (OPC), the historical uses of pozzolanic material (fly ash) and slags (GGBS, HMNS) in Portland cement and geopolymer technology. This chapter mainly focuses on the chemistry of geopolymer cement, the geopolymerization process and the factors

affecting the properties of geopolymers. The properties and application of geopolymer are also discussed in this chapter.

Chapter three presents an overall description of the materials and the methods used to determine the fresh and hardened properties, including the compressive strength and the splitting tensile strength of the geopolymer concrete produced. Testing equipment and preparation procedures of the specimens are also described. In addition the dynamic behaviours of geopolymer concrete under uniaxial dynamic compression are investigated in this chapter.

Chapter four mainly focuses on the microstructural characteristics of the manufactured geopolymer concrete. Micrograph analysis is performed using SEM/EDX analysis, while XRD analysis is used to identify the crystalline phases of the geopolymer concrete produced and the raw materials used. FTIR spectra are used to characterize the main new bonding created during the geopolymerization reaction. The matrix of interface bonding between aggregates and geopolymer is investigated using Optical Microscopy (OM).

Chapter five provides an experimental technique, mainly based on the Split Hopkinson pressure bar (SHPB) test, to measure the dynamic compressive strength of the final geopolymer product at high strain rates. The implementation of this dynamic technique is used to examine the dynamic behaviour of the designed geopolymer concrete.

Chapter six investigates the durability of the manufactured geopolymer concrete. The diffusion coefficient of chloride ions in the geopolymer concrete is obtained using ''The Rapid Chloride Permeability Test (RCPT)'' in accordance with NT Build 492 protocols.

Chapter seven studies the thermal behaviour and stability of the designed GP paste when subjected to temperatures as high as 900 ^{o}C. The effect of high temperatures on

the compressive strength of the paste, and changes in its colour and physical appearances are also discussed in this chapter.

Chapter eight comprises conclusions on the geopolymer concrete produced, a summary of limitations on its use, recommendations for future research.
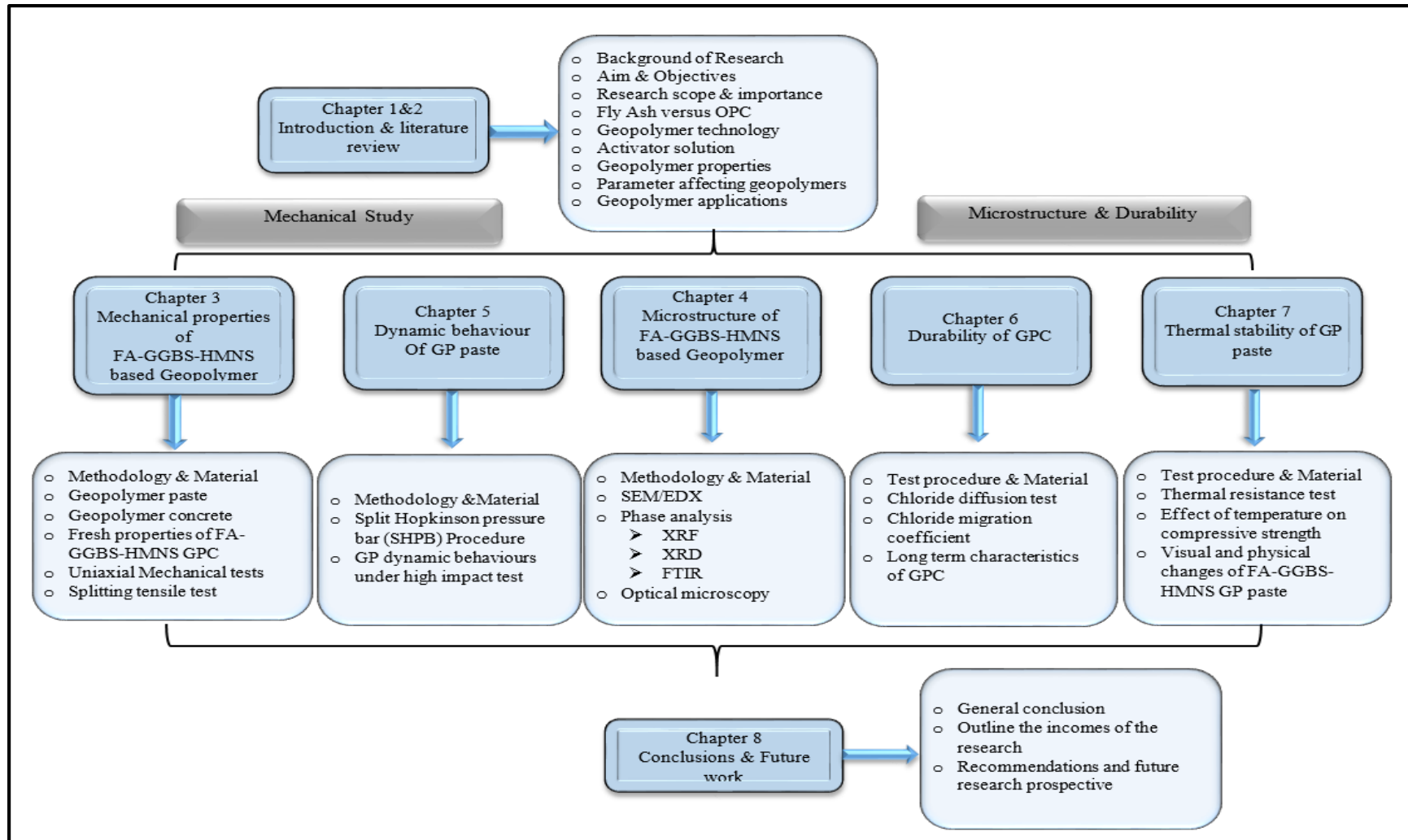
Figure 1. 1. Thesis architecture by Chapter.

Chapter 2‖

Literature Review‖

2.1. Fly Ash and the Conventional Cement

2.1.1. Ordinary Portland cement

Portland cement is considered the most extensively used largest hydraulic binder material utilised in the construction industry worldwide. Figure 2.1 shows the PC production process in which natural extracted raw materials (mainly consisting of Limestone ($CaCO_3$), Clay (SiO_2, Al_2O_3), Iron oxide (Fe_2O_3), Gypsum ($CaSO_4$) and Silica sand (SiO_2)) are crushed and blended as shown in
Table 2.1 (Suwan, 2016).
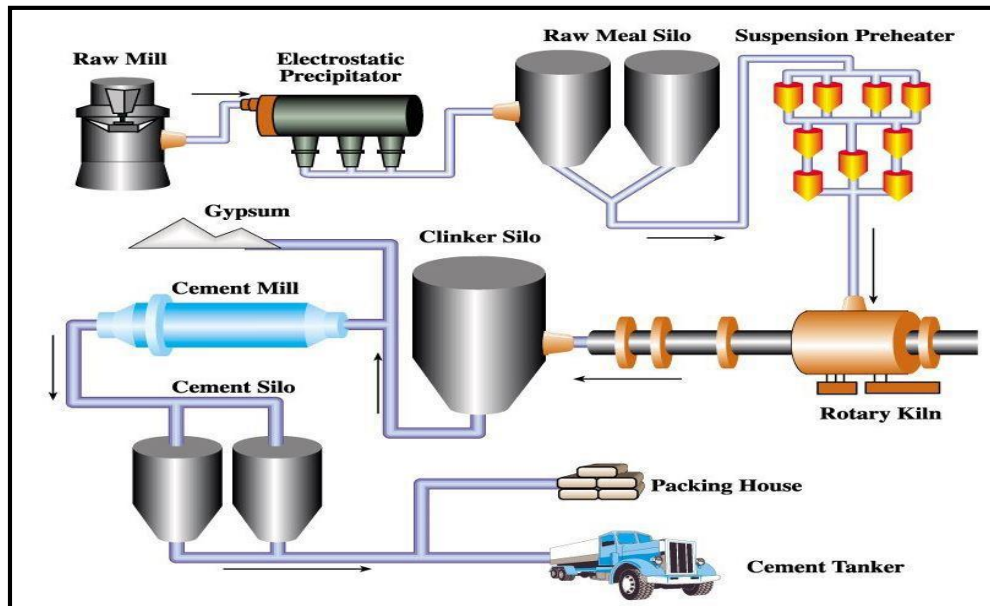
Figure 2.1. Portland cement production process

[(http://www.climatetechwiki.org/technology/energy-saving-cement)](http://www.climatetechwiki.org/technology/energy-saving-cement)

Table 2.1. Typical compositions of Portland cement

(Suwan, 2016)

Oxide	Common name	Symbol	Composition (wt. %)
CaO	Lime	C	62.0-67.0
SiO_2	Silica	S	18.0-24.0
Al_2O_3	Alumina	A	4.0-8.0
Fe_2O_3	Iron oxide	F	1.5-4.5
MgO	Magnesium oxide	M	0.5-4.0
K_2O	Potassium oxide	K	0.1-1.5
Na_2O	sodium oxide	N	0.1-1.0
H_2O	Water	H	Nil
SO_3	Sulfur trioxide	-	2.0-3.0
Free lime	-	-	0.5-1.5
LOI	Loss on ignition	LOI	1.0-3.0

About 40% of the carbon dioxide emissions resulting from the production of PC are due to the combustion of fuels used to create OPC clinker while around 5% come from the usage of energy in mechanical manufacturing processes. The chemical reaction shown in Eq (2.1) is the principal chemical process occurring during the formation of cement clinker. In this reaction, limestone reacts with silica to produce calcium silicates and carbon dioxide, the quantity of CO_2 being approximately 597kg for each ton of cement (Mcnulty, 2009).

$$5CaCO_3 + 2SiO_2 \rightarrow Ca_3SiO_5 + Ca_2SiO_4 + 5CO_2 \qquad \text{Eq (2. 1)}$$
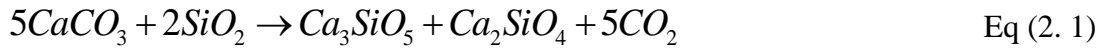
Hydration is the main reaction between water and calcium silicate in PC binders. Water introduces in the hydration process and is a significant material in the formation of the final structure of PC binders (Kim, 2012; Aliabdo *et al.*, 2016). The hydration of the silicate process is presented in Eqs (2.2), (2.3), (2.4), and (2.5) as follows:
For tri-calcium silicate (C_3S):

$$2(3CaO, SiO_2) + H_2O \rightarrow 3CaO, 2SiO_2, 3H_2O + 3Ca(OH)_2 + Heat \qquad \text{Eq (2. 2)}$$

Or: $2C_3S + 6H \rightarrow C_3S_2H_3 + 3Ca(OH)_2 + Heat \qquad \text{Eq (2. 3)}$
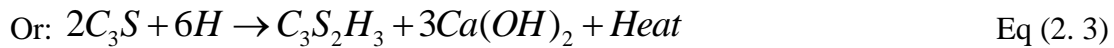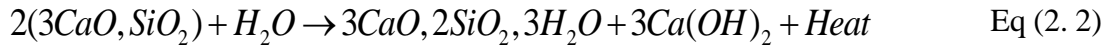
For di-calcium silicate (C_2S):

$$2(2CaO, SiO_2) + 4H_2O \rightarrow 3CaO, 2SiO_2, 3H_2O + Ca(OH)_2 + Heat \qquad \text{Eq (2. 4)}$$

Or: $2C_2S + 4H \rightarrow C_3S_2H_3 + Ca(OH)_2 + Heat \qquad \text{Eq (2. 5)}$
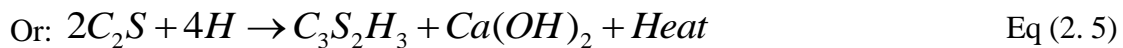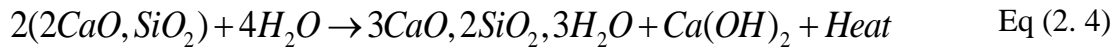
Calcium hydroxide (Ca(OH)$_2$) and heat are produced, due to the hydration of calcium compounds and the formation of calcium silicate gel (C-S-H). The hydrated C-S-H gel is the most significant developed product, which can improve the strength of cement by volume from 75 to 80 per cent, while 20 to 25 per cent of the strength is generated from the Ca(OH)$_2$ associated with heat as shown in Eq (2.6) (Suwan, 2016).

$$Portland\ cement + water \rightarrow C-S-H\ gel + Ca(OH)_2 + Heat$$ Eq (2. 6)
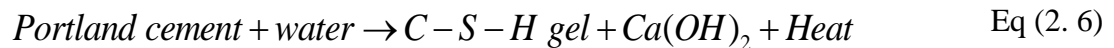
It is noted that the combusting process or calcination of raw materials produces a huge amount of carbon dioxide (CO$_2$) which is emitted into the atmosphere. According to the International Energy Agency's (IEA), the production of one tonne of cement releases approximately 0.8 to 1.0 tonne of CO$_2$ into the atmosphere (Eq (2.7)) (Suwan, 2016). Therefore, almost 5 to 7% of total global greenhouse gas emissions come from the production of OPC (Neupane, 2016).

$$CaCO_3(Limstone) \xrightarrow{\ (Calcinations)\ } CaO(Calcium\ Oxide) + CO_2$$ Eq (2. 7)

However, the rapid increase in global warming and climate changes have led the world to face significant new challenges, when compared to those previously considered. As a solution to the significant pollution from the manufacture of PC, alternative materials obtained from industrial by-products called Pozzolanic materials or commonly called fly ash (FA) have been investigated to replace PC, partially or fully (Suwan, 2016).

2.1.2. The Use of Pozzolanic Admixture (fly ash) in Portland Cement

FA is produced by a process involving coal-fired power stations in which the inorganic mineral substance becomes liquefied at an elevated temperature during the carbon burning-procedure (Jayant, 2013). The mineral admixtures thus created fall into three main categories: firstly, there are the low-activity admixtures such as limestone and dolomite; secondly, there are types of cementitious admixtures, for example, natural cement and blast furnace slag; and finally, there are Pozzolanic admixtures, which also

consist of natural pozzolan and pozzolan by-products, such as volcanic clay and pulverized fly ash (PFA) and silica fumes, respectively. The Pozzolanic FA (PFA) is the by-product material obtained from the combustion of coal during the generation of electric power in coal-fired plants as presented in Figure 2.2 (Suwan, 2016).
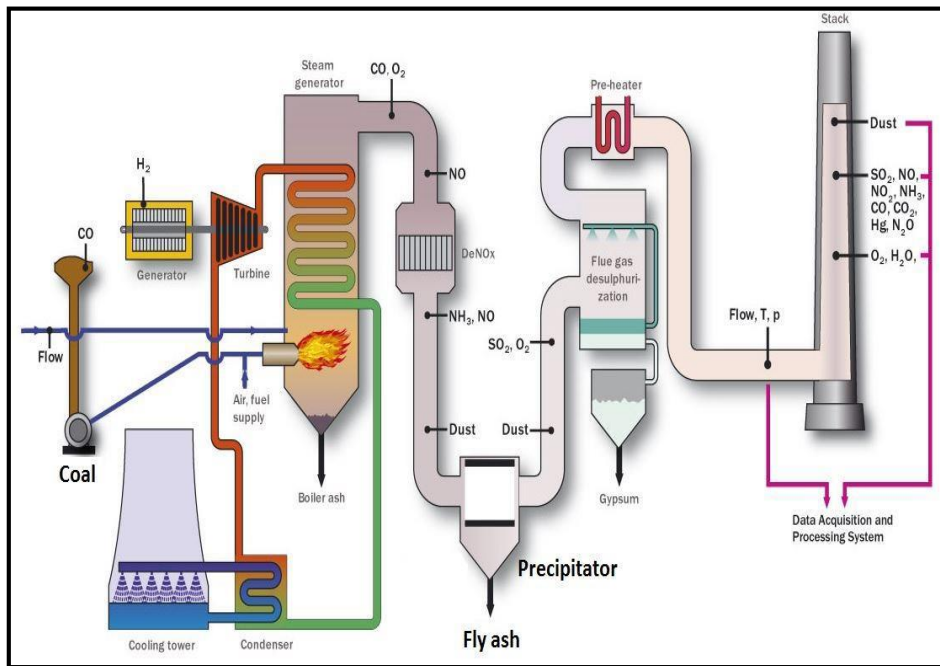
Figure 2.2. Coal-fired power station and fly ash collection
(https://www.silotransport.cz/3)

Figure 2.3 shows the physical characteristics of FA particles, as observed by scanning electron microscopy (SEM). FA particles, which are solid and shaped and categorized into two types. The first type are the hollow spheres, also known as cenospheres, which correspond to those ash particles hollow from the inside. The second type are the plerosphere particles which are hollow and packed with smaller ash spheres (Suwan, 2016).
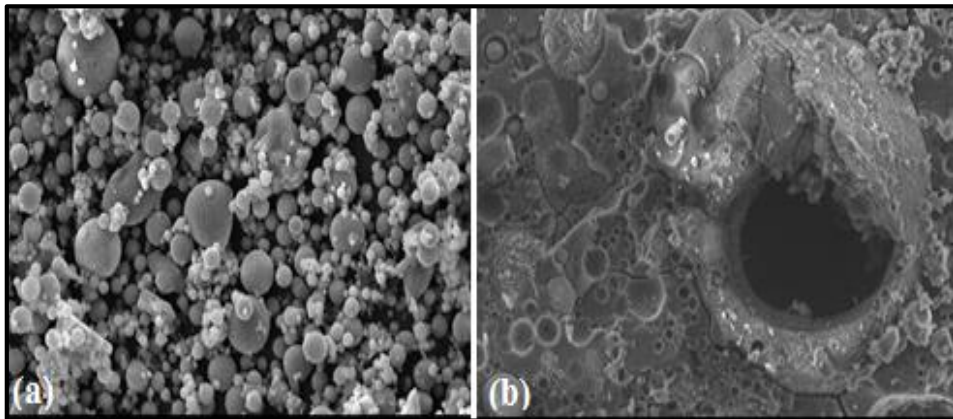
Figure 2.3. Scanning Electron Micrographs of FA: (a) cenosphere particles, (b) plerosphere particles

It has been reported that the small particles of FA, which fill the inside of the larger particles, are initially formed from the cracking of hollow particles and/or punched during a manipulation, but are not related to the smelting process (Topçu, Toprak and Uygunoğlu, 2014). Certain characteristics of FA particles, such as their shape and surface, potentially have an effect on the amount of water required for concrete. The friction between particles in the concrete mixture reduces, due to the spherical forms of particles, leading to an improvement in the concrete's flow properties and a reduction in the requirement for water. This occurs when FA replaces cement in concrete mixtures. In addition, when FA replaces OPC, many advantages have been reported in terms of improvements in the properties of different cements and concrete products (Jayant, 2013).

The presence of calcium hydroxide ($Ca(OH)_2$) in the hydration process of PC is considered a weakness, especially in acidic environments with a scaled pH from 12.4 to 13.5. Mehta (1986) considered that introducing FA as a part of the binder would lead to create a secondary C-S-H gel, due to a 'Pozzolanic reaction' between FA and calcium hydroxide $Ca(OH)_2$ as shown in the following chemical reaction, Eq (2.8) (Mehta, 1986; Suwan, 2016).

$$Fly\,ash\,(SiO_2, Al_2O_3) + water + Ca(OH)_2 \rightarrow \mathrm{Sec}\,ondary\,C-S-H\,gel \qquad \text{Eq (2. 8)}$$
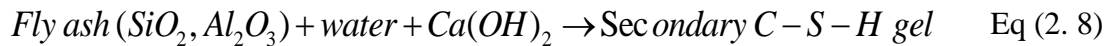
The spherical shape and structure of FA particles play a significant role in improving the workability of concrete. Further, the fineness of the FA particles has an important role in producing a denser, more compact concrete, which is more durable. It has been suggested that the proportion of FA which could replace cement might be as high as 50% (Wallah and Rangan, 2006). A successful replacement case was achieved by substituting around 50% of the OPC with FA, leading to the achievement of significant improvements in mechanical properties and durability. It has been reported that High Volume Fly Ash (HVFA) concrete has proven to be more durable and efficient in terms of resources compared to the OPC concrete (Malhotra and Mehta, 2002). In India, HVFA technology was used in road construction by replacing 50% of OPC with FA (Wallah and Rangan, 2006).

2.2. Geopolymer Cement

2.2.1. Chemistry and Fundamentals of Geopolymers

The geological process of the cementitious mechanism was firstly understood in 1967 by Victor Glukhovsky, who explained the formation of zeolites from volcanic rocks under specific temperature and pressure conditions. Alkaline activated cement is considered as a cementitious binder, as a result of the combination of zeolitic material and alkaline solutions of a high pH concentration (Pacheco-Torgal, Castro-Gomes and Jalali, 2008; Suwan, 2016). The term ''geopolymer'' was first established by Davidovits (1978), to describe the binders of alkaline activated solution with other chemical compositions. This is a material similar to zeolite which forms faster at low temperatures, but with an amorphous microstructure and non-crystalline phase (Wallah and Rangan, 2006).

The empirical formula given in Eq (2.9), shows the polymerization process on Si-Al minerals in the presence of a highly-concentrated activator solution. This leads to a faster chemical reaction and formulates what is called Poly (sialates) or three-dimensional polymeric chains and cyclic structure (Davidovits, Davidovits and James, 1999; Hardjito, 2005):

$$Mn\left[-(SiO_2)z - AlO_2\right]n \, . \, wH_2O \qquad \qquad \text{Eq (2. 9)}$$
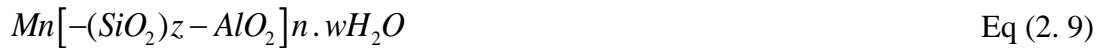
where M is an alkaline element or a monovalent cation, such as potassium, sodium or calcium and n is the degree of polycondensation or polymerization; z =1, 2, 3, or higher, up to 32.
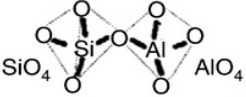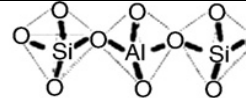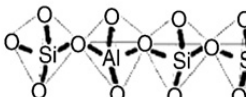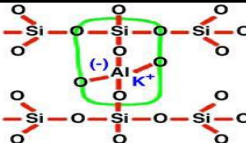
It is supposed that, based on the Si/Al ratio, there are three types of monomeric, which allow the geopolymeric structure to be distinguished, namely (i) the poly-sialate (–Si–O–Al–O) if Si/Al=1, (ii) the poly (sialate-siloxo) such as (-Si-O-Al-O-Si-O) if Si/Al=2, and (iii) the Poly (sialate-disiloxo) such as (–Si–O–Al–O–Si–O– Si–O–) when Si/Al=3 (Nuruddin *et al.*, 2016).

It has been suggested that aluminosilicate which is mainly introduced in the formation of geopolymers, is based on the poly (sialate) form, which is abbreviated by the term silicon-oxo-aluminate. The Polysialates is explained by a chain and ring of polymers, which consist of Si^{4+} and Al^{3+} cations. These cations are combined and re-arranged by oxygen atoms in IV-fold, which lead to the creation of an amorphous to semi-crystalline network, with high physical properties as shown in Table 2.2 (Davidovits, 2005).

Many factors could affect geopolymerization synthesis and make it very complex. The exact mechanism of geopolymer reactions is not yet completely defined. Nevertheless, many geopolymer researchers admit that the geopolymerization process consists of three main stages.

1. Dissolution or destruction which is explained by alkaline hydrolysis.
2. Re-arrangement or transportation of cations (also known as re-orientation).
3. The polycondensation process, or (hardening/solidification reactions) of free silicate and aluminates groups (Suwan, 2016).

Table 2.2. Chemical structures of polysialates
(Davidovits, 2005)

Si, Al Ratio	Name	Chemical bond	Chemical Schematic
Si/Al =1	Poly(sialate)	-Si-O-Al-O-	
Si/Al =2	Poly(sialate-siloxo)	-Si-O-Al-O-Si-O-	
Si/Al =3	Poly(sialate-disiloxo)	-Si-O-Al-O-Si-O-Si-O-	
Si/Al >3	Poly(sialate-multisiloxo)	Sialate Link	

The characteristics of the precursor materials and the activator solutions identify the final products of the geopolymerization reaction, which could be C-S-H (Ca + Si), zeolite/polymers (Si + Al) or C, N-A-S-H (Ca, Na + Al + Si) (Pacheco-Torgal et al., 2008a; Pangdaeng et al., 2014). A gel is formed from oligomers during the chemical reaction of geopolymers, while, at the same stage, molecules of water (H_2O) are released. Then, a three-dimensional structure in the form of gel network is created when the gelation process is re-arranged together through an exothermic reaction as shown in Figure 2.4 (Suwan, 2016).
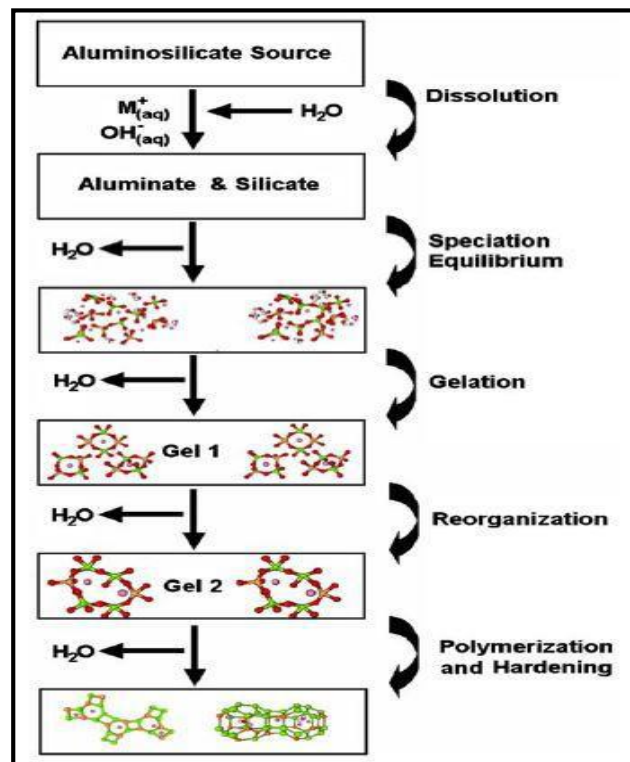
Figure 2. 4. Model of the geopolymerization process,

(Duxson *et al.,* 2007a)

2.2.2. Geopolymer Binder Constituants

2.2.2.1. Source of Materials

Silicon (Si) and Aluminium (Al) in amorphous form are considered to be the main source materials for geopolymers. These raw materials could be divided into three classes, namely industrial wastes, recycling materials, and natural materials. The main characteristics of the raw materials are listed as follows:

1. Industrial wastes:

A huge amount of industrial waste is produced by different manufacturing processes, for example, ash from fired coal, metallurgical slag, and mine and agricultural wastes (Sujatha *et al.,* 2012). As additives to PC, some of these materials are used to improve its properties. On the other hand, other industrial wastes such as fly and bottom ash, rice husk ash (RHA), granulated blast-furnace slag and steel slag are landfilled and stored in huge amounts.

2. Recycling materials:

Recently, worldwide consumption has increased, leading to a rise in wastage and recycling materials, such as in construction waste, and in paper and water sludge. Although the volume of these materials is limited compared to heavy industrial waste, it has generated an interest in reducing such as undesirable wastes and pollutants (Suwan, 2016).

3. Natural materials:

Several natural resources could be considered as raw materials for geopolymers, for example, kaolin (kaolinite or china clay), silty clay, and volcanic rock, among others. These materials can be found in different geological regions in limited amounts. It is believed that geopolymer produces from two main materials, previously mentioned as the raw materials and alkaline liquids, which are usually dissolved alkali metals such as Sodium (Na) or Potassium (K) (Wallah and Rangan, 2006). Further, it was thought that by using calcined source of materials, such as FA, slag and kaolin, it could be possible to achieve greater compressive strength than that of materials consisting of low or non-calcined materials, such as kaolin clay, mine tailings, and naturally occurring minerals (Barbosa, MacKenzie and Thaumaturgo, 2000). However, some researchers have found that the combination of both calcined and non-calcined materials gives rise to a significant improvement of strength in a short time (Xu and Van Deventer, 2002).

2.2.2.2. Alkaline Activators

In general, the activator solution most used in geopolymerization is a combination of sodium hydroxide (NaOH) or potassium hydroxide (KOH) with sodium silicate (Na_2SiO_3) or potassium silicate (K_2SiO_3) (Davidovits, Davidovits and James, 1999; Hardjito, 2005).

These alkaline activators comprise different ions such as Na^+, K^+ and Ca^{++}, which play a significant role in activating and accelerating the reaction between Si and Al and the binder. It has been reported that the use of sodium silicate solution, in a mix with sodium hydroxide solution, to activate the reaction between binder materials leads to a high geopolymerization reaction. This is due to a huge dissolution of NaOH in the solution compared to the KOH solution (Xu and Van Deventer, 2000). Hence, concrete based on alkali-activated fly ash is sensitive to the ratio of SiO_2/Al_2O_3 and Al_2O_3/Na_2O, which causes of complex and unclear chemical reactions of the geopolymerization mechanism (Ryu *et al.*, 2013).

Much research has focused on the positive impact during the geopolymerization process of the addition, of calcium to geopolymer cement or concrete, in terms of its mechanical properties and role. It is noted that the addition of calcium to geopolymer based fly ash can accelerate the hardening process and increase its strength (Van Deventer *et al.*, 2007; Topark-ngarm, Chindaprasirt and Sata, 2014). The strength increases when the geopolymer is cured at room temperature, whereas, curing under higher temperature conditions leads to weak mechanical properties, due to inhibition of the geopolymerization process and the development of a three-dimensional network structure or a so-called geopolymer-gel. However, some researchers (Komljenovic, Baarevic and Bradic, 2010; Kim, 2012) reported that both types of gel (C-S-H and geopolymer gel), which are formed during the hydration phase, and the geopolymerization process respectively, can have positive impacts on strength and give rise to the formation of a denser and more homogeneous binder (Kim, 2012). Table 2.3 presents, the achieved strength of a synthesised geopolymer, using different alkaline activator solutions.

Table 2.3. The compressive strength achieved by using different alkaline activators in the synthesis of geopolymer

No	Alkaline		Sample type	Comp.Strength		Starting Materials (% wt)	Additives (% wt)	Curing Condition		References
	Main (M)[a]	Addition		MPa	Age(d)			C°	Hrs.	
1	NaOH (12.5)	Na_2SiO_3	Paste	95.0	28	FA(100)class F[b]	-	85	20	Fernandez-Jimenez, et al.,2007
2	NaOH(75%)[c]	KOH(25%)[c]	Paste	95.0	28	MK(100)	-	40	20	Duxson et al., 2007c
3	NaOH(15)	Na_2SiO_3	Paste	92.1	7	FA(100)class F	-	75	7 days	Phoo-negernkham and Sinsiri, 2011
4	KOH(7)	Na_2SiO_3	Mortar	72.3	3	FA(100)class F	-	85	24	Kong and Sanjayan, 2010
5	KOH(7)	Na_2SiO_3	Paste	71.2	3	FA(100)class F	-	85	24	Kong and Sanjayan, 2010
6	NaOH(12)	-	Mortar	70.4	28	FA(100)class F	-	85	20	Fernandez-Jimenez and Palomo. 2005
7	KOH(-)	Na_2SiO_3	Paste	70.0	28	MK(100)	-	40	20	Duxson et al., 2007c
8	KOH(12)	K_2SiO_3	Paste	70.0	28	FA(90) class F	BA (10)	80	24	Hardjito and Fung, 2010
9	NaOH(-)	-	Paste	67.0	28	GBFS (100)	-	38	90 days	Khater, 2012
10	Na_2SiO_3(-)	-	Paste	45.0	28	FA(100)class F	-	60	28 days	Rashad and Zeedan, 2011
11	NaOH(-)	Na_2CO_3	Mortar	36.0	-	FA(100)class F	-	85	20	Fernanez-Jimenez and Palomo, 2005

[a]M = Molarity, [b] FA class F= low calcium fly ash, [c] percentage by weight (Suwan, 2016).

2.2.3. Geopolymer Constituents Design and Procedures

2.2.3.1. Concentration and Ratio of Alkaline Activators

Generally, in geopolymer cement or concrete, compressive strength increases when the concentration of alkaline activators is increased. Concentrated alkaline activators emit a considerable quantity of cations, which lead to a faster reaction in the polymerization process, and the dissolution of alumina-silicate materials (Raijiwala and Patil, 2010; Suwan, 2016). However, the optimum concentration of the alkaline solution could be influenced by many factors. For example, the properties of raw materials, the ratio between the alkaline activator and the raw materials, the liquid ratio SS/SH (Na_2SiO_3/NaOH) and the curing temperature and curing time, all have an influence. Several authors have studied the influence of sodium hydroxide solution on geopolymers using class F FA and various concentrations of NaOH (3-6M and 9M) (Görhan and Kürklü, 2014). Other parameters such as the sodium silicate/sodium hydroxide (SS/SH) ratio and sand /ash ratio were kept constant. The highest strength measured in seven days was given by an optimum concentration of NaOH of 6M: when the concentration of NaOH was lower (3M) or higher (9M) the strength was found to be less than the lower concentration, due to the insufficient reaction of NaOH in activating the geopolymerization; or caused by the precipitation of silicate in the case of higher concentration (Ken, Ramli and Ban, 2015).

In another study, in which the NaOH concentration was varied from 4.5M to 16.5M, the compressive strength increased as the NaOH concentration level was raised from 4.5 to 9.5M (Somna *et al.*, 2011). However, the strength increase was limited when the NaOH concentration increased from 9.5M to 14M, whereas, the compressive strength started decreasing once the NaOH concentration reached to 16.5M. Some authors believed that the alkali activation process is dominated by the types and the concentration of the alkaline activators (Komljenovic, Baarevic and Bradic, 2010). Five different activator solutions with diverse concentrations were used to make geopolymer mortars based on FA. The results of the compressive strength tests show

that the highest activation potential corresponds to the highest strength. These can be classified as follows; Na_2SiO_3, followed by $Ca(OH)_2$, NaOH, NaOH + Na_2CO_3 and KOH. It is believed that lower activation potential was given by KOH compared to NaOH because of the distinction between the ionic size of sodium and potassium ions/atoms (Ken, Ramli and Ban, 2015).

2.2.3.2. Ratio of Alkaline Activator-to-Raw material

A procedure design has been proposed by some authors for certain types of GPC, following Indian Standards (Anuradha *et al.*, 2012). The method designed was based on the selection of FA content and activator solution to FA ratio and based as well on a required strength. On the other hand, Ferdous et al. (2013) have suggested other mix designs containing FA based GPC. Several parameters have been considered in the suggested design, such as the variability of the concrete's density, the workability, required strength and specification of the raw materials, such as their specific gravity (Ferdous, Kayali and Khennane, 2013). The main concerns in the design process, are the ratio of selected activator solution to FA, also quantifying accurately the content of the activator solution, which corresponds to the selected FA (Pavithra *et al.*, 2016). However, it was believed that a high ratio of alkaline solution to FA leads to premature precipitation, before the geopolymerization process is complete, resulting in declining strength, due to the formation of sodium carbonate (Sukmak *et al.*, 2013). It is thought that, depending on the nature of the alumina-silicate materials, the ratio of alkaline solution to FA recommended to achieve the required strength and workability could range between 0.35 and 0.50 (Suwan, 2016).

In addition, water is considered a significant part of the mixture during the hardening process. In the case of the water to solid ratio (w/s), ''solid'' is given by the whole mass of solids, being the sum of FA, the mass of sodium hydroxide, the sodium silicate solid and of other added solids such as sand or aggregates, whereas the amount of water is given by the quantity of water in sodium hydroxide, sodium silicate solutions and the additional water added during the mixing. It was assumed that the ratio of w/s should be in the ranges 0.18 to 0.22 and 0.26 to 0.32 for fly ash-based geopolymer

paste and for concrete, respectively (Panias, Giannopoulou and Perraki, 2007; Chindaprasirt *et al.*, 2011; Suwan, 2016).

2.2.3.3. The Ratio of Na₂SiO₃-to-NaOH Solution (SS/SH)

The most significant parameter in the synthesis of geopolymer is the determination of the optimum ratio of sodium silicate to sodium hydroxide (SS/SH). It has been assumed that the proportions of SS and SH solutions are typically related to the percentage by mass of the alkaline solution in the ratio of AA/FA and also related to the water content and pH level (Suwan, 2016). Generally, geopolymerization will occur in two main steps. The first is the hydrolysis of the reactive silica by the free hydroxyl ions from the alkali solution, which leads to the formation of alkali-silica gel, followed by the second step which is water absorption by the formed gel which leads to an expansion in volume (Swamy *et al.*, 1992; Singh *et al.*, 2015).

Some researchers have studied the impact on the compressive strength of the GP paste of the ratios of FA to an alkaline activator (AA/FA) and of sodium silicate to sodium hydroxide (Na_2SiO_3/NaOH). Other investigations have been carried out by Mustafa Al Bakri et al. (2012) who agreed that the alkaline activator to FA ratio has a substantial influence on the compressive strength of GP paste. On the other hand, further researchers thought that the alkaline activator to FA ratio was not a significant factor for compressive strength in the geopolymerization process (Palomo, Grutzeck and Blanco, 1999). However, it has been found that the optimum ratio of Na_2SiO_3/NaOH, which corresponds to high compressive strengths, is in the range of 0.67 to 1.00 (Chindaprasirt, Chareerat and Sirivivatnanon, 2006).

Basically, the main raw material used for geopolymer is aluminosilicate, which is abundant in both alumina (Al_2O_3) and silica (SiO_2). The formation of a geopolymer based on these materials also is considered to be the main source of AL^{3+} and Si^{4+} ions during a geopolymerization process. Typically, the useful amount of the Al_2O_3 and SiO_2 elements which exist in the raw materials should be more than 70% (Cioffi, Maffucci and Santoro, 2003; Liew *et al.*, 2016).

Moreover, the mix of FA and the alkaline activator provides support to Na and Al sources, which are released from the alkaline activator solutions (SS/SH) and from the dissolved FA within the activator solution. The reactivity of FA can be determined by the amount of Al in the aluminosilicate gel. This is why the compressive strength of geopolymer could be affected by the AA/FA and SS/SH ratios. Much research has been carried out to determine the optimum ratios, which could lead to greater compressive strength being achieved (Al Bakri *et al.*, 2012). Some research has reported that geopolymer based on metakaolin as a raw material can achieve adequate strength when the Si/Al ratio ranges from 1.9 to 3.0. In practice the most suitable ratio of FA-based geopolymer comprises between 2.0 and 4.0 (Andini *et al.*, 2007). Based on this, it has been suggested that the appropriate Si/Al ratio for fly ash and metakaolin materials based geopolymers is around 2.0 to 3.0 (Suwan, 2016).

2.2.3.4. Preparation Process and Delay Time

The delay time is defined as the period of time that samples were left at an ambient temperature for moulding and wrapping before being transferred into the oven. A study carried out by Chindaprasirt et al. (2006) showed that delay times of 0, 1, 3 and 6 hours before FA based geopolymer specimens were placed inside the oven at 60°C, negatively affected the compressive strength of the geopolymer. These results were in agreement with those found by other authors (Hardjito *et al.*, 2004). It is believed that the optimum delay time for any geopolymer paste was found to be around a half of its primary setting time. For example, if the setting time is 2 hours, the delay time might be about 1 hour. Additionally, the characterization of the starting materials has an impact on the optimum delay time (Chindaprasirt *et al.*, 2011). However, the source of the materials could have a negative effect on the mechanical characteristics of the geopolymer, and the geopolymerization process could be prohibited by the extremely high temperatures during the curing period of heat (Ken, Ramli and Ban, 2015).

2.2.4. Geopolymers' Properties and Applications

The properties of geopolymer cement and its application have been reviewed in many research papers (Bakharev, 2006; Duxson *et al.*, 2007; Komnitsas, Zaharaki and Perdikatsis, 2007; Mohd *et al.*, 2013; Ryu *et al.*, 2013). Much research has focused on demonstrating that under various environmental conditions geopolymer cement has high mechanical and chemical properties whose significance can be listed as follows.

2.2.4.1. Mechanical Properties of Geopolymers

- Uniaxial Strength

An early strength and setting time are considered the most significant mechanical properties, the development of which can play an important role during the constructions of buildings. The hydration process is a chemical reaction that leads to the hardening of cementitious materials such as OPC. It has been reported that to achieve a short setting time for geopolymers, a higher curing temperature and higher concentration of alkaline solution are required, ultimately accelerating the rate of geopolymerization and leading to an early hardening of geopolymer cement (Hardjito, Cheak and Lee Ing, 2008). On the other hand, it has been stated that, if geopolymer pastes contain only FA as a binder, generally it takes a longer time to set, due to the slow rate of the chemical reaction at a low ambient temperature (Nath and Sarker, 2014).

Compressive strength is the most commonly-used test for evaluating the properties of geopolymers, due to its high descriptiveness and simplicity (Komnitsas and Zaharaki, 2007). It has been reported that high strength (up to 95 MPa) could be achieved after 28 days for fly ash based-geopolymer (Fernandez-Jimenez, García-Lodeiro and Palomo, 2007). Therefore, other studies demonstrated that geopolymer strength such as split tensile strength, flexural strength and bonding strength could be similar to, or

much greater than, that of OPC (Fernández-Jiménez and Palomo, 2005; Sofi *et al.*, 2007; Hu *et al.*, 2008).

- *Multi-axial Strength*

In past decades, much research focused mainly on the mechanical behaviours of geopolymer concrete when loaded under uniaxial stress. However, it has been pointed out that there is a lack of studies of the engineering properties of GPC under multi-axial loading. Nevertheless, the use of the multi-axial test to investigate OPC concrete has been considered by many researchers. Shi et al. (2014) examined through an experimental study, the dynamic multi-axial stresses of dam and wet screened concrete, and the results showing that the tri-axial stresses gave rise to massive distortions on the specimens before reaching failure point. The authors observed that specimen failure has occurred in different categories, such as plate, parallel and shear types, which has also been found to be the case by other researchers (Gabet, Malécot and Daudeville, 2008; He and Song, 2010; Shang, 2013). It has been concluded from those findings that the failure modes obtained from both concretes are mainly affected by the stress ratio, not by the strain rates (Shi *et al.*, 2014).

Drying shrinkage is shrinkage which can occur in cement or concrete by decreases in volume, due to the loss of uncontrolled water from the system (Liew *et al.*, 2016). This leads to a micro-cracks in the structure of concrete. Therefore, it has been reported that geopolymers possess good expansion resistance and superior shrinkage (20-25mm), with great thermal withstanding when subjected to high temperature ranging between 800°C and 1000°C (Panias, Giannopoulou and Perraki, 2007; Zuhua *et al.*, 2009).

2.2.4.2. Dynamic Properties of Geopolymer Concrete

Ren et al. (2015) examined the dynamic mechanical behaviours of geopolymer concrete immersed in water. A split Hopkinson pressure bar test (SHPB) was carried out to measure the dynamic compressive strength of the GPC, and the results showed that, compared to GPC tested before water submersion, the dynamic strength of the

immersed GPC increased around 12% with the decrease in the strain rate (10.76%) when compared to those indoors specimens. The authors, therefore, concluded that the quasi-static properties of the GPC could be negatively influenced by water, a conclusion in line with results obtained by other researchers, when OPC concrete was used. It has been explained that, the distribution of water into the concrete cracks could lead to a reduction in the potential energy of the surface which is needed for the crack expansion, which in turn, increases the stress loading at the crack tips (Yaman, Aktan and Hearn, 2002; Ren *et al.*, 2015).

However, due to the limited research on the strain rate effect in geopolymers, some recent studies have investigated the dynamic engineering of the GPC based on SHPB system. It has been stated that subjecting slag-ash geopolymer concrete to a high loading strain rate by using the SHPB test revealed a high strain rate sensitivity compared to that of OPC concrete (Luo *et al.*, 2013; Xin *et al.*, 2014). The same authors sought to explain that phenomena, saying it could have been due to the existence in geopolymer of three-dimensional hydration, which might play a significant role in transferring the resultant stress to the inner particles in the specimen. Another study has estimated the effect on the toughness of an alkali-activated slag concrete and concluded that the alkali-activated slag concrete, concluding that such concrete has considerable capacity to absorb energy under a high compression strain rate (Gao *et al.*, 2015; Ding, Dai and Shi, 2016).

2.2.4.3. Durability and Thermal Stability of Geopolymers

Many thermal standards have been established to assess the resistivity of geopolymers under heat or fire conditions. It was found that, in comparison with OPC, geopolymers have a high fire resistance, when temperatures varied rapidly between 200°C and 1000°C with a residual strength ranging from 20MPa to 31MPa, due to the limited amount present of calcium hydroxide (portlandite) $Ca(OH)_2$ (Rashad and Zeedan, 2011; Suwan, 2016).

A thermal stability study of geopolymer materials, made by using class F FA and both sodium and potassium alkaline activators upon heating at 800-1200°C, was carried out by Bakharev (2006). This study showed a rapid decrease in strength at 800°C, associated with an increase in the average pore size for those specimens made using a sodium-based activator. However, for those samples prepared using a potassium-based activator, the deterioration of strength started at 1000°C, with a significant increase in strength with a reduction in the average pore size which has also been observed. An experimental study, conducted by Türkmen *et al.*, (2016), showed that the strength of geopolymer concrete prepared using ferrochrome slag increased around 10% at a temperature range of between 100-300°C, where the highest strength, obtained at 300°C, was approximately 37.06 MPa.

A previous study of steel reinforced fly ash-based-geopolymer concrete panels of 125-175mm thickness indicated that exposing those panels to fire for two hours, resulted in a higher heat transfer rate, fewer cracks and spalls for the geopolymer concrete specimens. The same study demonstrated that the residual load capacity of the geopolymer samples was between 61% and 71%, compared to that of OPC concrete panels, which was between 50% and 53% (Kumar and Mcbeath, 2015). Kong and Sanjayan (2010) studied the behaviour of geopolymer paste, mortar and concrete under elevated temperatures (up to 800°C). The investigative study showed that the aggregate and specimen sizes were the main factors controlling geopolymer behaviour at temperatures up to 800°C. In addition, the strength loss of geopolymer concrete at high temperatures was mainly due to the incompatibility between the thermal expansion of the geopolymer matrix and the aggregate used in the GPC. Further, this thermal incompatibility caused internal destruction and thus negatively affected the strength of the concrete (Kong and Sanjayan, 2010).

It was revealed that concrete-based-Portland cement could be a durable material if its production was well designed. However, because the aggressiveness of environments such as chloride and other acids attacks the OPC concrete, it no longer resists and easily degrades under such conditions. The deterioration of concrete mainly occurs in

the form of reactions between various harmful chemicals and the matrix of concrete, and also the reactions of the chemicals with aggregates (Adam, 2009).

In general, marine and other acidic environments are considered the most corrosive and destructive towards concrete. This is because of the abrasion phenomena which can occur on the concrete, and also the rubbing, scratching and sliding of matter and substances on the surface of the concrete. Experimental work showed that due to its high homogeneity and structural bonding, geopolymer concrete performed better than OPC when both were exposed to marine environments (Pacheco-Torgal, Castro-Gomes and Jalali, 2007; Adam, 2009).

It has been reported that the development of ettringite gel as a new composition in the structure of OPC expands its volume, and also affects its microstructure, due to the damage which is caused by penetrating acids (Palomo *et al.*, 1999). Further, it has been observed that, after immersion in acid solutions, geopolymers showed less deterioration compared to OPC (Fernandez-Jimenez, García-Lodeiro and Palomo, 2007). An experimental study was carried out to investigate the durability of reinforced geopolymer concretes, which were designed from different FA sources and OPC. The results showed that, of all the specimens, the GPC samples displayed a lower chloride diffusion coefficient about 73% and had extremely limited corrosion product (Kupwade-Patil and Allouche, 2013).

Another study investigated the durability of low-calcium ferronickel slags-based geopolymer manufactured at 80°C for 48 hours and cured for 28 days. The geopolymer products were subjected to different corrosive environments, then immersed in freeze-thaw cycles from -15°C to +60°C for 4 months. The results showed that the compressive strength slightly decreased from 17 MPa at room temperature to 14.12 MPa (Komnitsas, Zaharaki and Perdikatsis, 2007). Chindaprasirt and Chalee (2014) investigated the penetration of chloride ions into a fly ash-based geopolymer concrete subjected to a marine environment for period of more than three years. The geopolymer concrete was produced using various NaOH concentrations ranging from 8, 10, 12, 14, 16 and 18M. The results revealed that the penetration of the chloride

ions increased with the increase of alkali molarity. The same authors investigated the effect of NaOH molarity on the chloride diffusion coefficient, where the results exhibited that high NaOH concentrations played a significant role in reducing the ingress rate of chloride into the geopolymeric material (Chindaprasirt, Chareerat and Sirivivatnanon, 2006; Chindaprasirt and Chalee, 2014).

2.2.4.4 Applications of Geopolymer Cement

In recent years, more and more industrial wastes is produced in every country worldwide, including metallurgical, mining sources and demolition materials. This industrial waste material can be used in the production of geopolymers such as concretes, coatings, and fire resistant precast components for building (Komnitsas, 2011). The use of geopolymers as the main construction material has many applications as follows.

Precast geopolymer components: The use of geopolymers in the fabrication of precast or assembled components is considered as commercial material for many applications (Suwan, 2016). It has been proven that, compared to OPC geopolymers could have a high resistance to chloride diffusion when cured at high temperatures. This allows geopolymers to be used in the production of precast concrete for marine constructions. Further, there is a high potential for using precast geopolymer material in-situ as an application for those structures exposed to a chloride environment under an ambient condition (Adam, 2009).

Geopolymer blocks and bricks: The use of different wastes or by-product materials to produce good construction bricks was the focus of many researchers. A study showed that more than 84% of hematite tailings can be combined with clay and low calcium fly ash to manufacture bricks (Chen *et al.*, 2011). Another study reported that high level of energy are consumed during the combustion process in the production of traditional bricks, so releasing huge amounts of greenhouse gases (Ahmari and Zhang, 2012). However, utilizing geopolymer in the production of bricks reduces the energy required for combustion, thereby reducing the emission of greenhouse gases. An

experimental study showed that lightweight geopolymer-blocks could be manufactured at an ambient temperature of 25°C (Andini *et al.*, 2007).

Reinforced geopolymer concrete: The OPC's standards have been used to study the application of reinforced-geopolymer concrete. It has been found that the bonding strength of geopolymer concrete proportionally increased with the increase of reinforcement-bar diameters (Singh *et al.*, 2015). Sujatha (2012) investigated reinforced geopolymer concrete columns of 100mm diameter, 1800mm length and 2.16% of reinforcements, the GPC activated by sodium silicate and sodium hydroxide and cured at 70°C. The results showed less deformation of the reinforced geopolymer concrete than of OPC manufactured with the same reinforcement steel bar under similar conditions. The same author stated that, due to the solidity of the bonding, a good reinforced geopolymer concrete product had been achieved (Sujatha, 2012). It was suggested that geopolymer concrete could be used in the production of railway sleepers, with less modification of the current OPC concrete equipment (Hardjito, 2005).

Composite and hybrid materials: Excellent properties such as high strength, lightweight nature, and good fire resistance are the main parameters, which could encourage the development of new composite materials. The use of geopolymer products as a composite material is a field which has been investigated by many researchers. An investigation showed that using melamine to produce geopolymer hybrid composites is an eco-friendly, particularly, when metakaolin and other metallurgical materials are used as precursor materials (Roviello *et al.*, 2015).

Immobilization of harmful elements: Typically, the industrial wastes might consist of heavy metals such as Pb, Cr, Cu, and Hg. These metals, however, could provide a serious risk to human health and the environment. It has been revealed that the immobilization of heavy metals from geopolymer mortar-based slag has a greater immobilization compared to that geopolymer without slag (Yunsheng *et al.*, 2007). Similar findings have been reported when the immobilization of heavy metals such as Pb, Cr and Se from high-magnesium nickel slag geopolymer has been efficiently

immobilized after the geopolymerization process (Zhang *et al.*, 2017). In addition, other authors have reported that heavy metals could easily be immobilized into the amorphous phase of aluminosilicate geopolymer (Hu *et al.*, 2008).

2.3. Factors Affecting Geopolymers' Properties under Ambient Conditions

Much research work has studied the characteristics and applications of geopolymers. It has been stated that heat plays a significant role in accelerating the geopolymerization process, which in turn enhances geopolymers' strengths (Nasvi, Ranjith and Sanjayan, 2014). Heat curing is considered to be the most significant limitation of geopolymer applications. Numerous studies have attempted to produce relevant geopolymer products with a high earlier strength and curing at ambient temperature (Phoo-Ngernkham *et al.*, 2013; Neupane, 2016). Because of this concern, some geopolymer studies have investigated the following factors, which might lead to achieving a significant earlier strength at ambient conditions.

2.3.1. Fineness and Shape of Particles

The fineness of particles plays a significant role in the improvement of the mechanical properties of geopolymers. Previous studies have shown that an increase in the fineness of FA from 290 m^2/kg to 907m^2/kg, can achieve greater strength and workability (Aydin, Karatay and Baradan, 2010). An increase in both flow and compressive strength was also reported, when there was a decrease in the fineness of particles (Sabitha *et al.*, 2012). Similar results have been found by other researchers indicating that the addition of finer particles of FA enhances the workability of the fresh geopolymer paste, due to the spherical shape and smooth surface of FA (Ken, Ramli and Ban, 2015). Other studies have revealed that, the fineness of high calcium FA particles significantly influenced by decreasing the setting time and the strength of fly ash-based geopolymer mortar. An experimental investigation based on the use of coarse, medium and fine FA particles, indicated that the highest strength was

achieved by using fine, medium and coarse FA particles, respectively (Chindaprasirt *et al.*, 2011).

2.3.2. The Concentration of Alkaline Activator Solutions

As previously indicated, the geopolymerization process is mainly controlled by the concentration of the activated solution used. The mechanical properties of alkali-activated FA-based geopolymer mortar could be affected by the concentration of the activator solution. The increase in activator concentration improves the compressive strength (Komljenovic, Baarevic and Bradic, 2010). Another study carried out by Al Bakri et al. (2012) shows that the compressive strength of a designed geopolymer rises with increases in the ratios of FA to the alkaline activator and of sodium silicate to sodium hydroxide (Na_2SiO_3/NaOH). Similar results have been found by the same authors when the NaOH concentration was changed (AL Bakri *et al.*, 2011). Furthermore, it has been reported that variation in the concentration of the alkaline activator considerably affects the development of early strength (Ryu *et al.*, 2013).

2.3.3. The Mixing Process

The combination of the richness alumina-silicate materials and activator solution leads to the formation of a geopolymeric cement (Lloyd and Rangan, 2010). In order to achieve a great workability of geopolymer mortar, 5% by mass of base water was mixed with FA and activator solution at a room temperature of 25°C. It has been revealed that considerable strength with a short setting time could be achieved, firstly when sodium hydroxide was mixed with the raw materials, then with the addition of sodium silicate solution (Chindaprasirt, Chareerat and Sirivivatnanon, 2006). Ferdous, Kayali and Khennane (2013) have presented a flowchart of a designed mix procedure to produce an appropriate fly ash-based geopolymer concrete (Ferdous, Kayali and Khennane, 2013).

2.3.4. Curing Conditions

Most of the previous studies have reported that heat can be the main reason for the improvement in strength of FA-based geopolymers (Suwan, 2016). In addition, geopolymers subjected to a high thermal temperature ranging from 50°C to 100°C improves their cementitious properties (Fernandez-Jimenez, García-Lodeiro and Palomo, 2007). It has been concluded from a study of different curing conditions that the temperature and humidity can have a significant curing role in the development of the microstructure and properties of FA-based geopolymer materials (Kovalchuk, Fernández-Jiménez and Palomo, 2007). Time and curing temperature also have an important effect on both compressive and flexural strengths and could affect the distribution of pores, which in turn influences the microstructure of the final geopolymer product. In addition, the curing of fresh geopolymer mixture under high temperatures leads to the development of early strength. However, a decrease in strength has been observed after 28 days (Rovnaník, 2010).

2.3.5. Calcium Content

The presence of calcium in the geopolymer mixture is considered as the main reason in the formation of a high early strength, due to the rapid reaction between the calcium and activator solutions. When compared with the other component oxides, it is believed that Al_2O_3 and CaO are the most significant. The AlO^{-4} combines with the silicate to form oligomers, which in turn introduces in the creation of geopolymer gels. while, the CaO can quickly react to form early C-S-H and/or (C, N)-A-S-H gels, which eventually improve the strength of the geopolymeric system (Xu and Van Deventer, 2002; Thomas and Nair, 2015).

It has been stated that using GGBS or adding calcium oxide (CaO) as a prime material in the production of geopolymers, enhances their strength at ambient temperature. Similarly it has been found that the mechanical properties of FA-based geopolymers could be affected by the amount of calcium components such as CaO and $Ca(OH)_2$

(Temuujin, Williams and van Riessen, 2009; Topçu, Toprak and Uygunoğlu, 2014; Nath and Sarker, 2016). Another study has shown that the formation of C-S-H gel during geopolymerization could have positive effects on the development of strength. The C-S-H gel plays the role of a micro-aggregate function in the geopolymeric N-A-S-H gel, resulting in a denser and more uniform system (Kim, 2012).

However, it has been observed that calcium silicate hydrate (C-S-H) increases with a significant decrease in calcium hydroxide crystals, due to the dehydration process of the crystals after the geopolymers are subjection to high temperatures. An elevated temperature accelerates the reactivity of pozzolanic materials, and converts the calcium hydrate crystals to calcium silicate hydrate (C-S-H), which in turn enhances the development of the geopolymer strength (Türkmen *et al.*, 2016).

2.4. Summary

The above literature review summarizes the main research outcomes of i) the use of fly ash in conventional cement (OPC), ii) the basics of geopolymer technology and iii) the main factors that can affect geopolymer properties at ambient temperature.

After water, Portland cement (PC) is the second most consumed material on earth, due to the vast scale of its use and the abundant availability of its component materials. The manufacturing process for OPC requires the burning of huge amount of fuels, which are needed for the decomposition of limestone, its main raw material. This process leads to the release into the atmosphere of large quantities of carbon dioxide. Significant attempts have been made to find other alternative pozzolanic cementitious materials, which might have similar or superior properties to those of OPC. Also, such alternative materials might provide a solution to the environmental issues caused by the production of OPC. Because of these concerns, much research has been done involving in geopolymer cement as a possible alternative binder to OPC.

Many studies have investigated the use of geopolymers as a replacement material for conventional cement (OPC). The fundamentals of geopolymers, such as their chemical composition, activation solution, physical properties and the characteristics of the prime materials have been examined. FA, GGBS and other by-products wastes are the raw materials most widely-used in geopolymers, due to their richness of alumina (Al) and silica (Si) constituents and also because of the morphological structure of their particles. To produce geopolymer products, a mix of activator solution prepared from sodium silicate and sodium hydroxide (SS/SH) is used to activate the aluminosilicate material. The concentration and ratios of the alkaline solution need to achieve high-level mechanical properties in the production of geopolymers, while the fly ash to activator ratio needs to be optimised. Loss of moisture is also a significant factor in the geopolymerization process, and can have negative effects on the geopolymer strength if it takes place too rapidly.

Recently, geopolymers have become a subject attracting much interest from many researchers. For such new, alternative geopolymers to be developed and become standardised commercial products, they must have better mechanical and physical properties than OPC. However, the main mechanism in the geopolymerization process is complicated and still not fully understood, in terms of the geopolymer matrix structure, the activation of the precursor materials, and its microstructural properties. A long-term assessment needs to be carried out to investigate geopolymer durability and its ability to withstand corrosive environments.

The literature survey described earlier reveals that the most research on the production of geopolymers is mainly focused on the use of one precursor or a combination of two materials. However, the use of ternary material together is a new concept in the production of geopolymers. This investigative research presents a novel process in the manufacturing of geopolymers using three by-product materials, in the purpose of developing a sustainable eco-friendly product.

Chapter 3

Mechanical Properties of FA-GGBS-HMNS based Geopolymer Concrete/Paste

3.1. Introduction

This chapter presents the mechanical properties of the designed FA-GGBS-HMNS based geopolymer concrete and paste. Also discussed in this stage the effect of curing time on uniaxial compressive strength and on the splitting strength of the manufactured geopolymer concrete. Test results for the properties of fresh geopolymer concrete and paste are also detailed. The mixed concrete specimens were cast into different mould shapes relevant to international standards before performing tests. The manufacturing process and the test procedures are presented in this chapter. The results obtained were plotted and presented in Figures and Tables by using the average values of at least 3 samples for each test.

This research aims to evaluate the potential for producing geopolymer concrete with high mechanical properties using various precursor by-product materials. The so-called geopolymer concrete is commonly known as concrete and has been investigated by many researchers for decades (Davidovits, 2005).

3.2. Materials and Testing

The materials used for casting GP concrete and paste specimens were aluminosilicate materials (class F FA, GGBS and HMNS), aggregates, and alkaline activator solutions, as shown Table 3.3. During this experimental work the mechanical and microstructure tests were conducted in ''Center of Excellence Geopolymer and Green Technology (CEGeoGTech), Universiti Malaysia Perlis, Malaysia.

3.2.1. Cementitious Materials

3.2.1.1. Fly Ash

As a source of aluminosilicate, class F FA material is used in the present experimental study. This material was obtained from the Manjung power plant at Perak in Malaysia. The distribution of the particle size of the FA used is shown in Figure 3.1. This shows that almost 90 % of the particles were distributed in the range 4 µm to 70 µm, while 10 % of the particles were distributed in the range 80 µm to 550 µm. It is noted that the distribution appears to be in bimodal form, the mode being located at 30 µm. The average particle size (X_{50}) of fly ash is 17.37 µm and its specific surface area is around 1.3 m^2/g. The chemical composition of class F FA, as shown in Table 3.2, were determined using X-ray fluorescence (XRF) analysis. The total amount of the main oxide components $SiO_2+Al_2O_3+FeO$ represents more than 70 %, while the amount of CaO is less than 10%. Scanning Electron Microscope (SEM) images of the materials used are shown in Figure 3.2.
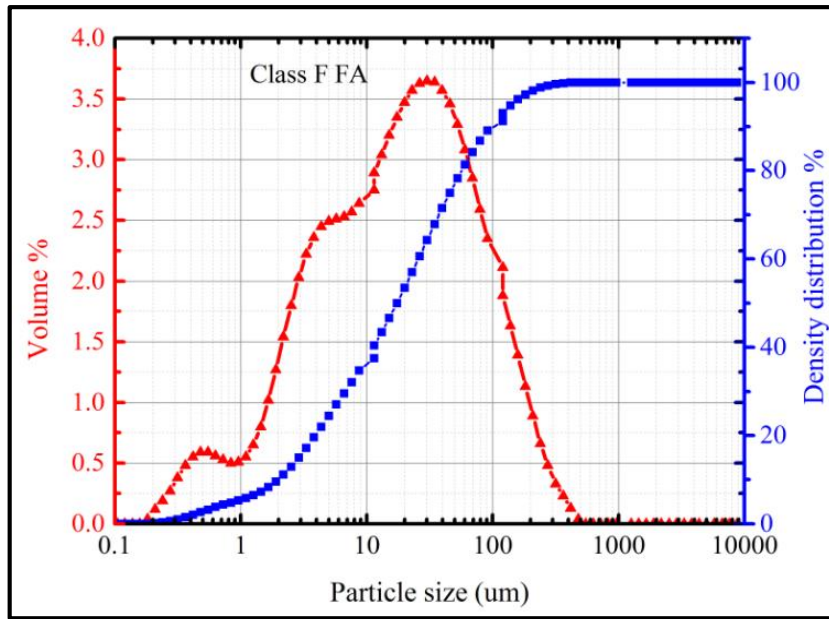
Figure 3.1. Particle size distribution of class F FA

As can be seen from Table 3.1, the FA used in this experimental study is classified as class F FA in accordance with the requirement of ASTM C618. The proportion of carbon in the FA is 3%, as determined using the loss on ignition (LOI) procedure. More details are presented in Appendix A. At less than 0.5%, the SO_3 percentage is low, a significant factor in the stability and durability of the final product.

Table 3.1. Class F FA characterizations

Constituent	Sum of (SiO_2, Al_2O_3, Fe_2O_3) (%)	SO_3%	LOI%
ASTM 618	≥ 70	$\leq 5\%$	$\leq 6\%$
Class F FA	90.7	0.27	3.04

Table 3.2. Chemical Composition of raw materials (%)

Compositions	Common name	Class F FA	GGBS	HMNS
SiO_2	Silica	55.7	28.2	43.22
Al_2O_3	Alumina	27.8	9.73	4.35
Fe_2O_3	Iron oxide	7.272	0.989	10.34
CaO	Lime	4.10	52.69	3.45
TiO_2	Titanium dioxide	2.29	1.01	0.1
SO_3	Sulfur trioxide	0.27	1.46	0.28
K_2O	Potassium oxide	1.55	1.22	0,18
MgO	Magnesium oxide	-	2.9	26.155
MnO	manganese oxide	-	0.749	0.89
P_2O_5	Phosphorus pentoxide	-	-	0.05
Na_2O	sodium oxide	-	-	0.232
Cr_2O_3	Chromium oxide	-	-	1.009
LOI	Loss on ignition	3.04	3.76	-0.3
Others	-	1.018	1.05	9.4
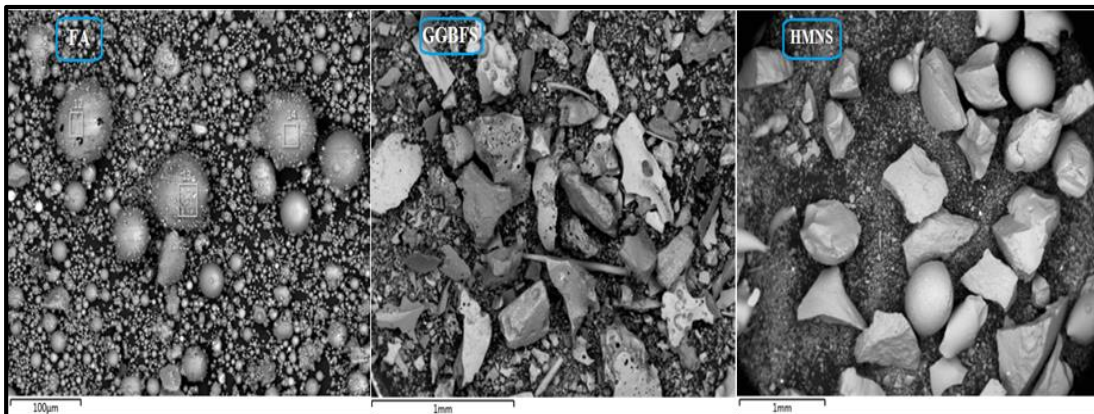
Figure 3.2. SEM images of the raw materials

Table 3.3. The main raw materials used for the study

Material	Function	Origin
Class F Fly Ash	By-product source of Aluminosilicate	Manjung power plant at Perak, Malaysia
GGBS	By-product rich of calcium and silicate	Steel plant in Penang, Malaysia
HMNS	By-product rich of Magnesium and silicate	Steel plant in Shaanxi, China (Mainland)
Sodium silicate	Alkaline activator	South Pacific Chemicals Industries Sdn. Bhd, (SPCI), Malaysia
Sodium hydroxide	Alkaline activator base	Formosoda-P Plastic Corporation, Taiwan.

3.2.1.2. GGBS

Ground Granulated Blast Furnace Slag (GGBS) was obtained from the steel plant in Penang, Malaysia. Its chemical composition is illustrated in Table 3.2. It is noted from the results that CaO has the major proportion of up to 52 %. The particle size distribution of GGBS, as provided by a particle size distribution analyser is shown in Figure 3.3. The average (X_{50}) particle size was 138 μm, while the mode peaked at ~250 μm. The specific surface area of the GGBS is around 0.106 m^2/g.
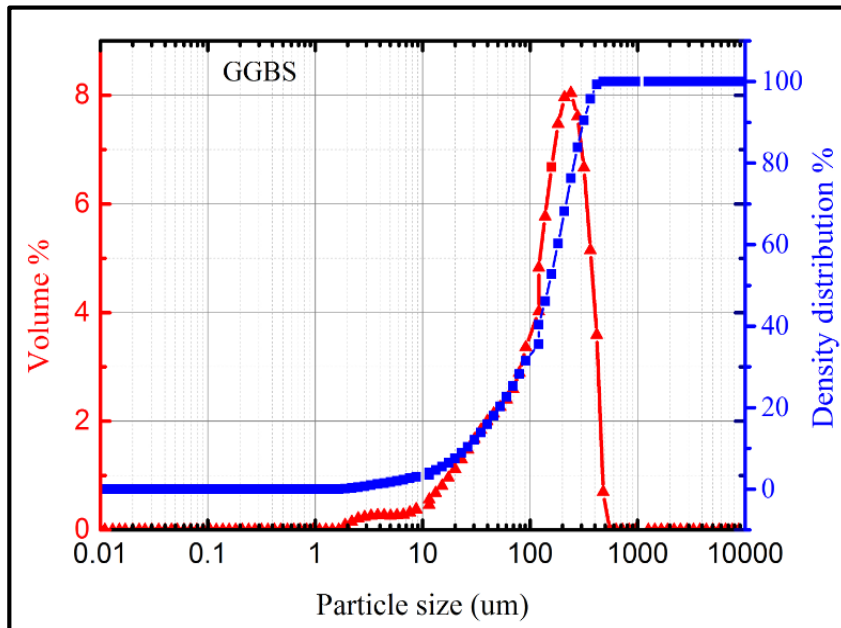
Figure 3.3. Particle size distribution of GGBS

3.2.1.3. HMNS

High Magnesium Nickel Slag (HMNS) was obtained from a steel plant in Shaanxi, China (Mainland). The chemical composition is presented in Table 3.2. It is noted from the results that SiO_2, MgO and Fe_2O_3 have the highest proportions at 43.22, 26.15 and 10.34% respectively. The particle size distribution of HMNS is given in Figure 3.4. The average particle size of HMNS (X_{50}) is about 280 μm, while the mode peaked at ~ 400 μm. The specific surface area of HMNS is approximately 0.0536 m^2/g. HMNS has a grey-black colour and mix of spherical and dendritic shape particles.
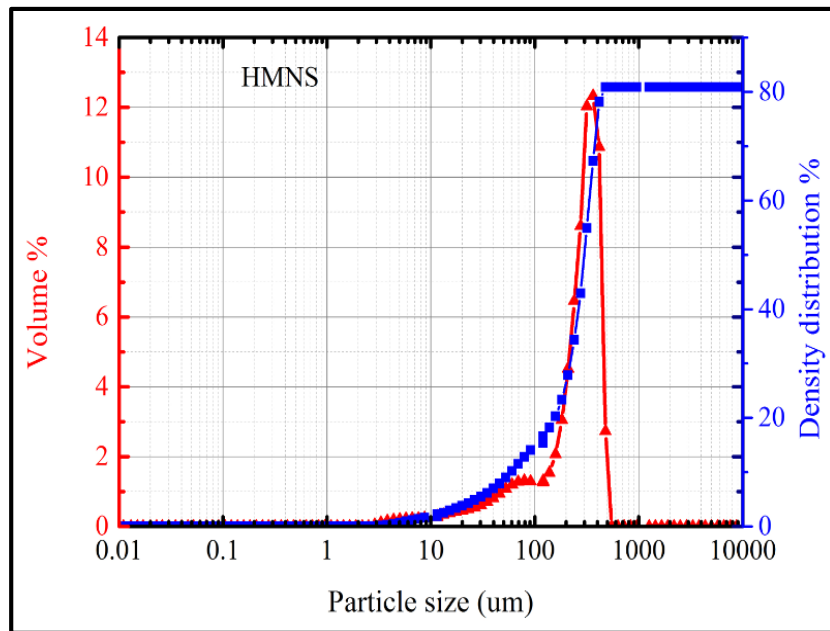
Figure 3.4. Particle size distribution of HMNS

3.2.2. Alkaline Activator Solution (AAS)

To prepare the alkaline solution, sodium silicate (SS) and sodium hydroxide (SH) were used to mix in a mass ratio of 2.5 (SS/SH =2.5). This solution was prepared and left overnight to ensure that it completely dissolved before being used in experimental work.

3.2.2.1. Sodium Silicate Solution (SS)

To synthesise the alkaline activator solution, sodium silicate and sodium hydroxide were mixed in a mass ratio of 2.5 (SS/SH =2.5).

Table 3.4 presents the main technical grade of sodium silicate as supplied by South Pacific Chemicals Industries Sdn. Bhd. (SPCI) Malaysia.

Table 3.4. Properties of sodium silicate solution

Properties	Specification
Molecular weight	122.06 g/mol
Silica (SiO_2)	30.1 %
Sodium Oxide (Na_2O)	9.4 %
Water (H_2O)	60.5 %
Activator Modulus (SiO_2: Na_2O)	3.20
Specific Gravity at 20 °C	1.4 g/cm^3
Viscosity at 20 °C	0.4 Pa.s

3.2.2.2. Sodium Hydroxide (SH)

Sodium hydroxide was selected over many other candidates to be an alkaline base activator due to its high reactivity and costless. The sodium hydroxide solution was prepared in the laboratory by dissolving sodium hydroxide pellets in water. To prepare the sodium hydroxide solution with a concentration of 12M, 480 grams of sodium hydroxide pellets supplied from Formosa Plastic Corporation, Taiwan were dissolved in 1 litre of distilled water. After cooling for 24 hours at room temperature, the sodium hydroxide solution was then mixed with sodium silicate solution. The main properties of sodium hydroxide flakes are presented in Table 3.5. Eqs (3.1) and (3.2) are applied to calculate the NaOH mass used during the preparation process.

Table 3.5. Properties of sodium hydroxide flakes

Properties	Specification
Purity	99.00%
Water solubility	100%
Molecular Weight	30 g/mol

$$Number\ of\ moles, n = \frac{M*v}{1000}$$

Eq (3. 1)

$$Mass\ of\ NaOH\ Pellet = n*Mw$$

Eq (3. 2)

Where M is the concentration of NaOH (in molar), v is the volume of NaOH (in ml) and Mw is the molecular weight of NaOH in (g/mol).

3.2.3. Aggregates

River sand of diameter sizes not exceeding 5mm and gravel of diameter sizes ranging between 5mm and 19mm were used as the fine and coarse aggregates, respectively. Their density is 1204 kg/m^3 for the coarse aggregate and 1640 kg/m^3 for the sand. For all specimens, the mass ratio of the sand-to-gravel was arbitrary kept as 3:7 which was close to that reported in literature (Kumar and Mcbeath, 2015). To ensure that the gravel would not over absorb the activator solution, the gravel was saturated in water for about two hours before being mixed with binders and alkaline activators.

3.2.4. Mechanical Tests

3.2.4.1. Compressive Strength Test

Compressive strength is one of the most significant mechanical properties which determine hardened concrete's resistance and quality. Concrete can develop most of its strength after 28 days. In this research compressive strength was determined in accordance to ASTMC109, where an Instron machine series 5569 Mechanical Tester as shown in Figure 3.5a, was used. Two types of cubic specimens, 50mm x 50mm x 50mm and 100mm x 100mm x100mm were used to determine the compressive strength of the GP concrete and pastes produced. The test was conducted at 7, 14 and 28 days for pastes specimens and at 7, 14, 28 and 90 days for GPC. The average of three samples was considered as the final result for all tests.

3.2.4.2. Splitting Tensile Strength Test

The split tensile strength of concrete is an indirect tension applied to a concrete specimen to measure its splitting strength (ASTM C 496/C 496M – 04, 2011). Cylindrical specimens measuring 75mm in diameter and 150mm in length were used for the test. The load is applied from the top horizontal side of the cylinders as shown in Figure 3.5b. In general, the tensile strength of concrete is approximately one-tenth of its compressive strength. Eq (3.3) was used to determine the splitting strength of the GP concrete designed.

$$f_{ct} = \frac{2P}{\pi LD}$$
Eq (3. 3)

where f_{ct} is the split tensile strength in (MPa), P is the applied load which splits the cylinder in (N), L is the length of the cylinder in (mm) and D is the cylinder diameter in (mm).

Figure 3.5. (a) Compression test, (b) Splitting tensile test

3.3. Geopolymer Paste Mixtures

Two types of GP pastes were mixed and tested. One was the GP paste in which the binder consisted of FA and GGBS. The other was the GP paste in which the binder consisted of FA, GGBS and HMNS. In both types of mixes, the binder-to-liquid (alkaline solution) ratio was kept at 2.0.

In the FA-GGBS based GP pastes, GGBS contents with 5%, 10%, 20%, 30% and 40% of the binder were selected. Nine specimens of 50mm x 50mm x 50 mm cube for each selected GGBS content were cast. Hence, there were a total of 5x3x3=45 cubic specimens that were cast. The compressive strength tests were carried out on these specimens at 7, 14, and 28 days, respectively. The purpose of the tests being to ascertain which the FA-to-GGBS ratio produces the greatest compressive strength.

In the FA-GGBS-HMNS based GP pastes, the GGBS content was fixed, based on the largest compressive strength of the FA-GGBS based GP pastes, whereas HMNS was used to partially replace FA at levels of 5%, 10%, 15% and 20%. Six specimens of 50mm x 50mm x 50 mm cube for each selected HMNS content were cast.

Hence, a total of 4x3x2=24 cubic specimens were cast. The compressive strength tests were carried out on these specimens at 7 and 14 days, respectively. The purpose of the tests was to find out which FA-to-HMNS ratio produces the greatest compressive strength. From this, the mix design proportions of the binders are determined at 70 %, 20 % and 10 % of FA, GGBS and HMNS respectively. The mix proportion of geopolymer paste is presented in
Table 3.6, while Figure 3.6 shows specimens of fresh and hardened geopolymer paste.

Table 3.6. Geopolymer paste mixture proportion

Materials	The proportion by mass % of FA	
Fly ash (low-calcium ASTM Class F)	70	Main material
Ground Granulated Blast Furnace Slag (GGBS)	20	Optimum
High Magnesium Nickel Slag (HMNS)	10	Optimum
Activator Solutions	Ratios	
Sodium silicate solution	-	
Sodium hydroxide solution	12 M	
(Na_2SiO_3/NaOH) (SS/SH)	2.5	
Solid / alkaline activator	2.0	

3.3.1. Mixing Procedure and Curing Condition

To prepare geopolymer concrete or paste, two chemical solutions (sodium hydroxide and sodium silicate) are required as alkaline solutions. Sodium hydroxide is classified as a corrosive solution with serious harmful potential, so for this reason, extreme precautions were considered during the preparations.

An auto mixer was used to prepare all the samples, and the following steps summarize the mixing procedure.

1. Manual mixing of the binder (FA, GGBS and HMNS) until the mixture becomes homogenous.
2. AAS was gradually added to the binder at a slow mixing speed (~150±10 r/min) for about 5 minutes.
3. The mixer speed was slowly increased to (400±10 r/min) for 1 minute.
4. The mixing was paused for 30 seconds, then run again for another 1 minute to ensure the homogeneity of the mix.

The final mixtures were poured into cubic moulds measuring 50mm x 50mm x 50mm as shown in Figure 3.6. These specimens were then compacted using a vibration table for around 30 seconds before being left at ambient temperature. According to the curing regime standard, the specimens were kept for 24 hours at a room temperature of 25±2ºC and relative humidity of 85-90% before being demoulded.

Figure 3.6. GP Paste specimens a); Fresh b); Hardened

3.4. Geopolymer Concrete (GPC)

The contents determined from the GP pastes in Section 3.3 for GGBS and HMNS were used to cast the FA-GGBS-HMNS based GP concrete. Three types of GP concrete specimens were cast: the first type was the cubic specimens of 100mm x 100mm x 100mm, used for conducting compressive strength tests at 7, 14, 28 and 90 days (3x4=12 specimens); the second type was the cylindrical specimens of 75mm diameter and 150mm in length, used for conducting splitting tensile strength tests, also at 7, 14, 28, and 90 days (3x4=12 specimens).

Cylindrical samples of 100mm diameter and 200mm in length were used for Rapid Chloride Permeability Test (RCPT) and more details will be given on durability in

Chapter 6. All of the FA-GGBS-HMNS based GP concrete specimens have the same mix proportion where the binder-to-liquid ratio is 2:1 and the binder-to-aggregate ratio is 3:7. Table 3.7 shows the details of the mix design proportions for both GP paste and GP concrete.

Table 3.7. Mixture proportions of GP paste and GP concrete (kg/m^3)

Materials	GP Paste	GP concrete	
	Cubic specimens	Cubic specimen	Cylindrical specimen
Coarse aggregates	-	1176	779
Fine aggregates	-	504	333.7
Class F FA	420	336	222.6
GGBS	120	96	63.6
HMNS	60	48	31.8
Na$_2$SiO$_3$ solution	214.28	171.43	113.6
NaOH solution (12M)	85.71	68.6	45.5
Na$_2$SiO$_3$/NaOH	2.5		
Solid/alkaline activator	2.0		

Figure 3.9 displays the preparation procedures for GPC. Various GPC mix design procedures have been proposed by many researchers (Anuradha *et al.*, 2012; Ferdous, Kayali and Khennane, 2013; Pavithra *et al.*, 2016), but it is noted that few studies report mainly on these. The current investigations are similar in terms of the general procedure, with slight changes regarding the researchers' techniques. In this study, the coarse aggregate (gravel) is firstly saturated in water for 2 hours, before being used in the mix to ensure the aggregate does not absorb the activator solution. Then the binder materials, aggregate and sand are mixed by a mechanical mixer for approximately 3 minutes. This is to confirm that the cementitious materials, especially FA, are consistently distributed onto the aggregate's surfaces. After that, the alkaline activator solution is gradually added to the dry mix (binder-aggregates) and mixed until uniform fresh GPC is achieved (see Figure 3.7b).

Figure 3.7. (a) Dry mix, (b) Fresh GPC mix

Figure 3.8. Fresh cylinders and cubes GPC
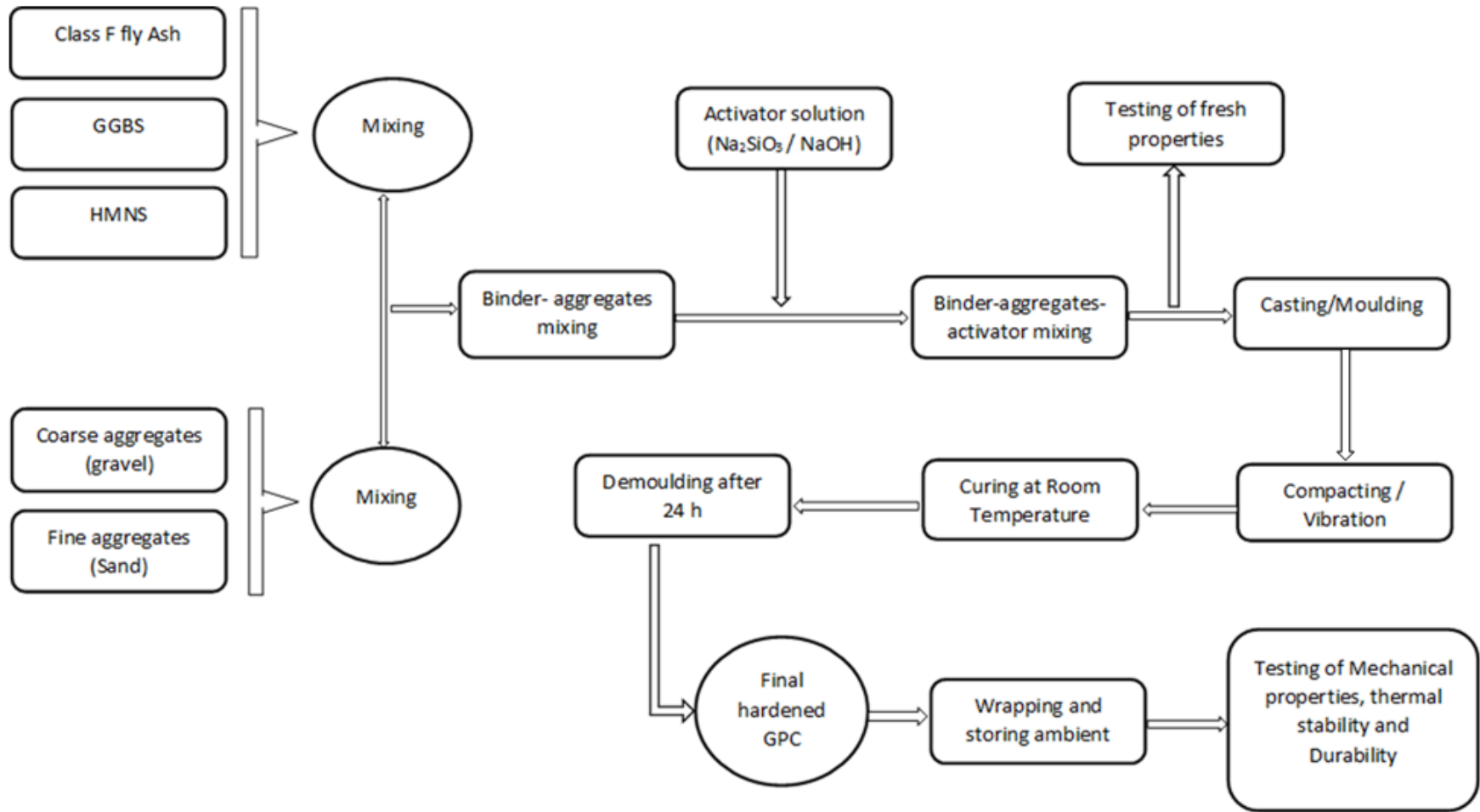
Figure 3.9. Flowchart of manufactured FA-GGBS-HMNS based GPC

It has been suggested that, to ensure the FA is well dispersed onto the aggregate's surface for GPC mixture, the sodium silicate (Na_2SiO_3) could be separately added to the dry mix (binder-aggregates), before the addition of sodium hydroxide solution (NaOH) (Palacios and Puertas, 2005). However, in this experimental research, the Na_2SiO_3 and NaOH are mixed together before being added to the mixture. The wet aggregates help the binders to stick and bind on their surface, which also ensures that the binders are well distributed onto their surface and start to create initial bonding between the binders and aggregates.

After preparing the mix of fresh GPC, a portion is used to test its properties (slump and setting time), while the left-over part is used for casting into cubic and cylindrical moulds (Figure 3.8) as has been discussed in section 3.4. Then the cast moulds are manually compacted using a steel bar rod and also vibrated on a vibrating table for no longer than 30 seconds to avoid any stiffness. Hence, the GPC samples are cured at a room temperature of 25±2ºC and a relative humidity of 85-90%. After 24 hours the samples are demoulded and wrapped in plastic film to avoid any evaporation of volatile substances and water, and then kept for further testing.

3.5. Results and Discussions

3.5.1. Setting Time

The slump and setting time tests are used to evaluate the workability of geopolymer paste and concrete. It is reported that the only procedure currently available to quantify and measure the setting time of geopolymer material is by using the Vicat needle apparatus shown in Figure 3.10a (Cheng and Chiu, 2003).

Figure 3.10. (a)Vicat apparatus, (b) Slump test

The setting time was obtained directly by using the Vicat apparatus ASTM C191. The initial setting time started when an activator solution was added to the dry mixture and lasted until the paste began to lose its elasticity, corresponding to 310 minutes, as shown in Figure 3.11. However, the final setting time elapsed at the moment the paste completely lost its elasticity, corresponding to 1490 minutes, as also shown in Figure 3.11. Both the initial setting time and final setting time seem reasonable for concrete, although the final setting time is slightly longer than the normal final setting time for traditional concrete. This could be due to the continuity of geopolymerization reactions taking place in the concrete because of the high amorphous phase of HMNS, which needs more time to react and to formulate (M-S-H or C-M-S-H) gels (Shinde and Kadam, 2016).
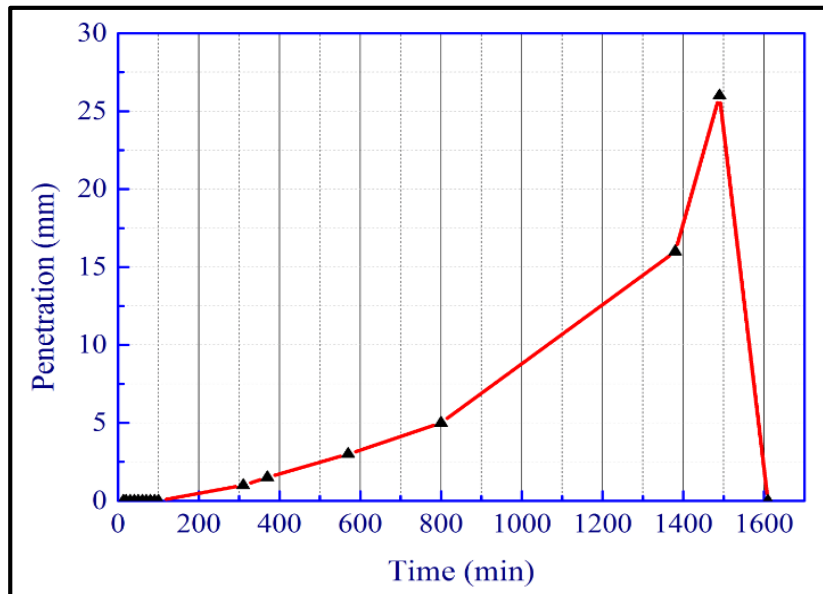
Figure 3.11. Setting time of GP Paste

3.5.2. Workability

A slump test was carried out to measure the workability of the fresh geopolymer concrete (see Figure 3.10b). The test was repeated several times, and demonstrated the good workability of the GP concrete designed. The manufactured GPC was manually tamped, due to the high viscosity of the geopolymer product (Ahmari *et al.*, 2012). It was noted that the workability of concrete was controlled not only by the binders but also by the aggregate and the alkaline activators.

Figure 3.12 presents the slump test result for the designed GPC, which corresponds to 220 mm, due to the high sodium silicate level which made the mixture stickier and more adhesive. It is believed that the mixed sizes and proportions of FA, GGBS, HMNS and aggregate played a significant role in the improvement of workability, which leads to creating what is called inter-particles dynamism of the system, which makes the released molecules of water easily penetrate between particles during

geopolymerization. It can be seen from Figure 3.12 that, after 40 minutes only some, the GPC slump falls to around 50 % of its initial level, and after 120 minutes only some 28% of the original slump remains. Therefore, the 28% of slump was kept until 160 minutes. It has previously been reported (Collins and Sanjayan, 1999) that GPC has better workability than OPC, and this is confirmed by this study.
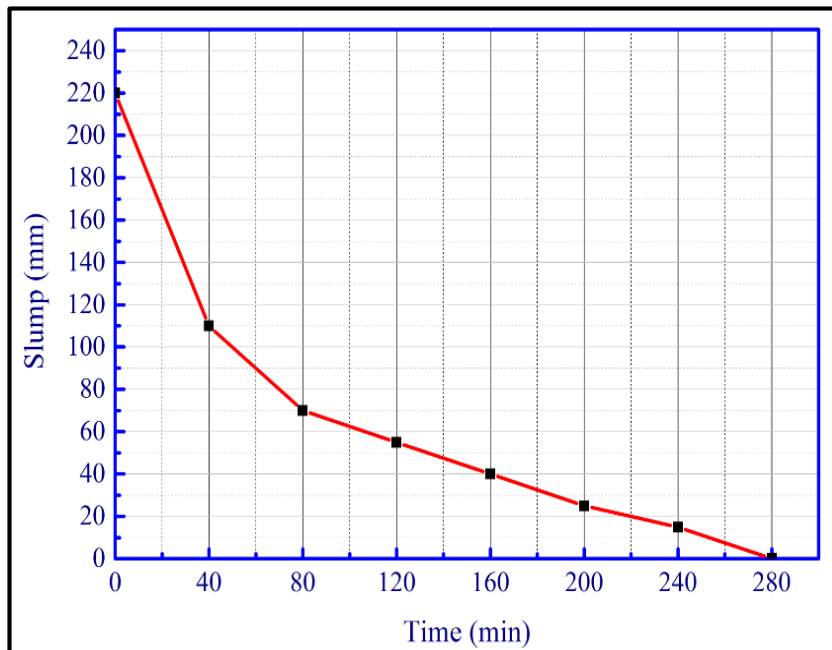
Figure 3.12. Slump test of GP concrete

The GPC produced would appear to offer many advantages in real applications, as was observed during its mixing and preparation process. Therefore, the main focus of this study is to design a suitable GPC in terms of high mechanical properties and the required workability.

3.5.3. Uniaxial Compressive Strength

3.5.3.1. Geopolymer Paste

In this experimental study, the GP paste produced was cast in 50mm x 50mm x 50mm steel moulds, as described earlier in this chapter. The specimens were prepared and tested for compressive strength at 7, 14 and 28 days. In line with the protocol adopted for the other tests undertaken, the results of the compressive strength tests were determined by the average of three specimens, and these figures are presented in Table 3.8. Figure 3.13 shows the compressive strength of the FA-based GP paste specimens with different GGBS replacements, tested at the ages of 7, 14 and 28 days. It can be seen from the figures that, for the GGBS replacement of less than 30%, the compressive strength increases with time. However, when the GGBS replacement reaches 30%, the compressive strength increases between 7 and to 14 days, but after 14 days it decreases with time. When the GGBS replacement reaches 40%, the compressive strength is found to decrease with time, the opposite of the increase in strength found in the specimens with a GGBS replacement of under 30%. This indicates that GGBS has a negative effect on strength development. Also, it can be observed from the figures that the compressive strength of the FA-based GP paste increases initially but then reduces with the increase of GGBS replacement. The maximum compressive strengths at 7, 14 and 28 days were found to be 38.5, 45.6 and 76.6 MPa respectively, which occurred for the 20% GGBS replacement. Comparing the compressive strength of FA-based GP paste without GGBS (73.86 MPa), the use of the 20% GGBS replacement can increase compressive strength by about 3.7%. A similar result was also found by Nath and Sarker (2014), who reported that the FA-based paste increased in strength when FA was partially replaced with GGBS. However, they found the maximum compressive strength was 30% for the GGBS replacement, slightly different from what was found here, possibly attributed to the different sources used for taking the FA and GGBS (Nath and Sarker, 2014).

Table 3.8. Mean compressive strength of geopolymer pastes

% By weight mass of FA	Compressive Strength (MPa)		
	GGBS		
	7 days	14 days	28 days
5	23.23	33.11	43.58
10	33.81	37.27	48.01
20	39.1	47.2	76.57
30	33.82	45.16	41.73
40	32.73	28.7	23.23
	HMNS		
5	35.69	47.54	-
10	39.95	60.82	-
15	32.79	38.56	-
20	33.15	47.78	-
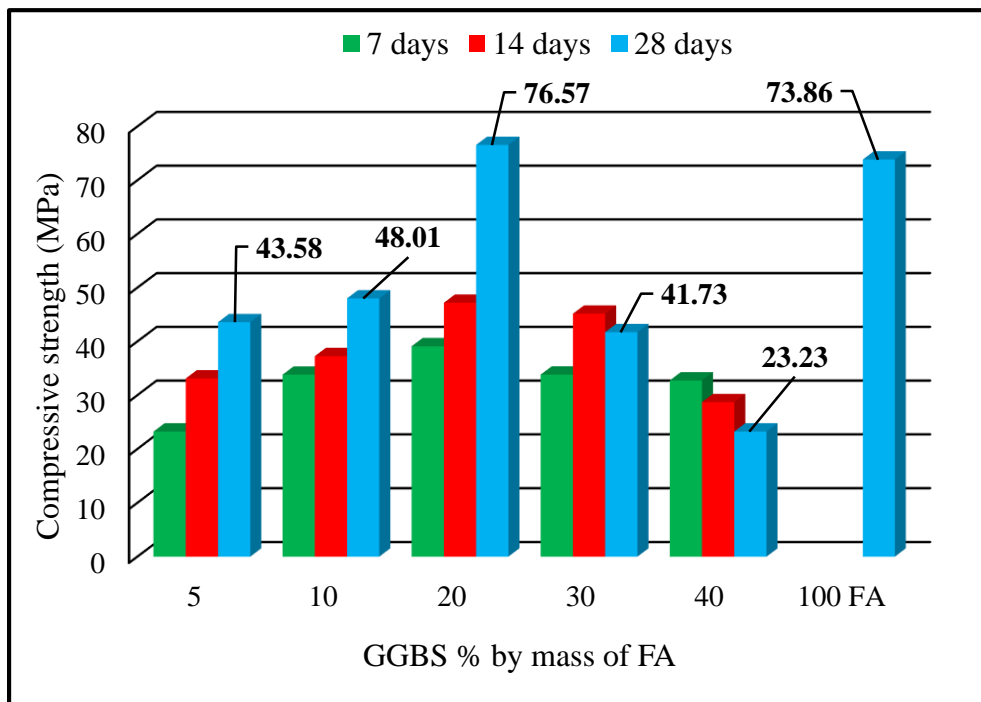
Figure 3.13.The compressive strength of FA-based paste with different GGBS replacement.

Figure 3.14 shows the compressive strengths of the FA-GGBS (20%)-based GP paste specimens with different HMNS replacements to FA, tested at 7 and 14 days, respectively (In this stage curing time was chosen at14 days, due to the short duration of laboratory testing. Also, after 14 days high strength was achieved, which led to an earlier selection of the optimum percentage of HMNS). It can be seen from the figures that, for all specimens tested, the compressive strength at 14 days was higher than that at 7 days, indicating that the HMNS has no negative effect on strength development. Also, it can be observed from the figures that the highest compressive strength was when 10% HMNS replacement to FA was used, giving a 14-day compressive strength of 60.8 MPa. Comparing the compressive strength of the FA (80%)-GGBS (20%) based GP paste without HMNS (47.2 MPa), the use of 10% HMNS replacement to FA can increase the compressive strength by about 29%, which is highly significant. This improvement in strength is mainly due to the high magnesium content in the mixture, which plays a similar role to the calcium and produces a new hydrate gel called hydrotalcite-like phase or magnesium-bearing silicate hydrates (M-S-H or C-M-S-H) (Yang, Yao and Zhang, 2014; Zhang *et al.*, 2017). Zhang et al. (2017) showed that the use of HMNS in FA-based GP concrete has a positive effect on compressive strength of the mixture when its replacement is not over 60% but otherwise, it will have a negative effect on compressive strength.

It is believed that the combined use of class F FA, GGBS and HMNS mitigates the porosity of the matrix, by reducing its dehydration which leads to mass loss of the produced geopolymer material. The use of 100 % of class F FA in the production of geopolymers mainly produces a major A-S-H gel phase, which is generally high porous as indicated in many previous research (Ismail *et al.*, 2013; Yang, Yao and Zhang, 2014). The combined use of FA and GGBS in GPC has been reported in literature and it has been demonstrated that the blending of these two materials in geopolymers can result in the formation of binary A-S-H and C-A-S-H gel phases, which improve the mechanical properties of the GP, and also control its fresh properties due to the influence of GGBS content. A previous study by Yang et al. (2014) showed that the C-A-S-H gel formed due to the incorporation of GGBS was vulnerable when exposed to a high temperature and showed a considerable

degradation. They also found that when HMNS was blended with GGBS it produces a high N-A(M)-S-H gel in the system.
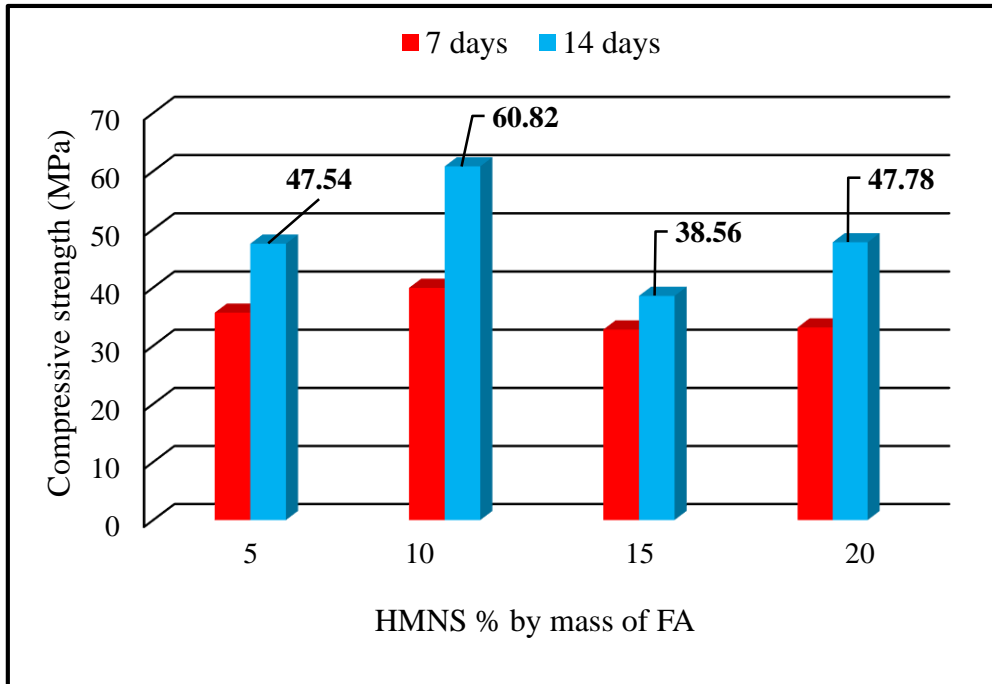
Figure 3.14. The compressive strength of FA-GGBS based paste with different HMNS replacements

3.5.3.2. Geopolymer Concrete

The cubic and cylindrical specimens of GP concrete were mixed using the proportions shown in Table 3.7. The compressive strength of the designed GP concrete cured under the same conditions at 7, 14, 28 and 90 days is shown in Figure 3.15. It can be seen from the figures that the compressive strength increases from 27.17 MPa at 7 days to 55.60 MPa at 28 days, and then reduces from 55.60 MPa at 28 days to 48.14 MPa at 90 days, indicating that the strength was fully developed during the first 28 days curing, with a subsequent strength reduction of about 14%. For the purpose of comparison, the compressive strengths reported by other researchers (Sofi *et al.*, 2007; Nath and Sarker, 2016; Pavithra *et al.*, 2016) for the FA-based GP concrete with

similar mixes and curing conditions are also superimposed in Figure 3.15, indicated as B, C and D respectively. Overall, the figures show that the designed GP concrete based on the test results of GP pastes has a compressive strength about 10% higher than of others. This improvement in strength of is partly because of the rapid formation of C-S-H and A-S-H gels during geopolymerization, as is confirmed by SEM/EDX analysis in Chapter 4, and partly because of the different particle size distributions of FA, GGBS and HMNS, which makes the mixed concrete less porous.

The development of C-M-S-H gel which is provided by the partial replacement of FA by HMNS also has a significant effect on the improvement in strength, because it causes a denser and more compact geopolymeric system. The decline in compressive strength after 90 days might be due to the decomposition of ettringite gel or possibly the evaporation of water from the geopolymeric system, which in turn leads to the formation of micro-cracks, then decreases the strength. It has been shown that the curing of GPC at ambient conditions give sufficient time to the hydration products to diffuse and precipitate homogeneously throughout the matrix (Bakharev, Sanjayan and Cheng, 1999).
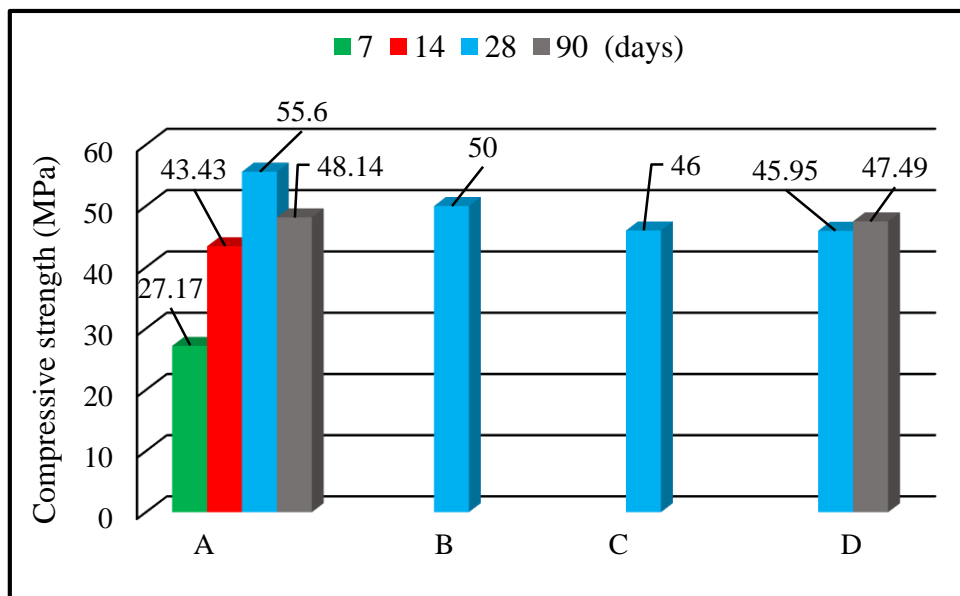
Figure 3.15. The compressive strength of GPC

3.5.4. Mean Density and Compressive Strength

After preparation of GPC at the laboratory, the specimen cubes measuring 100mm x100mm x 100mm, as used to measure the compressive strength, are used at the same time to determine the GPC's density.
Table 3.9 presents the average values for both density and compressive strength of the GPC produced.

The change in density of GPC specimens cured at ambient conditions is shown in Figure 3.16. After 7 days, the density of the manufactured GPC slightly decreased to about 0.17 %, which is relatively low. However, after 90 days, the maximum density loss of the concrete is around 2.4 %, which is reasonably good when compared to the long-term curing period. The loss in density was generally related to the evaporation of the quantity of watery phase in the mixture. Several authors have reported that the main cause of the decrease in the density of geopolymer concrete is the evaporation of water from the geopolymeric system (Yunsheng *et al.*, 2007; Sathia, Babu Ganesh and Santhanam, 2008).

Table 3.9. Average density and compressive strength

Mixture	Curing regime		Density (kg/m³)			Compressive strength (MPa)	
	Temperature (ºC)	Humidity (%)	1day density	Average	Standard of deviation	Average	Standard of deviation
7 days	25±2	85-90	2400	2396	25.65	27.17	0.49
14 days			2385	2368	20.20	43.43	2.12
28 days			2406	2375	30.41	55.6	1.03
90 days			2423	2365	47.69	48.14	6.58
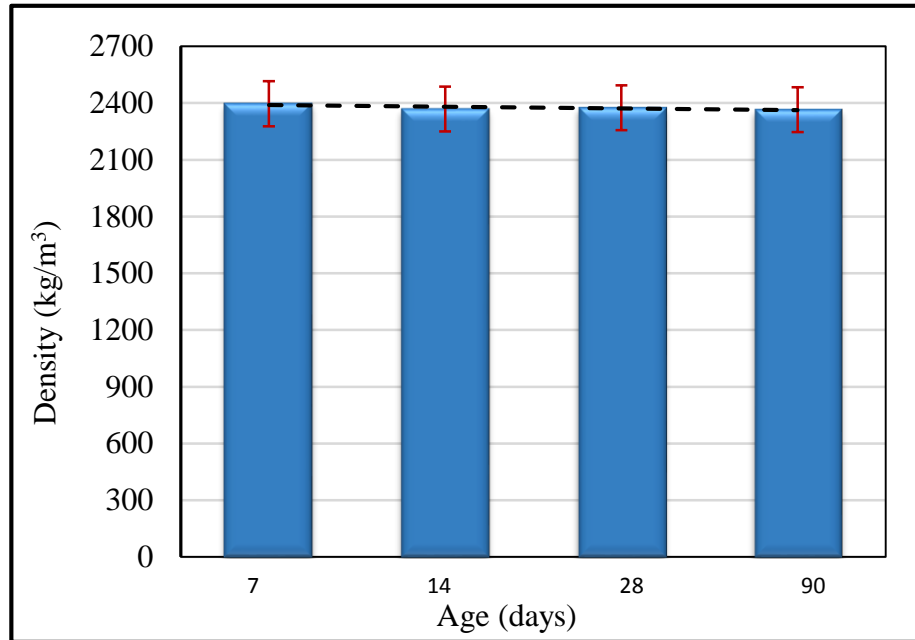
Figure 3.16. Change of density of GPC

3.5.5. Splitting Tensile Strength

The splitting tensile strengths of the designed GP concrete at 7, 14, 28 and 90 days are shown in Figure 3.17, these values being obtained experimentally by following ASTM C496 standard. It can be seen from the figure that the splitting tensile strength increases from 2.89 MPa at 7 days to 4.57 MPa at 28 days, then reduces from 4.57 MPa at 28 days to 4.12 MPa at 90 days. The variation of the splitting tensile strength with age is very similar to that of the compressive strength with age, indicating there is a good correlation between the compressive strength and splitting tensile strength. As with the compressive strength mentioned in 3.5.3.2. above, the splitting tensile strength of the designed GP concrete is also 10% higher than that of the similar GP concrete reported in the literature, as shown in Figure 3.17-A, where the GP concrete was made at room temperature and relative humidity >80% (Sofi *et al.*, 2007).

The increase in splitting strength might be attributed to many factors. First is the rapid geopolymerization process occurring between the binders and activator solution (Puertas *et al.*, 2000). The second factor is the strong bonding between the geopolymer matrix and the aggregates which are in agreement with the compressive strength results. The third factor is the denser and compacted GP concrete matrix obtained, due to the replacement of 30 % in a total mass of FA by GGBS and HMNS (Rashad, 2013). The fourth factor is the pH value of the activator solution which plays a significant role in the geopolymerization process and in determining the nature of C-S-H gel of the hydration products (Song and Jennings, 1999). It has been stated that to achieve an effective activation of hydration, the pH value should be higher or in the range of 11.5 (Fernández-Jiménez and Puertas, 2003; Rashad, 2013).

This decrease in splitting strength might be due to the formation of new pores, which are associated with the evaporation of water from the system during the geopolymerization reaction (Liu, Michael, Yong *et al.*, 2014). It has been reported that the splitting tensile strength of GPC is generally affected by the concrete's mix proportions, and increases with an increase in the compressive strength of the concrete (Topark-ngarm, Chindaprasirt and Sata, 2014). The relationship between the compressive strength and the splitting tensile strength of concrete has been explored by numerous researchers, with Eq (3.4) describing this relationship as follows.

$$f_{ct} = k\left(f'c\right)^{n} \qquad\qquad \text{Eq (3. 4)}$$

$$f_{ct} = 0.56\sqrt{f'c} \qquad\qquad \text{Eq (3. 5)}$$

$$f_{ct} = 0.59\sqrt{f'c} \qquad\qquad \text{Eq (3. 6)}$$

$$f_{ct} = 0.17\left(f'c\right)^{0.75} \qquad\qquad \text{Eq (3. 7)}$$

where f_{ct} is the splitting tensile strength in MPa, f_c' is the compressive strength in MPa, and k and n are constants obtained from the regression analysis of the experimental data.

According to ACI 318-08 (ACI 2008) and ACI 363R-92 (ACI 1997), the splitting tensile strength of normal and high strength concretes, could be calculated using Eqs (3.5) and (3.6) respectively. However, to estimate the splitting tensile strength of low-calcium fly ash-based geopolymer concrete, other authors have suggested Eq (3.7) (Ryu *et al.*, 2013). In this study, the splitting strength is measured based on the experimental data in accordance with (ASTM C 496/C 496M – 04, 2011) as has been indicated earlier. Table 3.10 presents a comparison between the splitting strengths as calculated by various methods reported in the literature. It can be seen that the results are comparatively close to each other with only minor differences.
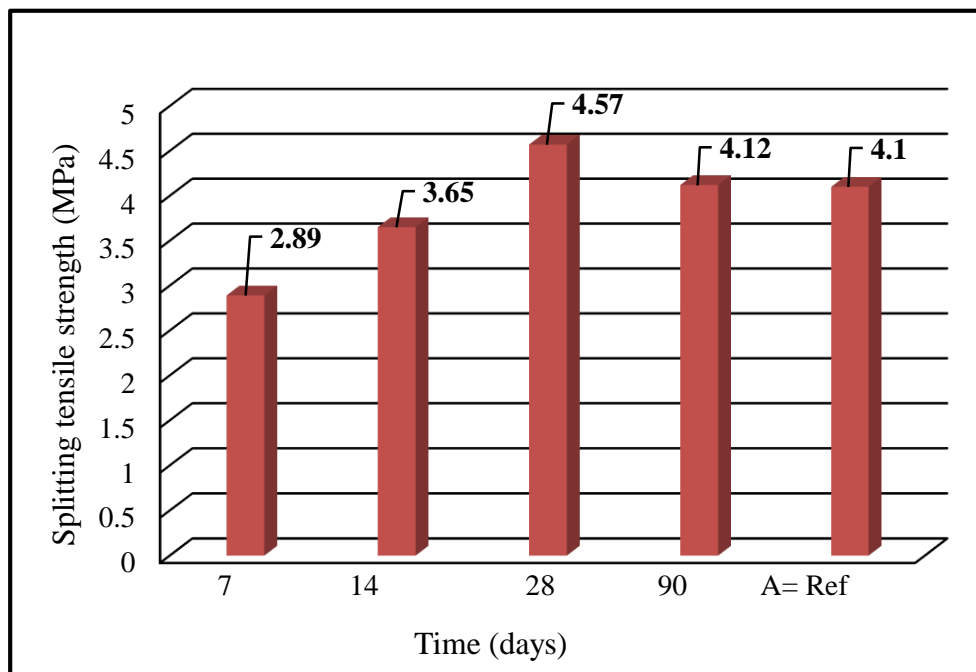
Figure 3.17. Splitting Tensile Strength of GPC

Table 3.10. Splitting tensile strength as calculated by different methods

Method	Splitting strength f_{ct} (MPa)			
	7 d	14 d	28 d	90 d
ASTM C 496/C 496M*	2.89	3.65	4.57	4.12
ACI 318-08	2.91	3.69	4.17	3.88
ACI 363R-92	3.075	3.88	4.4	4.09
Ryu et al. (2013)	2.02	2.87	3.46	3.10

*the standard which is followed in this research study.

Figure 3.18 displays the linear correlations between the splitting tensile strength and the compressive strength of the manufactured FA-GGBS-HMNS based GPC. Based on analysis of the various methods shown in Table 3.10, the correlation coefficient R^2 was obtained. It is obvious from Figure 3.18 that there are positive correlations between all methods with close values of R^2. In addition, the splitting tensile strength developed by FA-GGBS-HMNS based GPC with respect to the compressive strength obtained is greater than that calculated from the formulae proposed by Ryu et al., ACI 318-08 and is similar to that calculated by the formulae of ACI 363R-92. The high degree of similarity between the latter results could be due to the origin calculations from the formulas were used. It can be observed from Eqs (3.5), (3.6), (3.7) that for each single method the splitting tensile strength is calculated by multiplying the original compressive strength with a constant number obtained experimentally to correct the error in the experimental results.
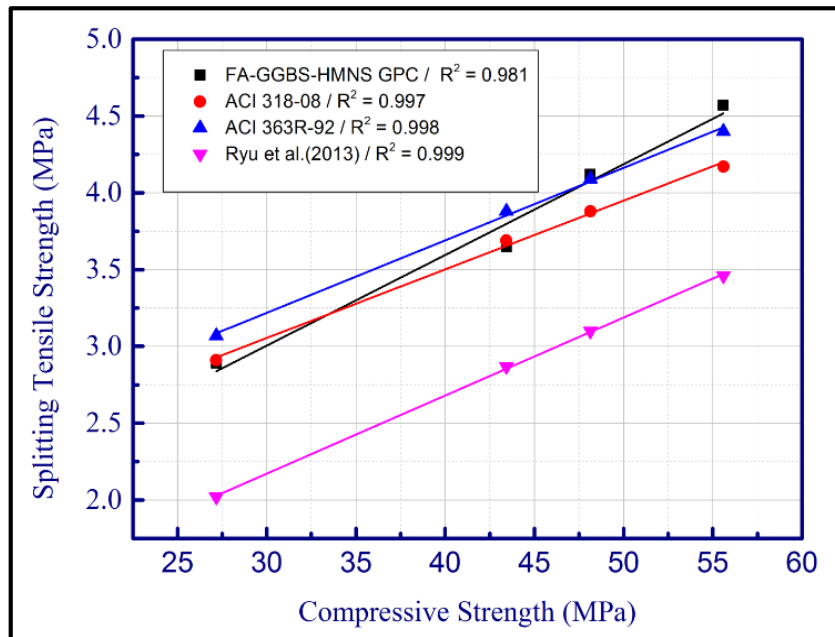
Figure 3.18. Correlation of splitting tensile strengths versus compressive strengths.

3.5.6. Theoretical Modulus of Elasticity E_c

In order to calculate the modulus of elasticity E_c of the designed GPC, Eq (3.8) is used, where f' is in MPa (Mamlouk and Zaniewski, 2011).

$$Ec = 4731 * \sqrt{f_c'}$$ Eq (3. 8)

where E_C in GPa is the modulus of elasticity, and f_c' in MPa is the compressive strength.

$E_c = 4.731*(55.6)^{1/2} = 35.27$ GPa

The modulus of elasticity (E_c) increases with an increase in the concrete's compressive strength. E_c could be determined through the empirical relationship shown in Eq (3.8).

It has been reported that the modulus of elasticity of fly ash-based geopolymer concrete varies between 23.0 and 30.8 GPa (Nath and Sarker, 2016; Noushini and Castel, 2016). However, this study shows that the manufactured GPC has a high modulus of elasticity of around 35.27 GPa after 28 days. Figure 3.19 shows the linear relationship between the compressive strength and the modulus of elasticity of the GPC produced. It has been found that the modulus of elasticity of the FA-GGBS-HMNS based GPC is correlated very well with its compressive strength with a correlation coefficient of $R^2 = 0.997$.
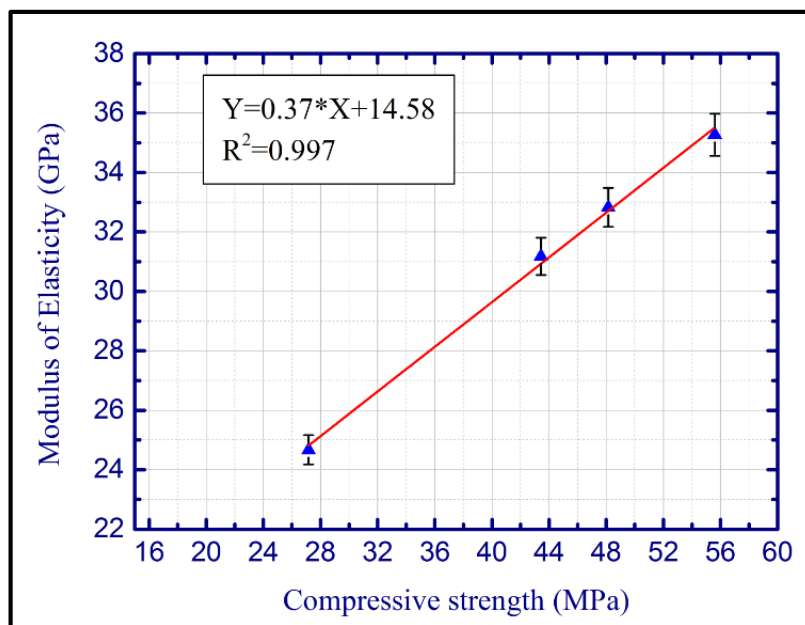
Figure 3.19. Modulus of elasticity vs Compressive strength

Based on the source of prime materials, activator solutions and curing regime, the compressive strengths of various mixes design as reported recently by other authors in geopolymer field, which also known as alkaline activated materials, is displayed in Table 3.11.

Table 3.11. Compressive strength of geopolymer as given by other research

NO	Materials mass %	Additional material	Nature of mix	Si-to-Al Ratio From precursors	Alkaline Solutions	Alkaline liquid-to-solid Ratio	Curing regime			Compressive strength (MPa)	References
							T (ºC)	Hours	Days		
1	Class F FA	CFRP and GFRP [a]	Concrete	2.12	Na$_2$SiO$_3$+NaOH	0.45	80	2-6h	28	23.2-33.8	(Lembo, Lokuge and Karunasena, 2014)
2	Class F FA	-	Concrete	1.58	Na$_2$SiO$_3$+NaOH +KOH	0.5	60	24	28	25.6-64.3	(Feng et al., 2015)
3	Slag	-	Concrete	-	Na$_2$SiO$_3$+NaOH	-	30	3 in water	-	39.3	(Gao et al., 2015)
4	Class F FA+GGBFS	MPCM [b] + OPC	Concrete	2.09-3.22	Na$_2$SiO$_3$+NaOH	-	20-40	in water	28	25-40	(Pilehvar et al., 2017)
5	Class F FA	-	Mortar	2.14	Na$_2$SiO$_3$+NaOH	-	60	24	91	47	(Ryu et al., 2013)
6	Class F FA	HMNS [c]	Paste	1.73-8.44	Na$_2$SiO$_3$+NaOH	0.42	20	-	28	60	(Yang, Yao and Zhang, 2014)
7	Class F FA	-	Mortar	5.24	Na$_2$SiO$_3$+NaOH	0.97-1.00-1.04	65-85	2-24	7	31.3-22	(Görhan and Kürklü, 2014)
8	High calcium FA	-	Mortar	3.76	Na$_2$SiO$_3$+NaOH	-	30-45-60-75	48	28	86	(Chindaprasirt et al., 2011)

9	Class F FA	OPC + Lime	Mortar	2.26	Na$_2$SiO$_3$+NaOH	0.5	80	24	7	29.94	(Shinde and Kadam, 2016)
10	BFS	-	Mortar/ Paste	3.21	Hydrated lime-Hydrate gypsum	0.48	24	24	28	35	(Neto, Cincotto and Repette, 2010)
11	Class F FA+GGBFS	-	Concrete/ Mortar	1.76-2.26	Na$_2$SiO$_3$+NaOH	0.2	20-23	24	28	55	(Nath and Sarker, 2014)
12	Class F FA	GGBFS [d]	Paste	2.04	NaOH + KOH	0.25-0.3	65-85	2-5-24	-	35	(Palomo, Grutzeck and Blanco, 1999)
13	Class F FA+GGBS+ HMNS	-	Paste	2.0	Na$_2$SiO$_3$+NaOH	0.5	25-27	-	28	76.57	(Bouaissi et al., 2019)
14	Class F FA+GGBS+ HMNS	-	Concrete	2.0	Na$_2$SiO$_3$+NaOH	0.5	25-27	-	90	55.6	(Bouaissi et al., 2019)
Control	Conventional OPC	-	Concrete	-	-	-	-	-	28	31.8	(Türkmen et al., 2016)
Control	Cement Repair (CR)	-	Mortar	-	-	-	-	-	28	46.1	(Hu et al., 2008)

[a] Carbon Fibre Reinforced Polymer (CFRP) and Glass Fibre reinforced Polymer (GFRP)

[b] Micro-encapsulated Phase Change Materials

[c] High-magnesium Nickel Slag

[d] The Granulated Blast Furnace Slag

3.6. Summary

In this chapter, the properties of both hardened and fresh FA-GGBS-HMNS based geopolymer concrete are discussed and evaluated. Discussion and analysis of the results from the main part of the chapter and focus mostly on the different mechanical properties such as uniaxial compressive strengths, splitting tensile strength and the modulus of elasticity. Further, the fresh properties including workability and setting time are also reported in this chapter.

In this section, a workable GPC has been designed, by following two procedures. The first is by formulating geopolymer paste with high strength characteristics. The second is by the preparing of GPC and investigating its mechanical properties by performing different fundamental tests. The GPC is found to have good fresh and hardened mechanical properties of 55.6 MPa and 4.57 MPa of compressive strength and splitting strength respectively, with an average density of 2340 kg/m^3. This manufactured GPC can be used in various structural applications, due to its high workability and significant strengths.

This chapter establishes a new mix design of GPC prepared from a binder of class F FA, GGBS and HMNS. This geopolymer material has adequate mechanical properties which are suitable for structural constructions. The manufacturing process of this GPC mixture follows a new design which can be practically considered as a low cost and eco-friendly product.

Chapter 4

Microstructural and Morphological Studies of FA-GGBS-HMNS based Geopolymer Concrete/Paste

4.1. Introduction

This chapter focuses on the microstructural and morphological studies of the produced geopolymer paste and concrete cured at ambient conditions.

As mentioned in the previous chapters, this research aims to produce a new mix design for a geopolymer technology product which will be both less costly and more eco-friendly. The selection of the precursor materials has significant advantages by expanding the sources of material which possesses cementitious or pozzolanic behaviours. A new mix design of GPC is successfully made by combining FA, GGBS and HMNS with alkali activator solutions. The main chemical and physical characteristics of the initial materials and the activator solution are detailed in Chapter 3, section 3.2.2. Regarding the chemical composition of the raw materials, as given by the XRF analysis shown in Table 3.2 Chapter 3, the CaO amount is less than 5% in

both FA and HMNS, but as high as 50 % in GGBS. However, all the binders have sufficient silicate (SiO_2) with a high magnesium oxide (MgO) content in HMNS. The microstructures analysis have been carried out in ''Center of Excellence Geopolymer and Green Technology (CEGeoGTech), Universiti Malaysia Perlis, Malaysia.

The Microstructure analysis of these materials and of FA-GGBS-HMNS geopolymer paste and concrete was carried out to characterize the structural changes in the geopolymer products occurring in the geopolymeric matrix, in terms of the degree of reactivity between the binders and the activator solution, the development of geopolymer gels, and the presence of micro-cracks and pores. SEM (Scanning Electron Microscopy) analysis was used to study the micrograph of geopolymer specimens aged 28 days. Energy dispersive X-ray spectroscopy (EDX) as an associate analysis technique was used to quantify the elementary atomic percentage in the geopolymer system.

X-Ray Diffraction (XRD) analysis was conducted to characterize and identify the crystalline and amorphous phases of the selected materials, as well as the transformed material to geopolymer product. An XRD-6000 Shimadzu X-Ray Diffractometer with Cu-Kα radiation machine was used to analyse specimens in powder form, while the results were analysed using ''X'Pert High Score Plus'' software specialising in automated search and matching peaks.

Fourier infrared spectroscopy analysis (FTIR) was performed to investigate various functional groups of the geopolymer product in comparison with the source material. Based on FTIR spectroscopy, it has been observed that the essential transformed phases from the raw material within a geopolymeric system have a significant effect on the mechanical properties of the final product. In addition, the FTIR spectra of the final product showed a vibration of various bands at different wave numbers, the details of these function groups are discussed later in this chapter.

4.2. Materials, Preparation and Testing Method

4.2.1. Chemical Group and Microstructure Characterization

The main chemical and morphological characteristics of the precursor materials and the GP paste and concrete are examined and analysed based on the following tests.

4.2.1.1. Morphology Characterization (SEM / EDX)

Scanning Electron Microscope (SEM), is an essential non-destructive analysis technique test, which can be used to analyse the morphological structure of geopolymer paste. By using this technique the specimens could be scanned under high magnifications (from 1000x to 10000x) with a scanning energy of 10 kV. An Energy Dispersive X-ray Analysis (EDX) is an associated test to the SEM analysis. EDX is used to determine the main elements and compositions by the percentage of weight found in the final product. In this study, a JEOL JSM-6460LA Scanning Electron Microscope machine as shown in Figure 4.1, was used to examine the morphological structures of both raw materials and final GP paste. All samples were embedded and polished in an epoxy resin. The resulting surface was metallised with gold before the analysis in back-scattering mode.

Figure 4.1. SEM and EDX machine

4.2.1.2. X-Ray Fluorescence Analysis (XRF)

The chemical composition of the initial material was determined using an X-ray fluorescence spectrometer (XRF), which is known as PANanalytic PW4030, model type MiniPAL. The specimens were loaded in an X-ray fluorescence spectrometer room. Then, they were exposed to a maximum voltage of 30kV and current of 1 mA. The main purpose of this procedure is to produce an X-ray radiation that is needed to stimulate and incite the atoms from the samples. The test was run for about 10 minutes with a precision of 1%.

4.2.1.3. X-Ray Diffraction Analysis (XRD)

X-Ray Diffraction (XRD) was used to characterize and identify diverse crystalline and amorphous phases of the designed GP materials. XRD-6000 Shimadzu X-Ray Diffractometer with Cu-Kα radiation generated under 40 mA and 44kv at room

temperature, was used to examine four selected specimens. The XRD analysis was performed at a scanning angle 2θ ranged between 10 and 70°. The analysis was run for 44 seconds per 2θ step. Then, the diffraction patterns were analysed using a software called ''X'Pert HighScore Plus'' to identify and auto-match the peaks.

4.2.1.4. Fourier Transform Infrared Analysis (FTIR)

Fourier Transform Infrared spectroscopy analysis (FTIR) was used to characterize the different functional groups which could be present in the GP paste produced. Basically, the vibration of molecules (based in turn on the vibrations of their functional groups) is key to identifying the nature of bands. The use of the FTIR analysis technique was mainly to demonstrate how the used FA reacts with the addition of GGBS and HMNS. The XRD results showed that, compared to FA and GGBS, HMNS contained a highly amorphous phase, which could possibly be involved in a series of chemical reactions leading to the formulation of new functional groups.

4.2.1.5. Optical Microscope Magnification (OM)

To investigate the micro-interface interaction between aggregates and the geopolymer matrix, an Optical Microscopy Motic MRL100, as shown in Figure 4.2, was used. It is evident that there were difficulties in obtaining sufficiently clear images of the GP concrete specimens, due to their gravelly nature and the non-uniformity of their shape. However, it is important to have specimens with a uniform shape and a horizontal plate surface to achieve high-resolution images. To examine further the bonding between aggregates and the geopolymer matrix, the specimens were subjected to visible light and observed under a magnification of 10, 20, and 50 Mpixel.

Figure 4.2. Optical Microscope apparatus (OM)

4.2.2. SEM/EDX Analysis of FA-GGBS-HMNS based Geopolymer

The geopolymer paste matrix is fairly homogenous as shown in Figure 4.3. It can be seen that most of the fly ash and slag grains had been dissolved by the activator solution. The GGBS particles were dissolved together with FA particles and contributed to the formation of C-S-H and A–S–H gels. However, HMNS grains were dissolved and led to the formation of C-M-S-H gel (Yang, Yao and Zhang, 2014). It is evident from the SEM images that the paste with 70% FA, 20% GGBS and 10% HMNS exhibits a denser microstructure and almost fully reacted matrix with some unreacted cenosphere and plerosphere FA particles. It was reported that the unreacted particles do not act as a filler in the mixture, but lead to an increase in the strength of the matrix with age, due to a growth in the physical bonding strength occurring during a complex chemical reaction between the surfaces of the particles as shown in Figure 4.3c2 (Ryu *et al.*, 2013).

The images shown in Figure 4.3(b1, b2, c1 and c2) demonstrate the geopolymerization products and show the presence of C-S-H and A-S-H gels which is mainly created from the activation of the 20% of GGBS, which in turn interacts with the FA, as can be observed on the EDX images. The high source of calcium and alumina-silicate in the mixture led to the formation of calcium alumina-silicate hydrate gel (C-A-S-H). GGBS, therefore, sourced an additional amount of calcium and contributed to an additional binding of products which in turn affected the setting behaviour of the geopolymer gel (Nath and Sarker, 2014). It is highly possible for the Mg^{2+} sourced from the HMNS to contribute to the formation of new gel phase as Na-Al(Mg)-Si-H gel, as evidenced by the EDX analysis. In addition, the XRD analysis in this study proves that the main HMNS components have all taken part during geopolymerization, where a complex chemical reaction with the other particles from the ternary mixture has occurred. The micro-cracks observed in some of the SEM features probably occurred during the mechanical tests, since the powders tested for SEM were taken from the specimens after the mechanical tests. Such micro-fissures could also be the result of multi-sequences of an internal stress occurring between particles during microstructural development (Fernandez-Jimenez, García-Lodeiro and Palomo, 2007).

The EDX analysis was used to determine the main elements of the geopolymer matrix. Figure 4.4 shows the SEM micrograph and the associated EDX spectrum analysis of the elements. The main hydration products were found as a mix between amorphous and crystalline C-S-H, A–S–H and C-M-S-H gels, with a, Ca/Si ratio of 0.53. It has been reported that if the Ca/Si ratio is below 1.5, then the C-S-H gel is classified as C-S-H(I) (Adam, 2009). However, the EDX analysis showed that the selected area has major elements of silicon, aluminium, calcium, sodium and magnesium. The average Si/Al and Mg/Si ratios in this study are around 2.73 and 0.34 respectively, with the exception of the ratios of the area 2 as this mainly consists of silica, as shown in Table 4.1. This, confirms that the matrix of FA-GGBS-HMNS based geopolymer concrete mainly contains Si-O-Al network with the incorporation of Ca^{++} and Mg^{++} in the

geopolymer gel. The EDX results were in good agreement with the XRD results, where certain patterns, such as quartz, remained, due to the partial dissolution of the raw materials.
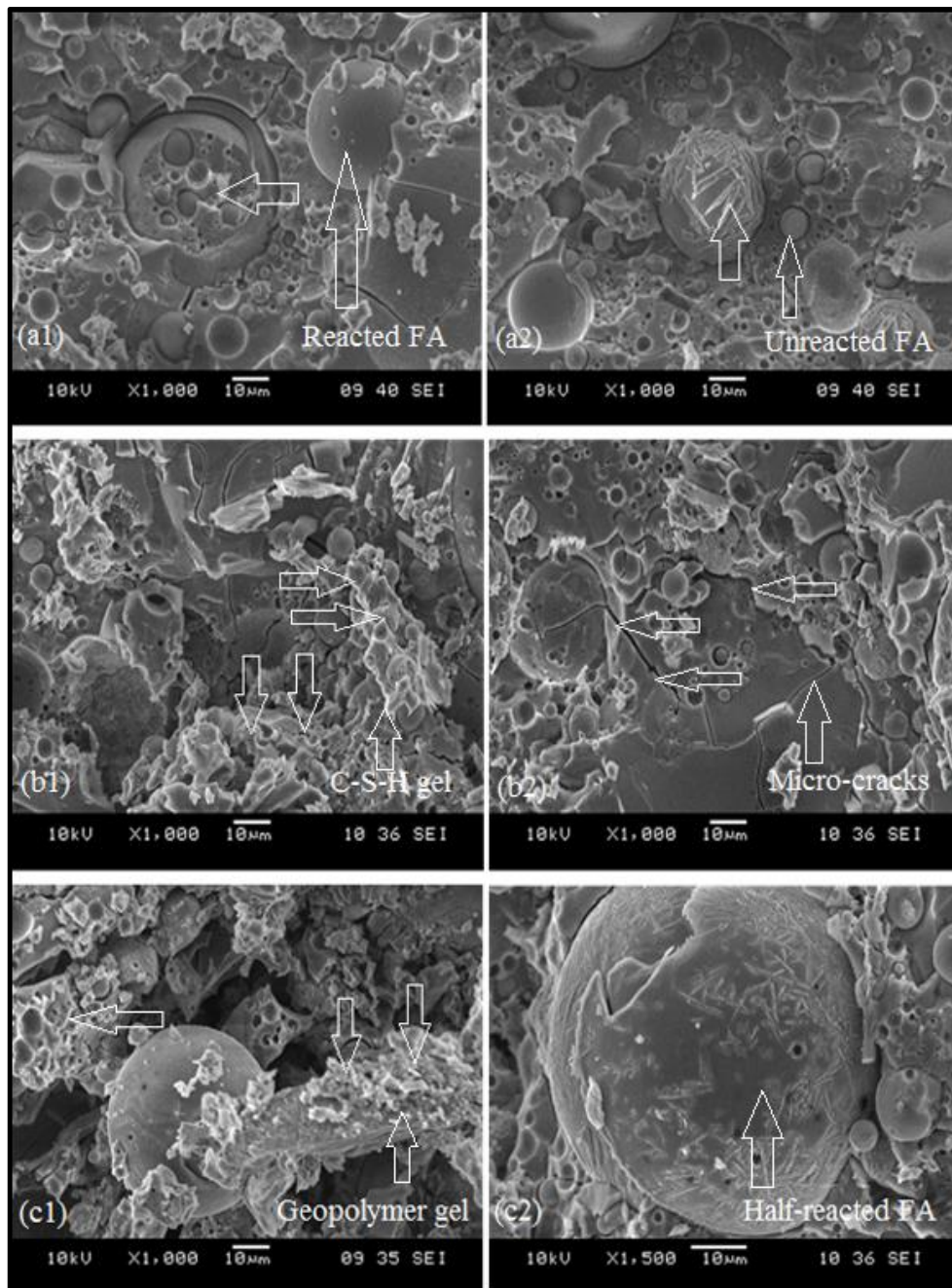
Figure 4. 3. SEM images of FA-based GP pastes
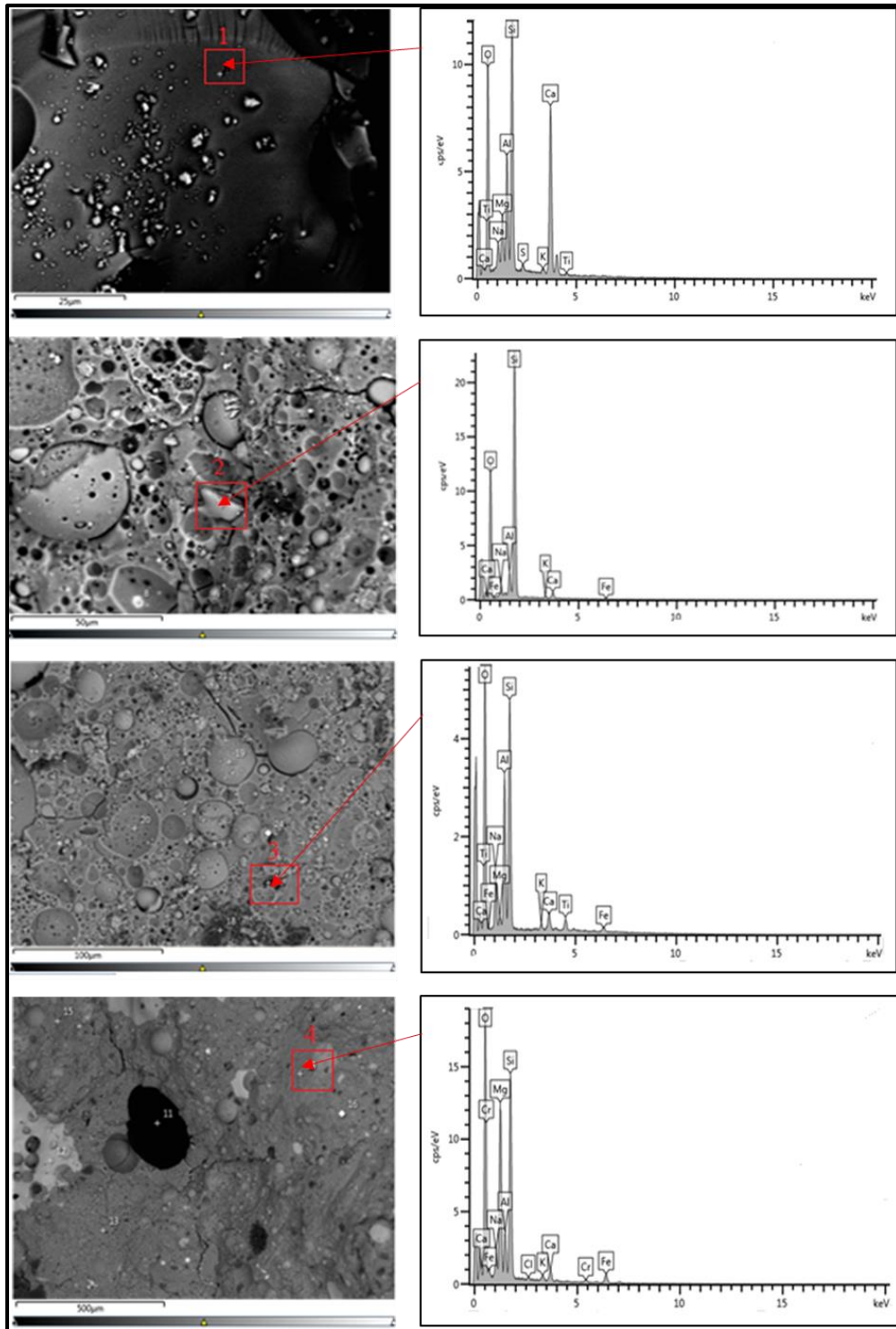
Figure 4.4. EDX analysis of the produced GP matrix

Table 4.1. Atomic elements of the GP Paste

Element (Wt %)	Area 1	Area 2	Area 3	Area 4
Si	18.0	39.7	22.4	21.4
Al	8.1	3.7	13.8	4.9
Ca	24.5	2.1	3.2	2.2
Mg	3.8	-	0.9	16.5
Na	2.0	2.5	7.0	3.0
Si/Al	2.22	10.72	1.62	4.36
Ca/Si	1.36	0.05	0.14	0.1
Mg/Si	0.21	-	0.04	0.77

4.2.3. Phase Analysis

4.2.3.1. XRD Patterns

The XRD patterns of the FA-based GP paste cured at ambient temperature are shown in Figure 4.5. It can be seen from the pattern in Figure 4.5a that the main crystalline peak identified in FA was the quartz (SiO_2) with a high intensity at $2\theta = 27°$, as is supported by the XRF results, where 55.7% of SiO_2 was detected. Mullite ($Al_6O_{13}Si_2$) was another significant peak, where it was detected in different ranges of 2θ ($17°$ and $65°$) (Nath and Kumar, 2013). Figure 4.5b shows that the main mineral elements found in GGBS were calcium carbonate ($CaCO_3$) and quartz (SiO_2) at $30°$ and $27°$-$50°$, respectively. The XRD pattern shown in Figure 4.5c suggests that many crystalline phases were characterized in HMNS with a high peak of protoensatite ($MgSiO_3$) at

$2\theta = 27^\circ$ (Rashad, 2013; Yang, Yao and Zhang, 2014), where albite (Na (AlSi$_3$O$_8$)) was stretched at $2\theta = 18^\circ$, 23° and 53° and forsterite nickeloan (Mg$_{1.4}$Ni$_{0.6}$O$_4$Si) at $2\theta = 32^\circ$ and 37°. Figure 4.5d shows the XRD patterns of the designed GP concrete. It is evident from Figure 4.5d that magnesium vanadium molybdenium oxide (Mg$_{2.5}$ (VMo) O$_8$) from HMNS is the main peak identified, with a high intensity at $2\theta = 27^\circ$. It is also seen from the XRD result shown in the same Figure 4.5d that new crystalline peaks, which appeared in the pattern, matched the calcium beryllium praseodymium oxide (CaBePr$_2$O$_5$), which has an orthorhombic crystallography and pnma space group. These new crystalline phases could be attributed to the presence of GGBS and HMNS, where their glassy phases were activated due to the high pH of the environment.

However, no formation of Mg(OH)$_2$ crystalline products is detected in the binder, which will lead to an undesired expansion of the geopolymer structure (Yang, Yao and Zhang, 2014). In addition, it can be observed from the XRD patterns revealed in Figure 4.5(a, b and d) that the geopolymerization has two main effects on the XRD patterns;

i) the first effect as it can be seen from the broad hump which clearly appears in FA, GGBS and GP paste XRD patterns, between $\sim15^\circ$ and $\sim40^\circ$. This hump corresponds to the formation of a new amorphous hump in the GP concrete and identifies the geopolymeric gel;

ii) the second effect regards to the decrease in the intensity of the crystalline peaks. This reveals a partial dissolution of the crystalline phases of the precursor materials, such as quartz (SiO$_2$) from FA and calcium carbonate (CaCO$_3$) from GGBS. It has been reported that the decrease in the intensity of the crystalline phases could be due to the high dissolution rate of SiO$_2$ in the presence of sodium silicate (Ahmari *et al.*, 2012; Vásquez *et al.*, 2016).
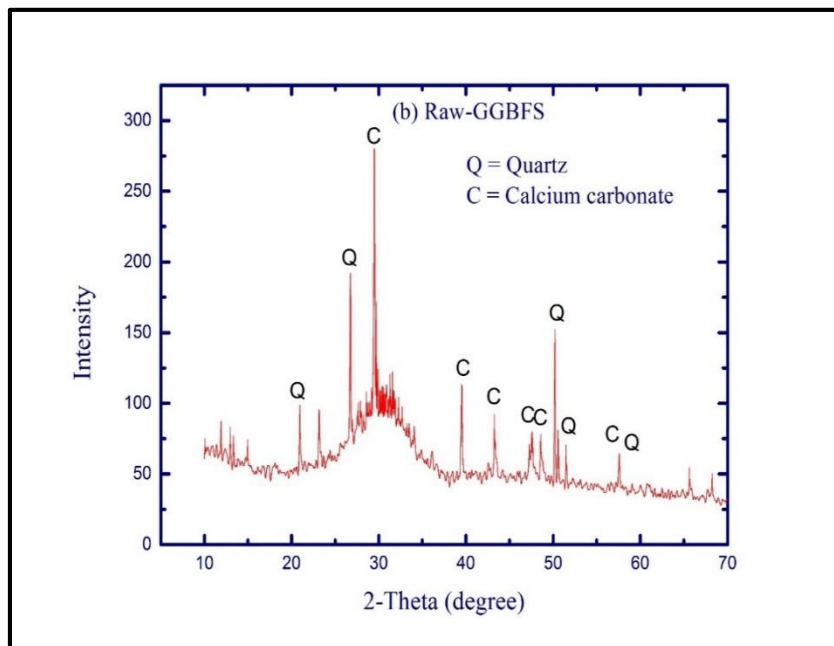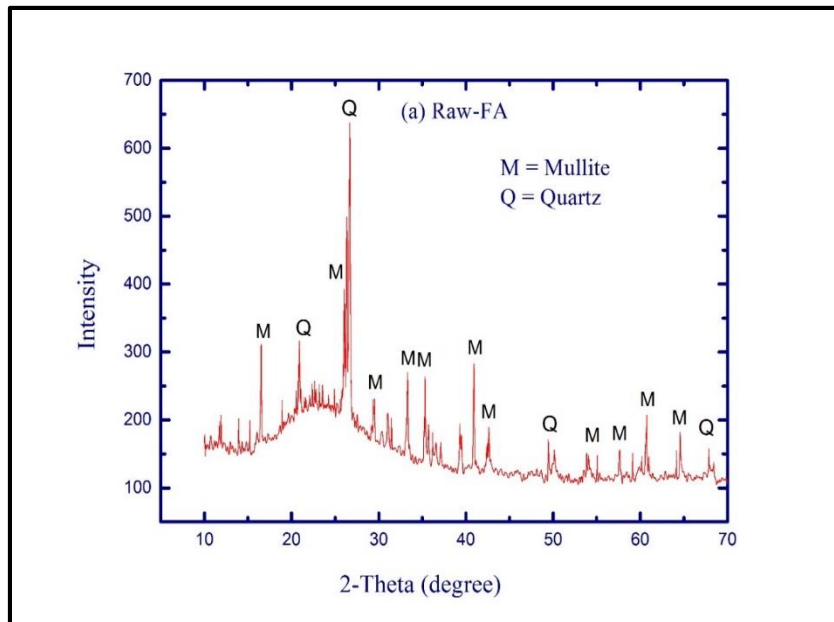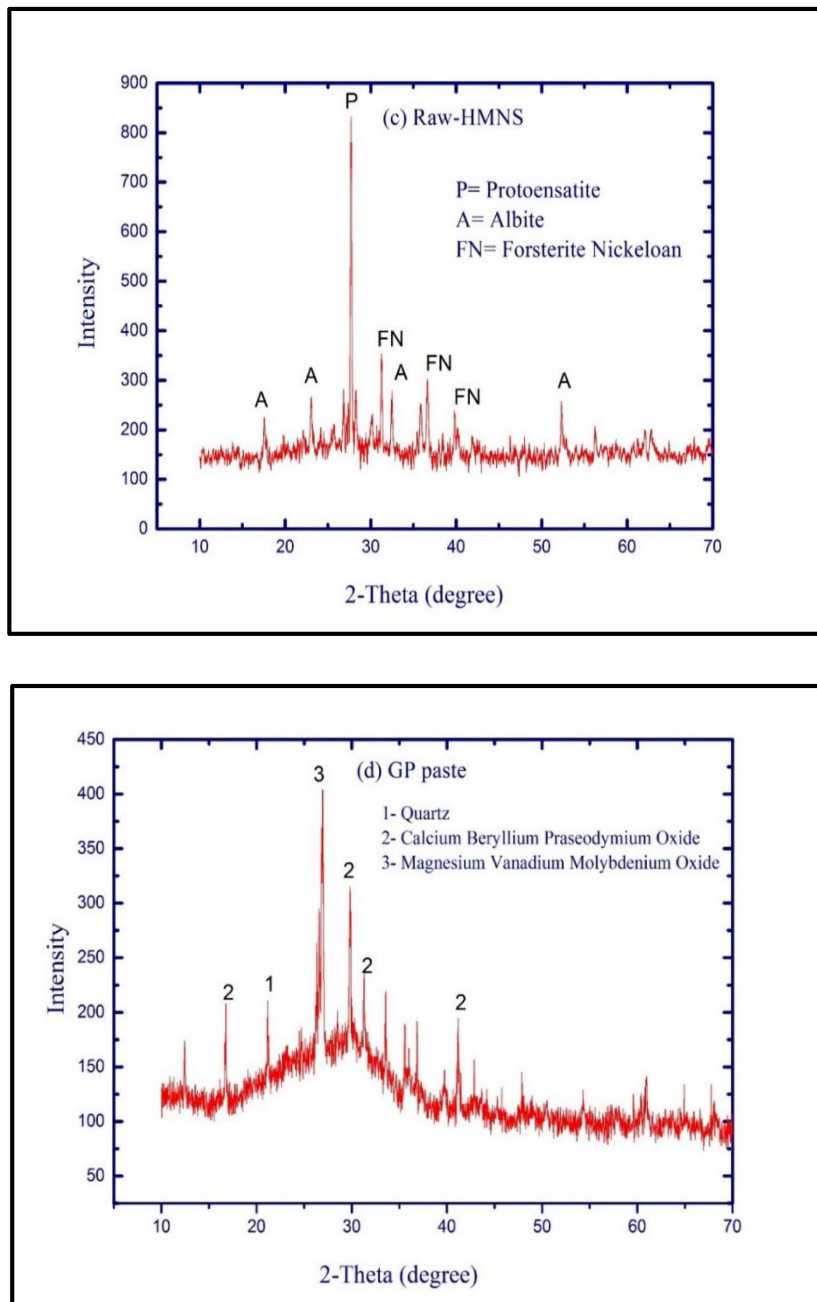
Figure 4.5. X-ray diffractograms of GP paste.

4.2.3.2. FTIR Analysis

In this study, Fourier transform infrared spectroscopy (FTIR) analysis was used to investigate the effect of the geopolymerization process on different chemical bonds of the precursor materials before and after the reaction. Spectra were obtained by using a Perkin Elmer FTIR Spectrum model RX1 Spectrometer. The spectra of the specimens covers wavelengths from 4000 cm^{-1} to 650 cm^{-1}.

The FTIR spectra of the GP concrete cured at room temperature at 28 days are shown in Figure 4.6. The difference in absorption frequency of the GP products is characterized by various bands and function groups formed during geopolymerization. The bands at ~ 3300-3600 cm^{-1} revealed that there is stretching vibration of O-H bending (Ahmari *et al.*, 2012; Yahya *et al.*, 2013; Faisal and Muhammad, 2016). However, the bands at 2000-2200 cm^{-1} could correspond to the stretching vibration of the functional group of Na_2CO_3, K_2CO_3 or sodium phosphate, formed by the activator solution and the binder material during the geopolymerization process. It has been reported that, if there is an excess of sodium ions due to the high concentration of alkali solution, a portion of these ions is transferred to the surface where it carbonates with the absorbed carbon dioxide from the atmosphere (Komnitsas, Zaharaki and Perdikatsis, 2007; Tatzber *et al.*, 2007). The stretching vibration frequency at ~ 2500 cm^{-1} can be C=O. The bands at ~ 1670 cm^{-1} present the H-O-H group. The frequencies of CO_3^{2-} with stretching vibrations of C-O groups were characterized at the peaks ~1470 cm^{-1} (Clara and Kumar, 2016). Therefore, it has been stated that the C-O bonds were created due to atmospheric carbonation. The broad-band at around 940-1005 cm^{-1} was ascribed to the asymmetric and symmetric stretching vibrations of Si-O-Si and Al-O-Si, formed during the dissolution of SiO_4 tetrahedra. The bands centred in these regions generally correspond to the C-S-H gel (Fernández-Jiménez and Puertas, 2003; Yunsheng *et al.*, 2007). However, the bands Si-O and Al-O were stretched at ~ 850 cm^{-1} and the stretching vibration of $-CO_3$ was counted at 875 cm^{-1} (Ahmari *et al.*,

2012; Cheng-yong *et al.*, 2017). The Characteristics of FTIR bands of the produced

Fly ash-based geopolymer paste is presented in Table 4.2.
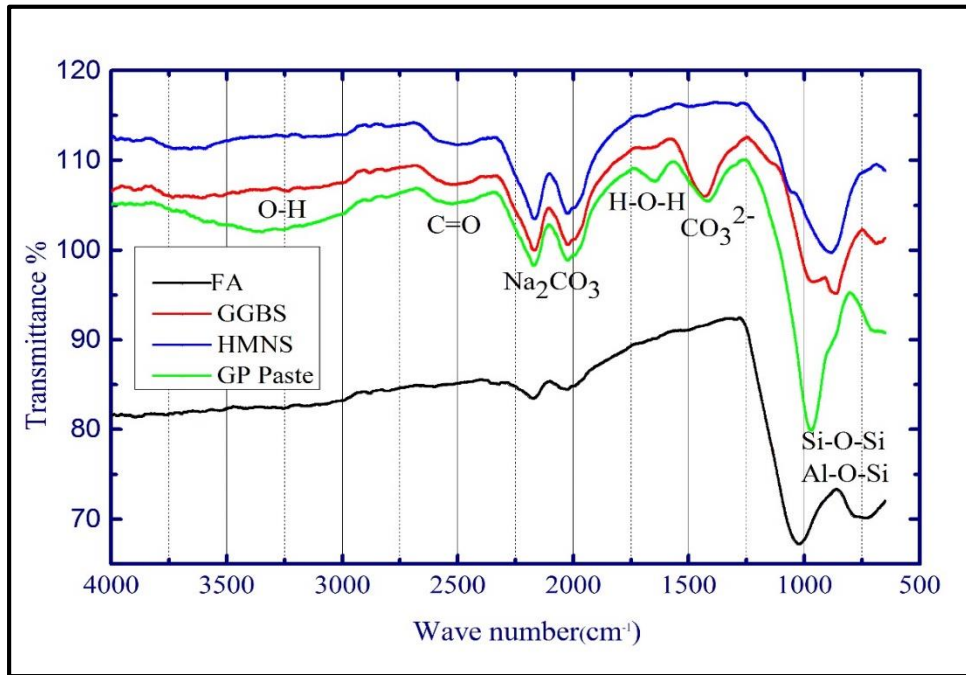
Figure 4.6. The FTIR spectra of raw materials and GP paste

Table 4.2. Characteristics of FTIR bands of Fly ash-based geopolymer

(Mohd *et al.,* 2013; Yahya *et al.,* 2013)

Wavelength (cm^{-1})	Assignment
2300-3500	Stretching vibration of (–OH, H-O-H)
1630-1650	Bending vibration of (H-O-H)
1410-1430	Stretching vibration of (–O-C)
990-1090	Asymmetric stretching vibration of (T-O-Si, T= Al or Si)

4.2.4. Optical Microscopy (OM)

Optical microscopy is used to observe the effect of aggregates on the geopolymeric binders. The use of this optical-analysis tool provides a physio-visual description of the GPC microstructure (Komnitsas and Zaharaki, 2007). The interfacial zone between aggregates and the geopolymeric matrix is captured under a magnification of 5, 10, 20, and 50 Mpixel. Figure 4.7 presents the optical microscopic images of the geopolymeric system. Figure 4.7 (A, B), which corresponds to a magnification of 5 Mpixel shows the distribution of macro-particles of fine aggregates.

Figure 4.7 (C, D) corresponds to the images observed under a magnification of 10 Mpixel, where micro-cracks and a clear distribution of geopolymer gel on the surface of aggregate are observed. The images shown in Figure 4.7 (E, F) and (G, H) reveal the GPC under a magnification of 20 and 50 Mpixel, respectively. It is evident that the aggregates are bonded to the geopolymer matrix, which significantly contributes to an improvement in strength. This might be due to the reaction of aggregates' surface with the geopolymeric system, leading to the creation of an attractive potential in the geopolymer binders. Further, the source of aggregates (originally sourced from crushed stone) may contain some calcium components, which in turn contribute to the geopolymerization reaction. Nevertheless, the presence of micro-cracks is mainly due to the implementation of mechanical force during the preparation of the GPC specimens.
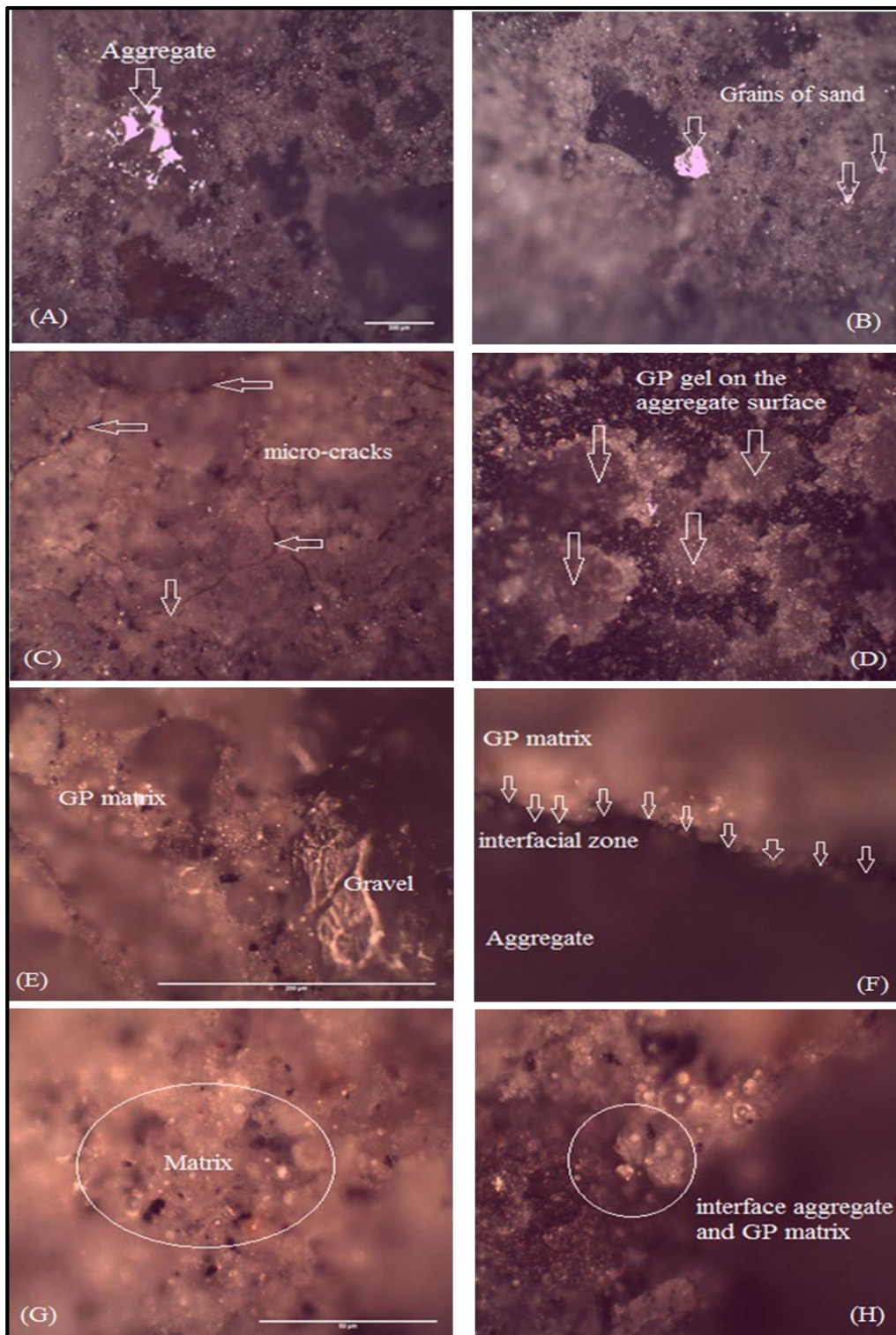
Figure 4.7. Optical micrographs of GPC

4.3. The Effect of HMNS on the Mechanical and Microstructural Properties

This study shows a good improvement of the mechanical and microstructure properties of the GP concrete mixed using FA, GGBS and HMNS. The combination of those three materials led to the formation of ternary gel phases, due to the occurring of different chemical reactions in the mixture with the presence of the alkali activator solution. It was also demonstrated that the M-S-H or C-M-S-H gel sourced from the HMNS is denser and morphological less porous when compared with the A-S-H and C-S-H gels formed from FA and GGBS. It is clear that the incorporation of HMNS with class F FA and GGBS introduces a significant improvement on the engineering properties. The sourced Mg^{++} cations from HMNS improve the geopolymerization of geopolymeric system. The chemical nature of the magnesium allows the Mg^{++} cations to form a strong intermolecular bonding with other cations such as Si^{+4} and Al^{+3} through sharing of oxygen atoms as schematised in Figure 4.8. The proposed model shown in Figure 4.8 is fundamentally similar to that proposed by (Davidovits, 1994). Further, the presence of Mg^{++} in the geopolymeric chain provides chemical stability or what is called interatomic-bonding in the matrix, due to the formation of different chain-links such as Si-O-Mg, Si-O-Al, Ca-O-Si and Si-O-Si. Therefore, it is believed that such intermolecular forces created in the system can be a reasonable explanation for the improvement of the GP properties (Bouaissi *et al.*, 2019).
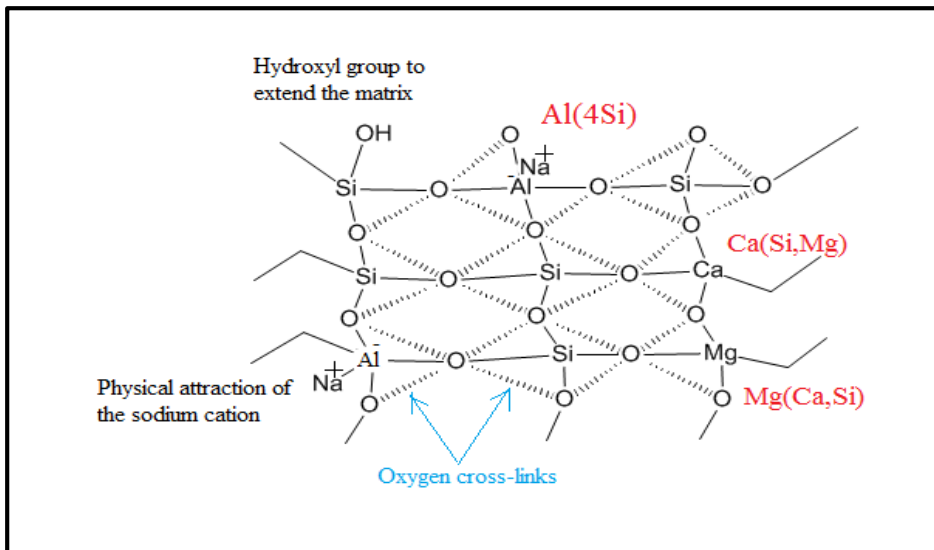
Figure 4.8. Proposed model of the ternary A-S-H, Ca-S-H, and C-M-S-H gel phases

4.4. Summary

The morphological characteristics of the GPC and the precursor materials used have been discussed in this chapter. The SEM micrographs showed a fairly homogenous geopolymeric matrix, due to the high reactivity between the binders and the alkali activator solution. However, the SEM photographs indicated some micro-cracks on the GP matrix, due mainly to the effect of the mechanical tests on the specimens, since the powders tested for SEM were taken from the specimens after the mechanical tests. On the other hand, the SEM images showed a full reaction of the precursor materials, with fewer unreacted FA particles. The main mineralogical elements were determined by using EDX analysis. The EDX spectrum revealed that silica, aluminium, calcium, sodium and iron were the major elements which contributed to the hydration process and then in the formation of C-S-H, A–S–H and C-M-S-H gels.

The XRD patterns displayed the crystallinity of raw materials and the GPC. The most crystalline phases found in the initial materials are; Quartz, Mullite, Calcium Carbonate, Albite, Protoensatite, Forsterite. However, the crystalline peaks detected in the geopolymeric system are; Quartz, Calcium Beryllium Praseodymium Oxide, Magnesium Vanadium Molybdenium Oxide. The presence of Quartz in the geopolymeric system is due to the richness of aluminosilicate in the precursor material. The high calcium level provided by GGBS is a significant contribution to the formation of a new crystalline phase during geopolymerization. A typical amorphous phase has been detected after the geopolymerization process, which indicates a wide diffraction hump ranged at 2θ angles of $\sim 15^\circ$-40°.

The FTIR analysis is considered an effective technique providing relevant information on the molecular bonding during the geopolymerization reaction. The FTIR spectrum showed that the geopolymer and its raw material mainly consist of Si-O and Al-O bonds, due to the high content of Si and Al in the binder. However, it was noticed that the H-O and H-O-H bonds may refer to the formation of water molecular, while the C-O bonds may correspond to the formation of alkali carbonates due to atmospheric carbonation.

Chapter 5
Dynamic Behaviours of FA-GGBS-HMNS based Geopolymer Paste

5.1. Introduction

In practical engineering, many structural materials may undergo high strain rates and dynamic loadings, due to the implementation of many actions, caused by nature or human beings themselves. The dynamic strength of materials is considered to be one of the most important indexes, which can be applied to evaluate the materials when used in critical applications such as earthquakes. However, due to the limited research into the dynamic properties of geopolymers (Feng *et al.*, 2015; Ren *et al.*, 2015), it is pointed out through this study that a good understanding of the mechanical and dynamic behaviours of geopolymers under high strain rates, could be a significant contribution to standardizing and expanding their application in the construction industry. The Split-Hopkinson Pressure Bar (SHPB), also known as the Kolsky apparatus, is an experimental technique, commonly used to measure the dynamic compressive strength of materials or concrete-like materials at high strain rates. This chapter examines the dynamic properties of the FA-GGBS-HMNS based geopolymer paste using the SHPB technique. The work was performed by using SHPB to investigate the impact behaviour of FA-GGBS-HMNS based geopolymer paste specimens at various different impact velocities.

5.2. Materials and Testing

To implement the dynamical compressive impact test at high strain rates, three pre-prepared cylindrical specimens with diameters of 33, 36 and 37mm respectively, and thickness of 18mm, were sliced from cast cylinders of FA-GGBS-HMNS based geopolymer paste and were used for the impact test. The dynamical impact test has been carried out in ''Guangdong Provincial Key Laboratory of Durability for Marine Civil Engineering, Shenzhen University''.

5.2.1. Preparation of Specimens

In order to prepare FA-GGBS-HMNS based geopolymer paste specimens, the following powder materials were used. Class F FA with a specific surface area of 1.3 m^2/g and average particle size (X_d) around 17.37µm was obtained from the Manjung power plant at Perak in Malaysia; GGBS with a specific surface area of 0.106 m^2/g and an average particle size of approximate 138µm, was obtained from the steel plant in Penang, Malaysia, and HMNS, with an estimated specific surface area of around 0.0536 m^2/g and average particle size of 280µm, was sourced from the steel plant in Shaanxi, China (Mainland). The alkaline activators used in the present experimental study were sodium silicate (Na_2SiO_3) and sodium hydroxide (NaOH). The sodium silicate solution consists of the chemical composition of Na_2O=14.7%, SiO_2=29.8%, and water 55.5% by mass. The sodium hydroxide solution was prepared in the laboratory by dissolving sodium hydroxide pellets in water to make the solution of 12 M concentration. After cooling for 24 hours at room temperature, the sodium hydroxide solution was then mixed with the sodium silicate solution. The mass ratio of sodium-silicate to sodium-hydroxide solution was 2.5. The freshly prepared GP paste was poured into cylindrical tubes of different diameters. After 24 hours they were demoulded and cured at room temperature of 25±2ºC with a relative humidity of 85-90% before being used for testing.

5.2.2. The Principle of the Split-Hopkinson Pressure Bar Compressive Test

The SHPB system mainly consists of two long slender metallic bars, between which the specimens to be tested is placed. The SHPB principally works in one direction of wave propagation. The SHPB apparatus mainly consists of a gas gun, a striker bar, incident and transmission bars as shown in Figure 5.1. These bars are made from the same material and have a similar cross-section area. During testing time, both incident and transmission bars should remain elastic and be concentrically aligned in order to ensure an accurate measurement. When the striker bar is boosted by the gas pressure, a stress wave is generated and propagated through the incident bar towards the specimen. At the moment when the wave reaches the specimen, part of the stress wave created is transmitted through the transmission bar (transmitted pulse), and another part is reflected back to the incident bar (reflected pulse).

The remaining wave in the transmitter bar will be absorbed by a stopper, which is known as a shock absorber (see Figure 5.1). To measure the incident pulse, the transmitted pulse and the reflected pulse, strain gauges are fixed on both incident and transmitted bars (see Appendix C). Due to the direct proportional relationship between the strain rate in the specimen and the amplitude of the reflected wave, the elastic strain created in the incident and transmission bars are used in the calculation of stresses and strains occurring in the specimen.
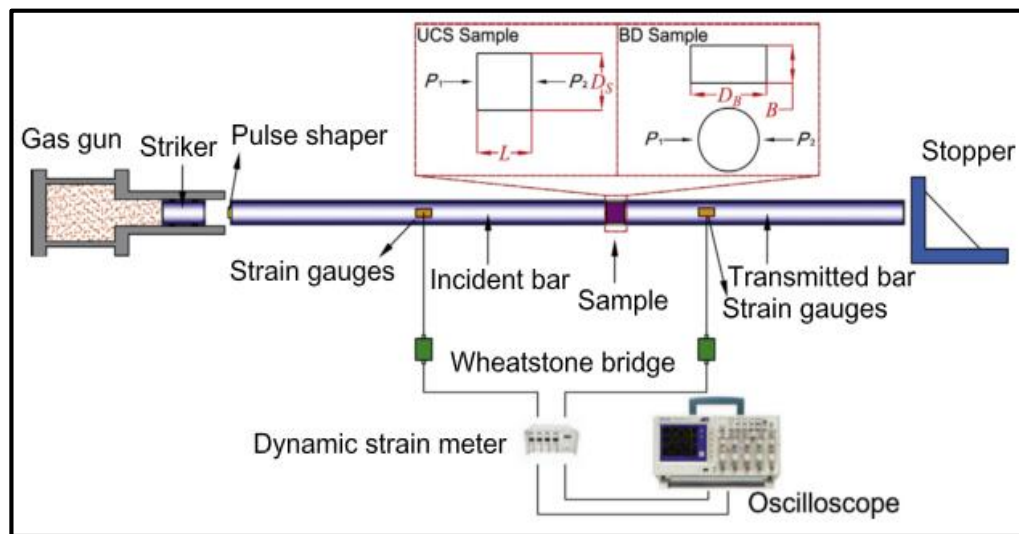
Figure 5.1. Schematic of the Split Hopkinson Pressure Bar system

(Yao *et al.*, 2019)

5.2.3. Test Procedure

This section describes the main steps used in the SHPB test. In order to prepare the test specimens, 3x9 = 27 cylindrical discs of 33, 36 and 37mm diameter and 18mm thickness were sliced from cast samples (see Figure 5.2) of FA-GGBS-HMNS based geopolymer paste, using an electrical diamond machine as shown in Figure 5.4a. To ensure the high consistency and uniformity of the specimens, both end surfaces of the specimens were carefully polished and parallelized (see Figure 5.4(b, c)). The SHPB system was calibrated before starting the test, to ensure that the wave propagation through the incident and the transmission bars was homogenous, uniform and isotropic over the full system as shown in Figure 5.5. The length and diameter of both incident and transmission bars were 2000mm and 40mm respectively. In order to reduce the friction between the specimen and two bars, a film of lubrication was used to coat the contact surfaces the bars. It has been reported that strain rate loading ranges from 50-370 s^{-1} and from 300-1500 s^{-1} could be used for concrete and mortar specimens,

respectively (Feng *et al.*, 2015).

However, in this study, three impact velocities were adopted in the experiment work, which was approximately 2, 4 and 6 m/s. During the test, the failure pattern of the specimens under different conditions (before impact, after impact and failure mode) was recorded by the camera. It is worth mentioning that, during the test, the SHPB device (see Figure 5.3) was triggered by mistake several times, which resulted in the collection for some experimental data being missed by the dynamic strain indicator.

Figure 5.2. Geopolymer paste for SHPB Test

Figure 5.3. SHPB apparatus
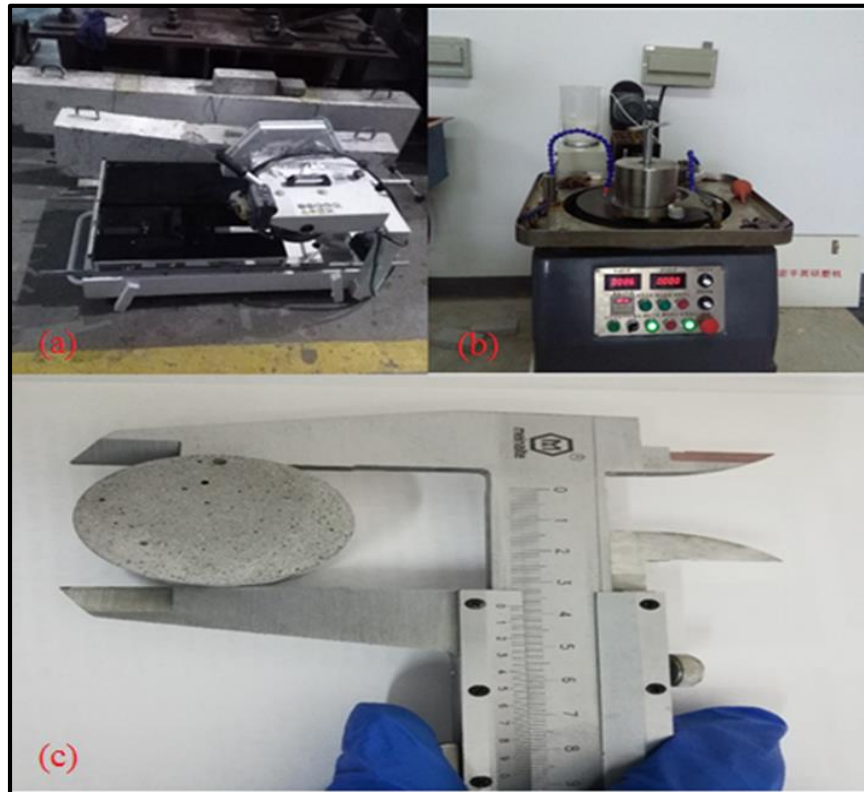
Figure 5.4. (a) Cutting machine, (b) Grinding equipment, (c) specimen measurement
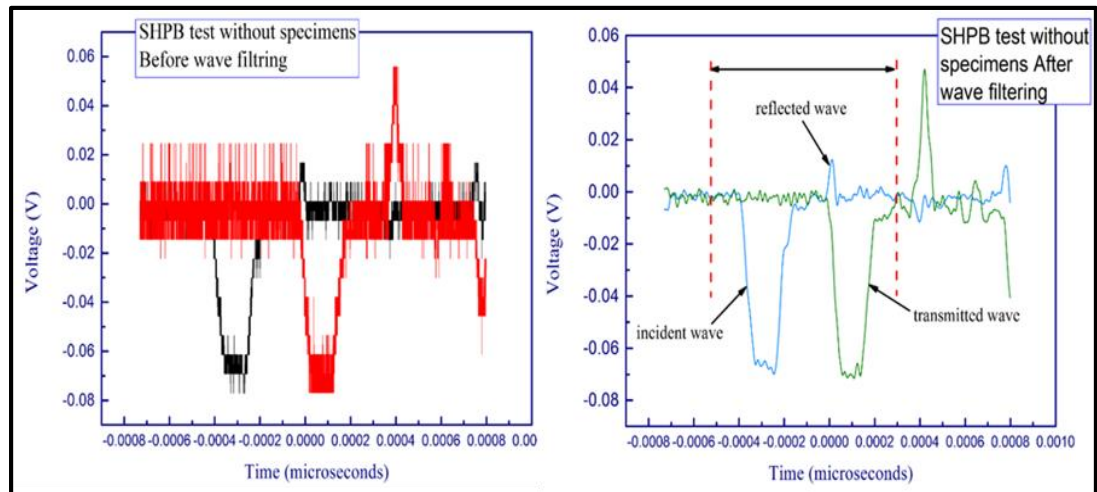
Figure 5.5. Original wave test without specimen, before and after filtering

5.2.4. The Fundamental Equation of SHPB

The main mathematical equations which explain the one-dimensional relationship between stress σ and strain ($\frac{\partial u}{\partial y}$) where u is the axial displacement are presented as follows.

As a result of the impact of the striker bar on the incident bar, a compression force F_1 and F_2 will be created on the differential elements as shown Figure 5.6.

At the end of each element section, the forces F_1 and F_2 could be written regarding the stresses as follows:

$$\sigma_1 = \frac{F_1}{A_0} \ and \ \sigma_2 = \frac{F_2}{A_0}$$

Eq (5. 1)

where A_0 is the cross-section of the bar. The stress applied to the element can be related to the strain as follows:

$$\sigma = E\varepsilon = E\frac{\partial u}{\partial y}$$

Eq (5. 2)

where E is the Young's modulus and ε is the strain. From Eq (5.1) and Eq (5.2), F_1 and F_2 could be written as follows (see Figure 5.6):

$$F_1 = EA_0\frac{\partial u_1}{\partial y} \ and \ F_2 = EA_0\frac{\partial u_2}{\partial y}$$

Eq (5. 3)
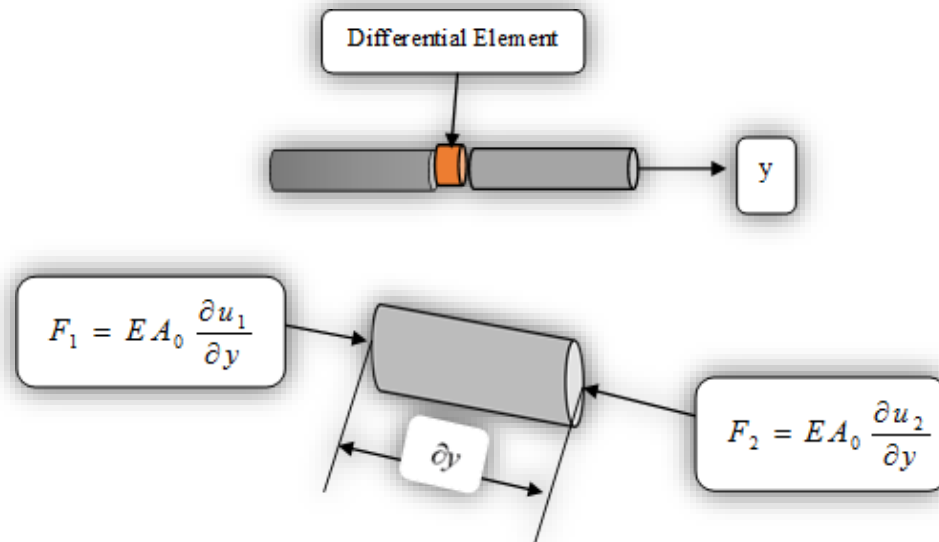
Figure 5.6. Differential pressure bar element under compression

Applying Newton's second law yields:

$$EA_0 \frac{\partial u_1}{\partial y} - EA_0 \frac{\partial u_2}{\partial y} = A_0 \partial y \rho \frac{\partial^2 u}{\partial t^2} \qquad \text{Eq (5. 4)}$$

where t is the time and ρ is the density of the bars.

Taylor Series expansion could be used to determine u_1 and u_2 as displayed in Figure 5.7.
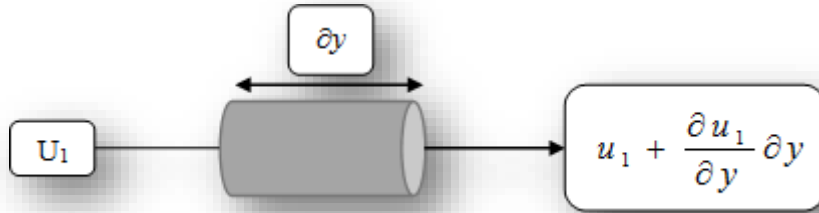
Figure 5.7. Taylor series expansion for displacements

(Lang, 2012)

$$u_2 = u_1 + \frac{\partial u_1}{\partial y} \partial y \qquad\qquad \text{Eq (5. 5)}$$

By differentiation of u_2 in function of y Eq (5.5) yields:

$$\frac{\partial u_2}{\partial y} = \frac{\partial u_1}{\partial y} + \frac{\partial^2 u_1}{\partial y^2} \partial y \qquad\qquad \text{Eq (5. 6)}$$

It is known that the wave velocity C_0 of one dimension is given by Eq (5.7) as follows (Kaiser, 1998):

$$C_o = \sqrt{\frac{E}{\rho}} \qquad\qquad \text{Eq (5.7)}$$

By replacing ρ from Eq (5.7) into Eq (5.4) it yields to:

$$EA_0 \frac{\partial u_1}{\partial y} - EA_0 \frac{\partial u_2}{\partial y} = A_0 \partial y \frac{E}{C_0^2} \frac{\partial^2 U}{\partial t^2} \qquad \text{Eq (5. 8)}$$

The substitution of Eq (5.6) into Eq (5.8) with simplification of both sides of the equation can be written as:

$$EA_0 \frac{\partial u_1}{\partial y} - \left(\frac{\partial u_1}{\partial y} + \frac{\partial^2 u_1}{\partial y^2} \partial y \right) = A_0 \partial y \frac{E}{C_0^2} \frac{\partial^2 u}{\partial t^2} \qquad \text{Eq (5. 9)}$$

$$C_0^2 \frac{\partial^2 u_1}{\partial y^2} = \frac{\partial^2 u}{\partial t^2} \qquad \text{Eq (5. 10)}$$

The solution of Eq (5.8) for the incident bar could be given as:

$$u = f(y - c_0 * t) + g(y + c_0 * t) = u_i + u_r \qquad \text{Eq (5. 11)}$$

where f and g are the functions describing the incident and reflected wave which travel in a positive and negative y-direction, respectively. The strains through the incident bar could be obtained by the differential displacements of Eq (5.11) with respect to y-direction and time.

With respect to y direction it yields:

$$\varepsilon = \frac{\partial u_i}{\partial y} + \frac{\partial u_r}{\partial y} = \varepsilon_i + \varepsilon_r \qquad \text{Eq (5. 12)}$$

With respect to time t yields:

$$\dot{u}_1 = c_0 \left(-\varepsilon_i + \varepsilon_r \right) \qquad \text{Eq (5. 13)}$$

For the transmitted bar differentiating displacements yields:

$$u = h\left(y - c_o * t\right) = \varepsilon_t \qquad \text{Eq (5. 14)}$$

$$\dot{u}_2 = -c_o \varepsilon_t \qquad \text{Eq (5. 15)}$$

where ε_t corresponds to the strain created in the transmitted bar and h is the function which describes the transmitted wave through the bar.

The strain rate occurring in the tested specimen could be obtained through the following Eq (5.16) as schematised in Figure 5.8.

$$\dot{\varepsilon} = \frac{\left(\dot{u}_1 - \dot{u}_2\right)}{L_S} \qquad \text{Eq (5. 16)}$$

$$\dot{\varepsilon} = \frac{c_0\left(-\varepsilon_i + \varepsilon_r + \varepsilon_t\right)}{L_S} \qquad \text{Eq (5. 17)}$$

where $\dot{u}_1$ and $\dot{u}_2$ correspond to the velocities at the interface of the incident and transmitted bars, respectively, and L_S is the instantaneous length of the test specimen (Gao *et al.*, 2015).
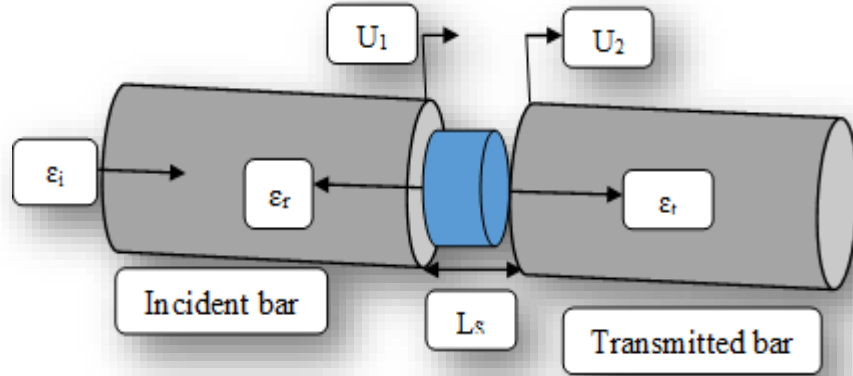
Figure 5.8. Schema of different acting strain on the specimen through the incident and transmission bars

To simplify Eq (5.17), the theory of conservation of momentum to the striker bar, incident and transmitted bars and test specimen was applied. The strain rate in the test specimen can be estimated as:

$$\varepsilon^{\bullet} = \frac{V}{L_S}$$

Eq (5. 18)

where V is the velocity of the striker bar before impacting the incident bar.

The engineering stress in the tested specimen can be calculated by dividing the force by the original area of the specimen. Because the FA-GGBS-HMNS based GP paste specimen is considered an incompressible material, the volume before impact by the striker bar could be related to the volume after impact which could be written as:

$$A * L = A_S * L_S$$

Eq (5. 19)

where *A* and *L* correspond to the cross-section area and the length respectively of the specimen before impact, and A_S and L_S correspond to the instantaneous cross-section area and the specimen length after impact.

The engineering stress could be determined from the strain gauge measurements of the transmitted force and divided by the instantaneous cross-section area.

$$\sigma = \frac{AE\varepsilon_t}{A_S}$$

Eq (5. 20)

$$\sigma = \frac{AE}{A_S}\left(\varepsilon_i + \varepsilon_r\right)$$

Eq (5. 21)

Eq (5.20) corresponds to one wave of stress, since the only values used are from the transmitted wave. However, an accurate estimation of the stress can be measured by two-wave methods, at the incident bar and at the specimen interface as shown in Eq (5.21). Nevertheless, when applying Eq (5.21), the influence of high transient which occurs when the loading starts in the incident bar and specimen interface should be considered especially at the beginning of the test (Lang, 2012).

5.3. Results and Discussions

5.3.1. Dynamical Compressive Properties

The dynamical mechanical properties of all FA-GGBS-HMNS based GP paste groups tested are presented in Figures 5.9 and 5.11.

5.3.1.1. Dynamic Stress-Strain Curves

It can be seen from Figure 5.9 that the dynamic stress-strain curves of all groups of FA-GGBS-HMNS based GP pastes reveal similar variation trends to strain rate. It is clear from the same figure that the GP paste specimens tested under different velocities and strain rates show remarkable plasticity of behaviour, which obviously appear from the nature of the line-graph. The stress-strain curves can be divided into three different stages as follows (Luo *et al.*, 2013):

Stage I: It can also be known as the compaction phase, and in this stage, the stress linearly increases with the strain. This increase is mainly related to the dynamic compression applied, where the micro-cracks and the micro-spaces between the particles of the GP specimens become collapsed and morphologically closed. In this stage most stress is achieved. Also it is clearly shown in Figure 5.9 that this stage is shorter compared to the other two stages.

Stage II: This is the softness and the yielding stage, as can be observed from Figure 5.9. It is longer than the first stage and with a prolonged strain. According to the same figure, the stress maintains its increase until reaching the maximum value, which is known as a peak-stress point. The latter can be clearly distinguished from the GP specimens of the group (a) as shown in Figure 5.9, where the stress-strain curves appear as concave instead of plateau forms. It is believed that there is irreversible

plastic deformation behaviour, which can be seen from the plateau forms of the stress-strain curves.

Stage III: This corresponds to the failure stage, during which the stress-strain curves exhibit observable failure features. During the elastic stage (stage II), and because the load is gradually increased, many more cracks develop and subsequently propagate slowly into the specimens, which leads to complete failure of the specimen. Also, due to the difference of strain rates and velocities, different forms of damage are evaluated during the whole process as shown in Figure 5.10.

From these different stages, dynamic compressive strength can be defined as the achieved peak stress on the stress-strain curve of each specimen, which in turn reflects the strength characteristic; whereas, the peak strain can be defined as the critical strain which corresponds to the peak stress which reflects the deformation features. Some research has reported that the behaviour of the strain rate dependent under a dynamic loading could be described as the huge quantity of energy consumed during the starting formation of micro-cracks. While the increase of strain rate leads to much development of micro-cracks, which in turn required high energy to control the inertial strength of the material (Su and Xu, 2013).

In addition, as shown in Figure 5.9, the dynamic mechanical behaviours (dynamic compressive strength, critical strain and ultimate strain) of the FA-GGBS-HMNS based GP paste specimens increase with the increases strain rate. It can be seen from the same figure that the non-linear deformation stages before achieving the peak stress increase in all groups (a, b and c), which explains the plasticity behaviours of the material. Quasi-similar behaviours can be observed after peak stress, where the slopes of the stress-strain curves increase with increasing strain rates, which also increase the ultimate strains before the specimens completely crashed.
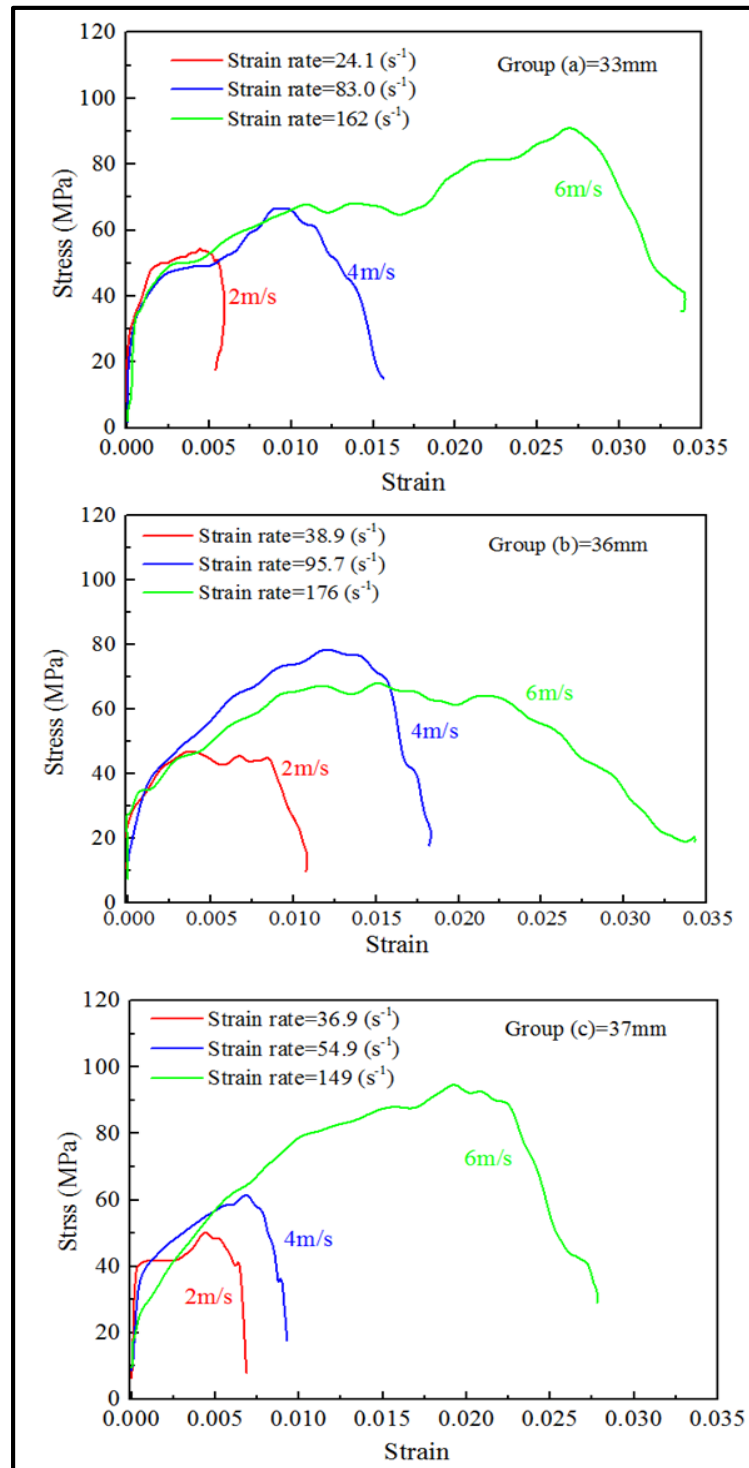
Figure 5.9. Stress-strain curves of FA-GGBS-HMNS based GP paste with different strain rates and velocities

5.3.1.2. Failure Patterns

The failure modes of the FA-GGBS-HMNS based GP paste specimens under different strain rates and/or impact velocities are presented in Figure 5.10. It is evident that the failure form of the GP paste specimens after dynamic compression tests shows a strong dependency on the strain rate and changes with the increase of strain rate. Also, it is worth indicating that fragment size and amount are directly related to the strain rate. When the strain rate is 24.1 s^{-1} the damage form of the specimens after impact undergoes in several large pieces. When the strain rate was between 83 s^{-1} and 162 s^{-1}, the specimens were crushed into fine fragments. The fracture theory maintains that, when the specimens are subjected to an impact, the failure should propagate from the edge to the centre (Gao *et al.*, 2015). However, in concrete like material, it is extremely difficult to obtain highly homogeneous or ideal isotropic material, which will mainly affect the amount of damage.

As depicted in Figure 5.10, larger amounts and smaller size fragment, are generated when a higher strain rate is applied. Chen, Wu and Zhou (2013) state that the cracks in cement paste are mostly straight and long when compared to those in concrete or mortar specimens. In this study, it was found that when the strain rate was less than 51.2 s^{-1} (which is the most critical case), the stability of FA-GGBS-HMNS based GP paste is still good. However, the complete deformation of the GP paste specimens was observed when the strain rate reached 149 s^{-1}. Similar findings have been reported by other researchers, where their cement-like material showed good stability at a strain rate of less than 50 s^{-1}, but was totally destroyed when the strain rate reached 63 s^{-1} (Cao, Yilmaz and Song, 2018). In our study, however, the FA-GGBS-HMNS based GP paste specimens showed good outstanding resistance at a high strain rate almost three times higher than those reported by previous researchers before they broke completely.
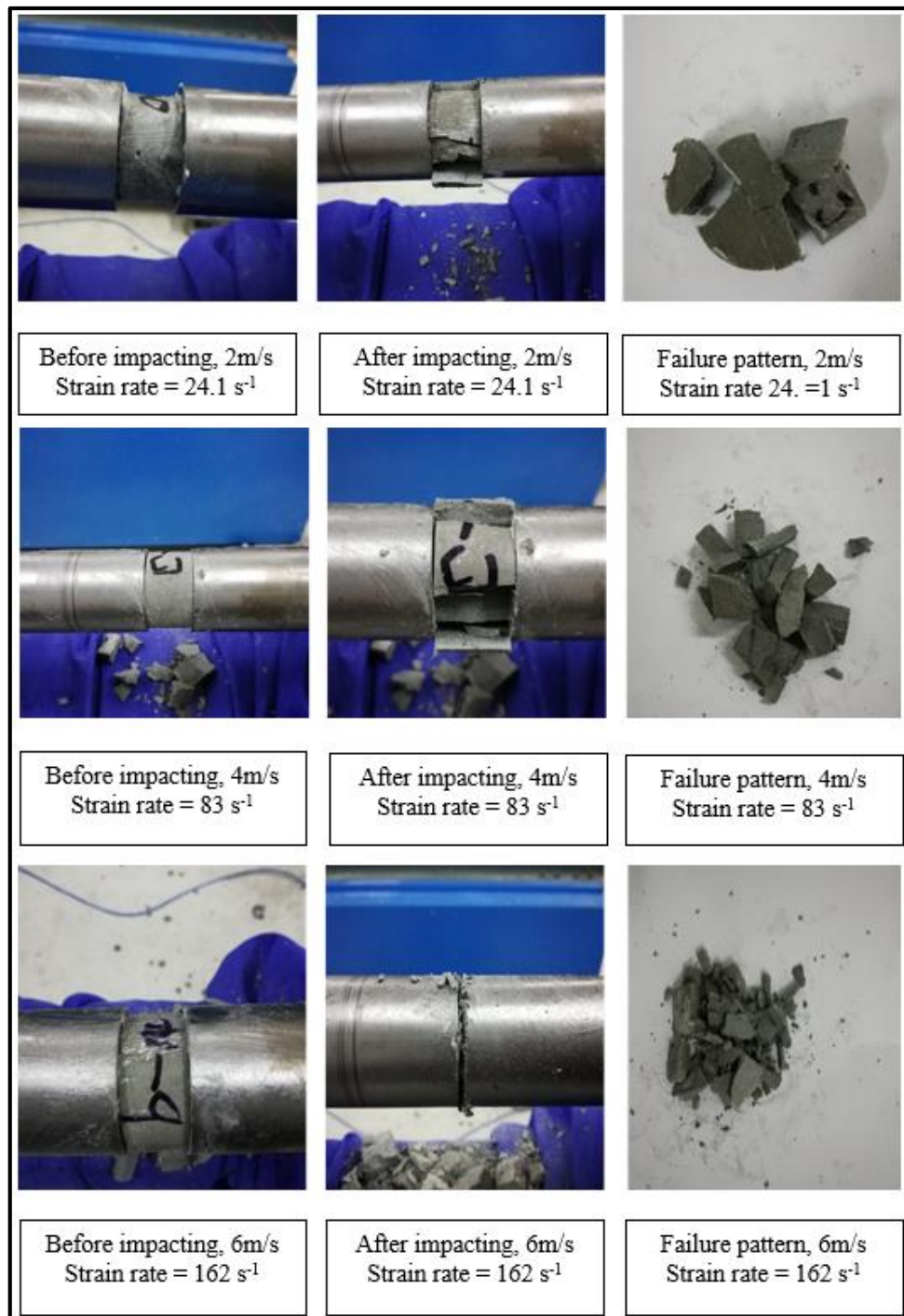
Figure 5.10. Failure modes of FA-GGBS-HMNS GP Paste specimens under different impact velocities and strain rates

5.3.2. Dynamic Compressive Strength

Figure 5.11 reveals dynamic compressive strength against strain rates of FA-GGBS-HMNS based GP paste. From Figure 5.11, it is evident that there is a prominent dependency between the dynamic compressive strength and strain rates, with an approximately linear increase in dynamic strength with strain rates, a part from some evident scatters which can be seen due to the homogeneity effect of the specimens. Some researchers believe that the proportional increase in dynamic compressive strength with strain rates could be related to the creation and dynamic development of micro-interaction. The effect of micro-interactions under high impact loading accelerates the propagation of cracks, subsequently leading to specimen failure within a short time, which is contrary to the one under quasi-static loading (Chen, Wu and Zhou, 2013).
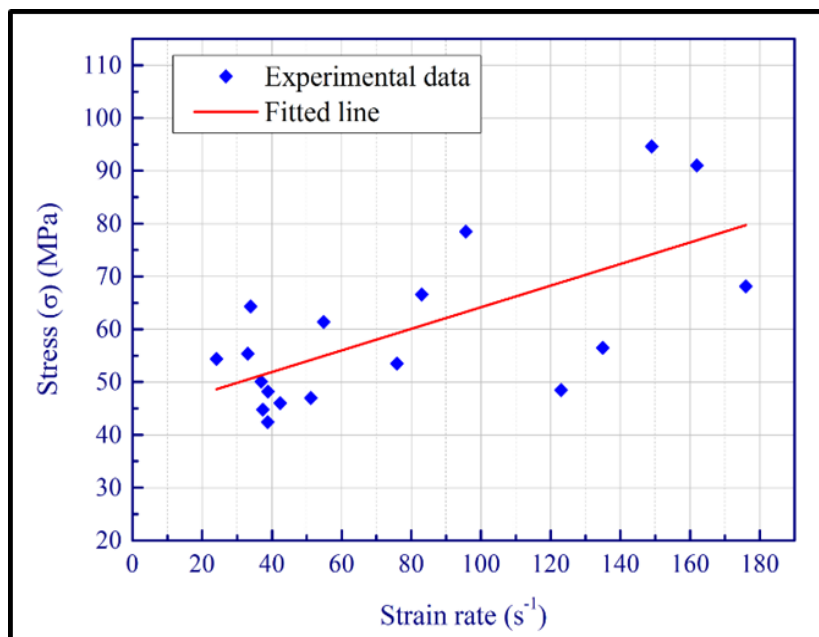
Figure 5.11. The law between dynamic compressive strength and strain rate for FA-GGBS-HMNS based GP paste

It is therefore believed that, the moisture in the cementitious material or so-called concrete-like material plays a significant influence on strain rate sensitivity, which could be an additional effect to the inertial effects of water, increasing the fracture toughness of moist-concrete compared to dry concrete. According to previous studies, there mainly seem to be two reasonable explanations for rate sensitivity; the first related to the viscoelastic of the hardened paste, the second referring to the time-dependent nature of micro-crack expansion (Kim *et al.*, 2010; Chen, Wu and Zhou, 2013). For concrete-like material, it is believed that there is sufficient time for micro-cracks to grow into macro-cracks under quasi-static loading, which can accordingly cause final deformation of the material. Nevertheless, when the specimen is exposed to a dynamic impact loading, more micro-cracks are generated and in a short time develop into macro-cracks, before the specimens ultimately reach complete failure. The development of a large number of both micro and macro-cracks leads to a considerable consumption of energy (see next section, Figure 5.12), subsequently causing higher ultimate strength, which explains why the dynamic compressive strength is greater than that of quasi-static (Su and Xu, 2013).
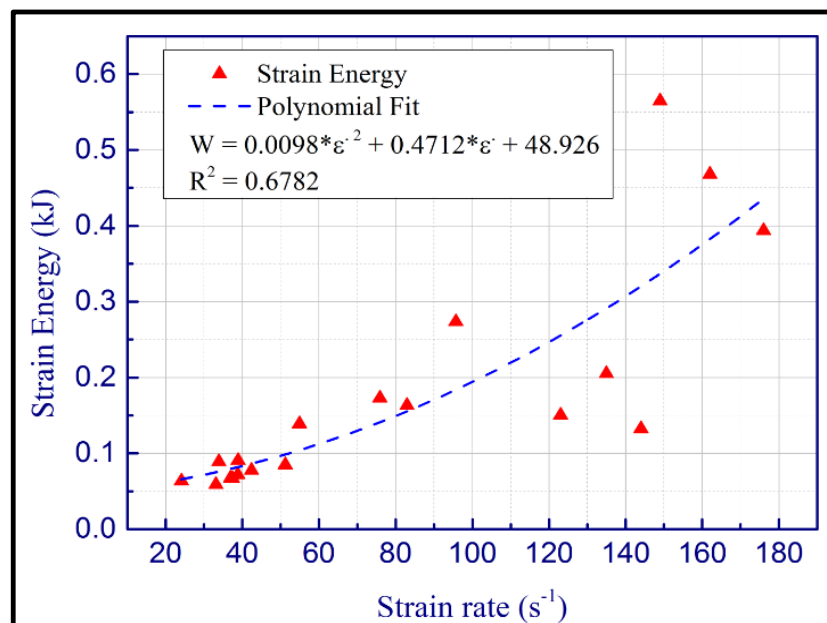
Figure 5.12. Strain Energy (w) versus strain rate of FA-GGBS-HMNS GP paste.

The energy absorbed by the FA-GGBS-HMNS GP paste specimens in the function of strain rate is presented in Figure 5.13. From Figure 5.13, it is obvious that the amount of energy consumed by the GP specimens during the impact test proportionally increases with strain rate, clearly shown by an adequate polynomial fitting line. Further, it can be also seen that at a high strain rate range of 24.1 to 176 s^{-1} the energy consumed ranges from 48.8 .10^{-5} to 85.94.10^{-5} kJ, which indicates that under impact the FA-GGBS-HMNS GP paste reached a good level of toughness. The law between the energy absorbed and the strain rate with respect to the considered range could be written as follows:

$$W_{ab} = -2*10^{-5}\varepsilon^{\bullet 2} + 0.0065\varepsilon^{\bullet} + 0.3059 \ \ with \ R^2 \approx 0.982 \qquad \text{Eq (5.22)}$$

where W_{ab} is the energy absorbed and $\varepsilon^{\bullet}$ is strain rate of the dynamic compressive strength.
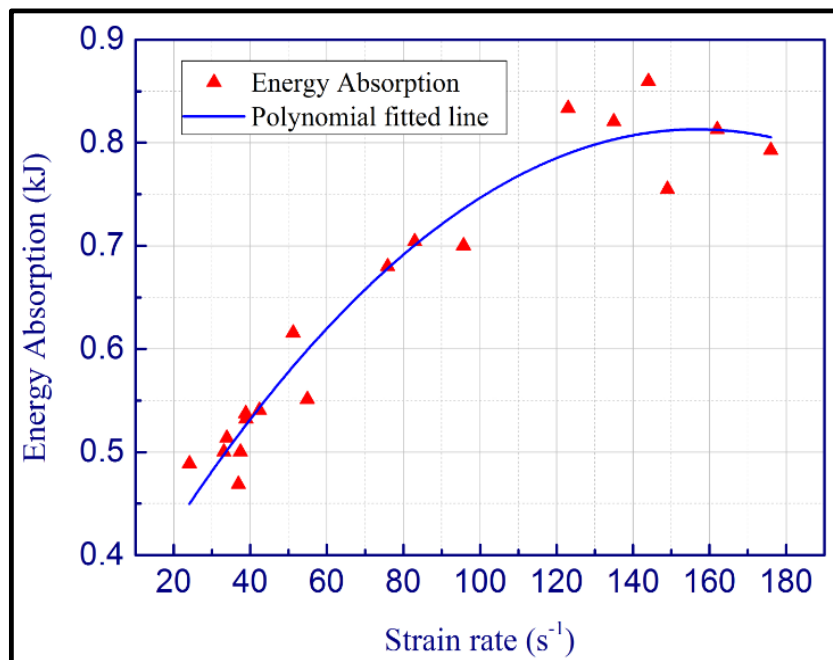
Figure 5.13. Energy absorption of FA-GGBS-HMNS GP paste at different strain rates

5.3.3. Dynamic Increase Factor (DIF)

The effect of strain rate on the compressive strength could be defined as the ratio between the dynamic compressive strength and the quasi-static strength, which is well known as the dynamic increase factor (DIF). As widely reported in previous research, the DIF has been used in order to assess strain rate sensitivity for cementitious materials (Su and Xu, 2013; Ren *et al.*, 2015; Fu *et al.*, 2018; Yang *et al.*, 2018). It is believed that there is a linear relationship between the DIF and the logarithmic strain rate for concrete-like material (Fu *et al.*, 2018). In this study the relationship between the DIF and the strain rate for FA-GGBS-HMNS based GP paste is given by Eq (5.23) as follows:

$$DIF = \frac{DPCS}{\sigma_S} \qquad\qquad \text{Eq (5.23)}$$

where *DPCS* corresponds to the dynamic peak compressive strength and σ_S reflects the peak compressive strength at the quasi-static loading rate. In this study, the conventional rate of loading for 50mm x 50mm x 50mm cubic samples equals 0.57 kN/s, which corresponds to the average peak compressive strength of 48.4 MPa. Apparently, the total stress which will be created in the cubic samples will be higher than that in the cylindrical samples, resulting in higher compressive strength in cubes than cylinders, hence the following Eq (5.24), which describes the relationship between cylindrical and cubic compressive strength (Graybeal and Davis, 2008).

$$Compressive\ strength\ of\ cylinder = 0.96 * Compressive\ strength\ of\ cube \qquad \text{Eq (5.24)}$$

In order to determine the relationship between the DIF and the strain rate for the dynamic compressive strength, the DIF values are calculated based on Eq (5.23) and Eq (5.24) as shown in Appendix C. The variation between DIF and the decimal

logarithm of strain rate is presented in Figure 5.14. From the same figure the linear law between the DIF and the logarithm of strain rate can be expressed by the following Eq (5.25).

$$DIF = A * \log \dot{\varepsilon} + B \qquad \text{Eq (5.25)}$$

where A and B correspond to the correlation coefficients, and $\dot{\varepsilon}$ is the strain rate of the dynamic compressive strength of FA-GGBS-HMNS GP paste.

From the fitting line of the experimental data shown in Figure 5.14 Eq (5.25) can be written as:

$$DIF = 0.657 * \log \dot{\varepsilon} - 0.0748 \qquad \text{Eq (5.26)}$$

In order to compare the DIF of the current study, some DIF expressions have been selected from the literature (Tedesco *et al.*, 1997; Chen, Wu and Zhou, 2013), and plotted in the same figure with the corresponding fitted lines as revealed in Figure 5.14. Two formulae are recalled as follows:

1- The DIF expression proposed by Tedesco et al. (1997) applicable for concrete.

$$DIF_{Concrete} = \begin{cases} 0.000965 * \log \dot{\varepsilon}_d + 1.058 & \text{for } \dot{\varepsilon}_d \leq 63.1 \text{ s}^{-1} \\ 0.758 * \log \dot{\varepsilon}_d - 0.289 & \text{for } \dot{\varepsilon}_d > 63.1 \text{ s}^{-1} \end{cases} \qquad \text{Eq (5.27)}$$

where $\dot{\varepsilon}_d$ is the dynamic strain rate.

2- The DIF expression proposed by Chen et al. (2013) suitable for paste.

$$DIF_{Paste} = 0.10 * \log(\dot{\varepsilon}_d / \dot{\varepsilon}_s) + 1 \qquad \text{Eq (5.28)}$$

where $\dot{\varepsilon}_d$ and $\dot{\varepsilon}_s$ are the dynamic and quasi-static strain rates respectively.
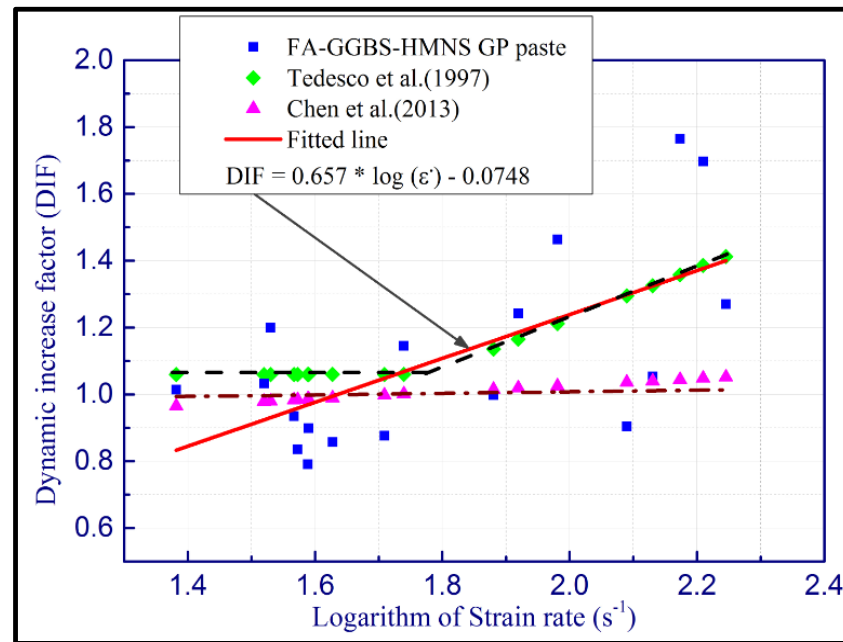
Figure 5.14. The relationship between DIF and the strain rate

It is clear that the above equations are in good agreement with the logarithmic curve of Eq (5.25), while the experimental data displayed in Figure 5.14 fits well with the formulae selected, where high linearity can be observed. But a slight difference can be underestimated of FA-GGBS-HMNS GP paste, which mainly contributes to the effect of the characteristic of the material itself, as both formulae are only applicable to concrete-like material. In other words, the influence of different factors such as chemical compositions, microstructure and the geotechnical characteristics of the material are not considered in the selected equations. However, the proposed formula of the present study mainly reflects the relationship between the DIF and the strain rate. As shown in the same figure, the DIF values of the GP paste increase with the

strain rate, which is confirmed by the significant slope value in Eq (5.26). These viewpoints are also supported by other results reported by (Ren *et al.*, 2015).

5.3.4. Lateral Inertial Confinement

One of the significant influencing factors on the dynamic compressive strength enhancement of concrete with an increase of strain rate is the lateral inertial confinement. In general, the lateral confinement generated as a result of high impact loadings occurs on both surfaces of the specimen and the lateral inertia. It has been reported that concrete-like material shows a high sensitivity to the confining pressure and, further, that the specimens may undergo lateral deformation when subjected to a high-speed impact compression. Therefore, in concrete-like material, the dynamic strength can be influenced by lateral inertial confinement, which also affects the DIF due to the inertial forces (Hao *et al.*, 2013). In the present study, it is strongly believed that the dynamic compressive strength of GP paste specimens is influenced by the lateral inertial confinement. This influence is mainly shown from the different trends of stress-strain curves obtained as revealed in Figure 5.9. The main reason behind this considerable effect is related to the specimens' dimensions, where the diameter-to-length ratio of most specimens is approximately half. This point of view is supported by other studies, where it is reported that the influence of lateral inertial confinement on concrete-like material is sensitive to the specimen-diameter and the material density (Zhang *et al.*, 2009; Hao *et al.*, 2013).

5.4. Summary

This chapter aimed to investigate the dynamic mechanical behaviour of FA-GGBS-HMNS based geopolymer paste under high impact loading. The experimental study of the impact test was conducted using a 40mm diameter SHPB apparatus. A total of 27 GP paste specimens, divided in three groups with diameters of 33, 36 and 37mm and an average thickness of 18.5mm were used in this investigation. The stress-strain curves, failure patterns, strain energy, energy absorption and dynamic increase factor (DIF) of the GP paste were also evaluated. The following points can be drawn, based on the different experimental results analysed and discussed in this study.

- The dynamic compressive strength of the GP paste specimens increases with the increase in strain rate remarkably, where the curves appeared as plateau forms. This is believed to be the result of the influence of the diameter-thickness ratio of the specimens, which is approximately 2 in this study.
- The experimental results revealed an approximately linear increase of the dynamic strength with the strain rates, which showed a strong dependency between the dynamic compressive strengths and the strain rates of FA-GGBS-HMNS GP paste.
- The strain energy and the energy absorbed under different impact velocities increased with strain rates and fitted by adequate polynomial lines.
- A linear relationship between the DIF and the logarithmic strain rate experimentally demonstrated the strain rate sensitivity of the GP paste–like material.
- Different failure modes were observed under different strain rates ranging from 24.1 to 176 s^{-1}, where the specimens are broken into large, small and finely crushed fragments.

Chapter 6‖

Durability of FA-GGBS-HMNS based‖

Geopolymer Concrete/Paste‖

6.1. Introduction

The durability of the FA-GGBS-HMNS based geopolymer concrete is investigated in this chapter. The diffusion of chloride ions is considered the most significant issue in durability of concrete, due to its potential role in the deterioration of the concrete's construction. Concrete's life expectancy is mainly related to its resistivity, in other words, it depends on its durability through inhibiting the ingress of the ions from severely aggressive environments such as seawater. Until now, there have been only limited studies investigating the durability of geopolymer concretes, which undergo deterioration in constructions exposed to, or partially submerged in corrosive and/or marine environments. However, there are many procedures such as Bulk Diffusion Test, Rapid Migration Test (RMT) and Wet Candle Test which could be used to investigate the effect of chloride ions on concrete. To evaluate the durability of the designed geopolymer concrete, a Rapid Migration Test (RMT), also known as Rapid Chloride Permeability Test (RCPT), was carried out in this research due to its visible and rapid results and simple testing procedure.

To better understand the significance of the durability of concrete, Figure 6.1 displays the mechanism of concrete deterioration, which is mainly related to the action of different physical and chemical phenomena. The Corrosion phenomenon of rebar steel in a reinforced concrete is shown in Figure 6.2. This figure also exhibits the diffusivity of different ions such as Cl^- and OH^-, which are the most effective and yet the most harmful particles in terms of concrete damage.
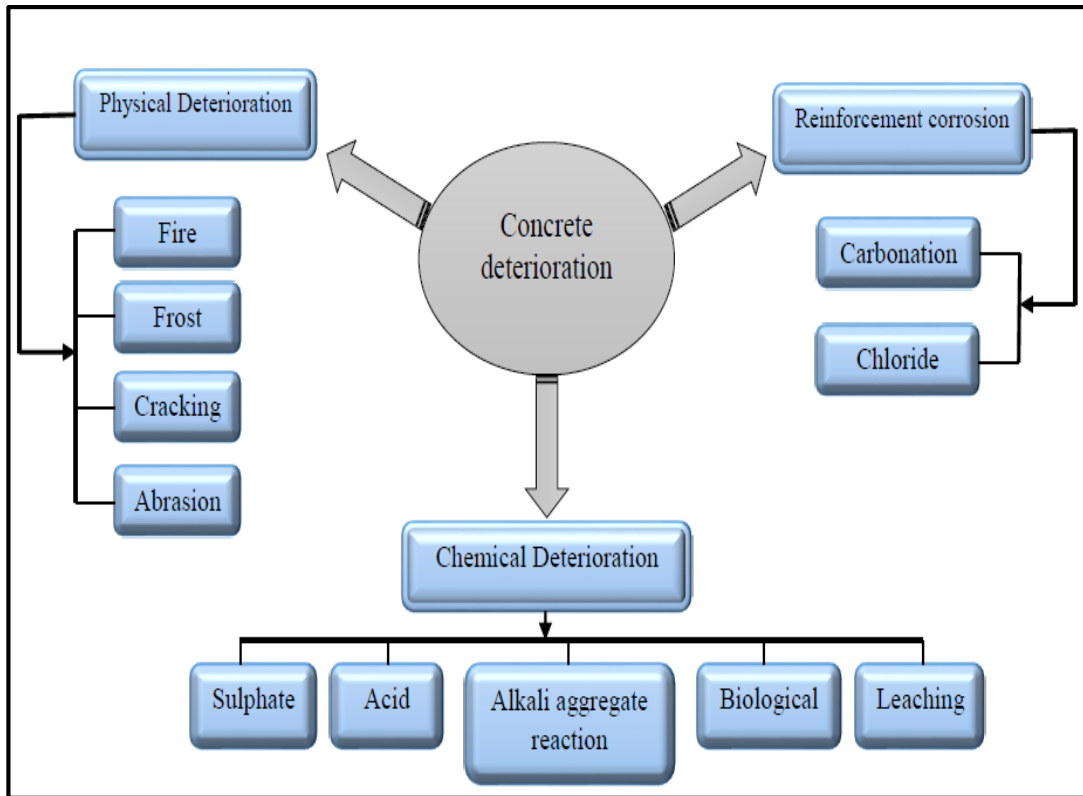
Figure 6.1. Diagram shows the deterioration of reinforced concrete

(Adam, 2009)
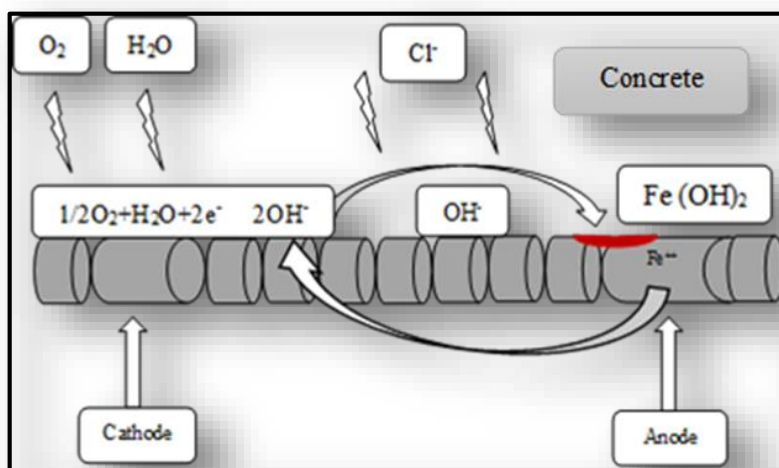
Figure 6.2. Corrosion phenomenon of rebar steel in the concrete

6.2. Materials and Testing

6.2.1. The Rapid Chloride Permeability Test (RCPT)

To investigate the migration of chloride ions onto the manufactured geopolymer concrete, a Rapid Chloride Permeability Test (RCPT) was conducted at the ''Guangdong Provincial Key Laboratory of Durability for Marine Civil Engineering, Shenzhen University'', as indicated above. The test procedure was in accordance with the method described in Nord Test standard (NT Build 492, 1999), which is experimentally used to investigate the migration of chloride ions in a non-steady state, and also to determine the resistivity of concrete by calculating its chloride migration coefficient. This procedure is mainly applicable to hardened cylindrical specimens cast in the laboratory or to drilled cores with a diameter 100mm and a thickness of 50mm. for the test, three samples sliced from a cylindrical specimen with a minimum length of 200mm and diameter of 100mm, were used.

6.2.1.1. Test Procedure

The configuration of the RCPT apparatus is shown in Figure 6.3. The RCPT system, generally is powered by DC potential supply as a cathode and anode connected to negative and positive poles respectively. As shown in Figure 6.3, the catholyte reservoir is filled with 10% by mass of NaCl and 90% by mass of tap water (100g of NaCl for each 900g of water). The anolyte solution in the rubber sleeves is filled with 0.3 M of NaOH in de-ionised water. The specimens are then fitted into rubber sleeves and secured with anti-corrosion pair clamps. The rubber sleeves, therefore, are placed on plastic supports in the catholyte reservoir. Before starting the test, both cathode and anode are connected in series to a multi-meter and the temperature is maintained in the range of 20-25 ℃. The final temperature and current is carefully recorded at the end of the test before the experiment is concluded.

a. Rubber sleeve   e. Catholyte
b. Anolyte   f. Cathode
c. Anode   g. Plastic support
d. Specimen   h. Plastic box
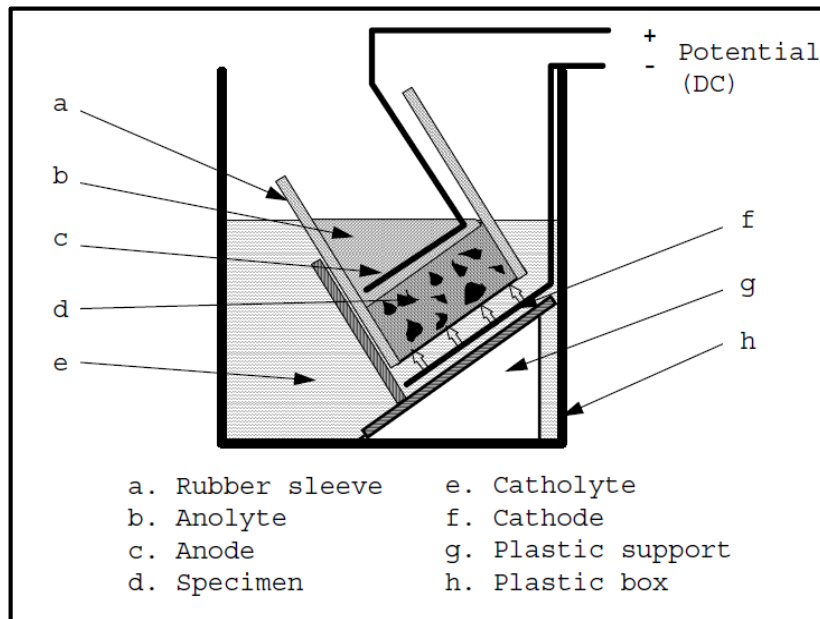
Figure 6.3. RCPT Apparatus

(NT Build 492,1999)

After the required time, mainly determined according to the initial current, the specimens are removed from the rubber sleeves, rinsed with tap water, well dried, and then split axially into two sections. A silver nitrate solution (AgNO₃) of 0.1N is sprayed onto the freshly split sections of the specimens, resulting in a chemical reaction between the chloride and the silver ions as shown in Eq (6.1). After a period of 15 minutes, the white silver chloride precipitation (evident from a change in colour) is clearly visible on the split sections, and by using a ruler and calliper, the measurements of the penetration depth is taken at intervals of 10mm to obtain a minimum of seven measures, as shown in Figure 6.4. The average for the results obtained can then be used for determining the chloride migration coefficient by applying Fick's second law.

$$Ag^+ + Cl^- \rightarrow AgCl\ (white)$$ Eq (6. 1)

However, in the areas without chloride ions, the silver ions react with the hydroxides present in the concrete and form a brownish colour, as shown in Eq (6.2).

$$Ag^+ + OH^- \rightarrow AgOH \rightarrow Ag_2O \, (brown)$$

Eq (6. 2)
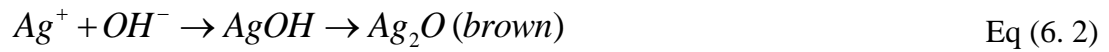
6.2.1.2. Chemical Reactions of Corroded Concrete Caused by Chloride Ions

The penetration of chloride ions into the reinforced concrete could cause corrosion of the rebar steel leading to a deterioration of the concrete structures. The following chemical reactions manifest the reaction between the chloride ions and the main product of the concrete, which is mainly formulated as calcium hydroxide $Ca(OH)_2$.

$$Ca(OH)_2 + 2NaCl \rightarrow CaCl_2 + 2NaOH$$

Eq (6. 3)

$$Ca(OH)_2 + CaCl_2 + H_2O \rightarrow Ca(OH)_2.H_2O.CaCl_2$$
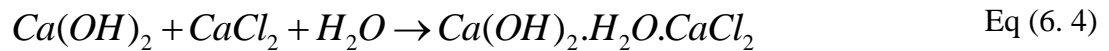
Eq (6. 4)

The product from Eq (6.4), which is called alkaline calcium chloride [$Ca(OH)_2$. H_2O. $CaCl_2$], is the main cause of the destruction of concrete due to its volume expansion during the crystallization process. Further, the steel reinforcement of the concrete could also be affected by the chloride ions (Cl^-). The presence of these chloride ions contributes to a chemical reaction with the iron and produces ferric chloride ($FeCl_2$), which in turn reacts with the water to create what is called rust [$Fe(OH)_2$] and also hydrochloric acid (HCl). The hydrochloric acid affects the reinforcing steel bars by forming pits and cavities on their surface. Eqs (6.5) and (6.6) below detail the main chemical reactions which occur between the iron and chloride ions:

$$Fe + 2Cl^- \rightarrow FeCl_2 + 2e^-$$

Eq (6. 5)

$$FeCl_2 + 2H_2O \rightarrow Fe(OH)_2 + 2HCl$$

Eq (6. 6)
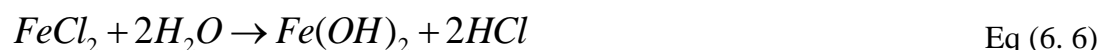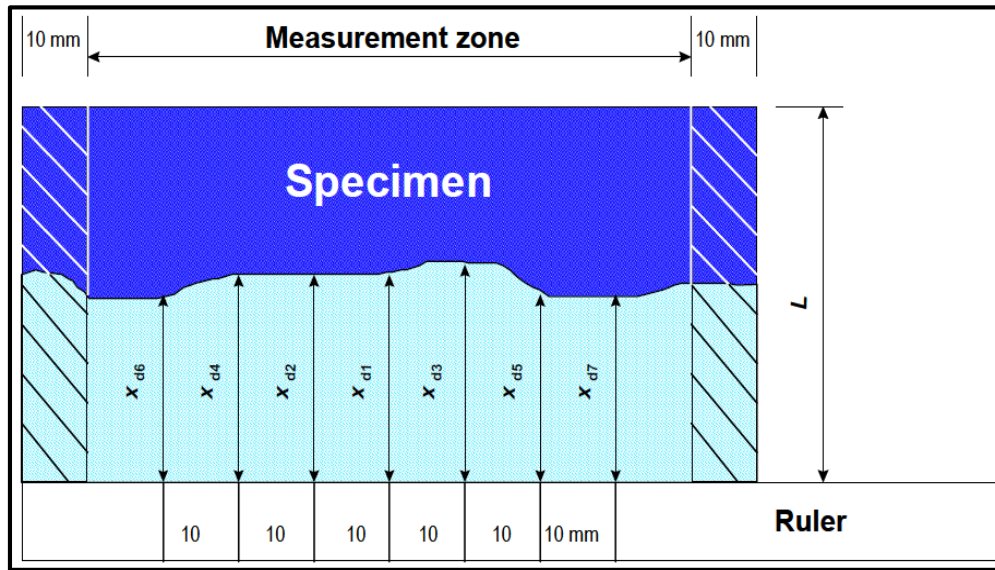
Figure 6.4. Measurements for chloride penetration depths

(NT Build 492, 1999)

Table 6.1. Test voltage and duration-NT Build 492 method

(NT Build 492, 1999)

Initial current I 30v (with 30v)(mA)	Applied voltage U (after adjustment)(V)	Possible new initial current I_0 (mA)	Test duration t (hour)
$I_0 < 5$		$I_0 < 10$	96
$5 \le I_0 < 10$	60	$10 \le I_0 < 20$	48
$10 \le I_0 < 15$		$20 \le I_0 < 30$	
$15 \le I_0 < 20$	50	$25 \le I_0 < 35$	
$20 \le I_0 < 30$	40	$25 \le I_0 < 40$	
$30 \le I_0 < 40$	35	$35 \le I_0 < 50$	
$40 \le I_0 < 60$	30	$40 \le I_0 < 60$	
$60 \le I_0 < 90$	25	$50 \le I_0 < 75$	24
$90 \le I_0 < 120$	20	$60 \le I_0 < 80$	
$120 \le I_0 < 180$	15	$60 \le I_0 < 90$	
$180 \le I_0 < 360$		$60 \le I_0 < 120$	
$I_0 \ge 360$	10	$I_0 \ge 120$	6

6.2.1.3. Experimental Work

The method is straightforward and physically shows the penetration depth of the chloride ions into the fabricated FA-GGBS-HMNS based geopolymer concrete. The RCP test was performed in accordance with the NT Build 492 method as mentioned in section 6.2.1. Three cylindrical specimens of 100mm in diameter and 200mm in length, as shown in Figure 6.5b, were prepared and cast in a similar way to the designed GPC detailed in Chapter three. Then the samples were kept at a room temperature of 20±2ºC and a relative humidity of 40-50%. A total of six discs of 100mm diameter and 50mm thickness were sliced from the GPC cylinders by taking out both edge surface of each cylinder. After cutting, the surface of the specimens was washed using tap water and then dried utilising soft paper (Figure 6.5a). The sliced specimens were saturated in a desiccator at a pressure in the range of 10-50 mbar for around 3 hours, as presented in Figure 6.6. Further, a saturated $Ca(OH)_2$ solution was poured into the desiccator until the specimens were visibly immersed as illustrated in Figure 6.7a. The specimens in the system were then maintained and left for 18±2 hours before being transferred to the RCPT cells.

Figure 6.7b displays the RCPT montage. After fixing all the tests preconditions and preparations, the voltage was set at 30V and the initial current, which passed-through each individual sample, was subsequently adjusted. The initial temperature of each electrolyte solution was recorded using a thermometer, then the appropriate test duration was set according to the initial current recorded, as given in Table 6.1. Before disconnecting the test, the final temperature and current were carefully recorded, due to the necessity for calculating the chloride migration coefficient. Afterwards, the test was stopped and each specimen was removed from the rubber sleeves, rinsed with tap water, well-dried with soft paper and axially split into two perpendicular sections (see Figure 6.8). In order to measure the depth of chloride penetration, a silver nitrate solution of 0.1M as a colourimetric indicator was sprayed onto the freshly split cross-sections of each specimen. These specimens were left for around 15 minutes with the purpose of giving the silver nitrate time to react with the chloride ions and to formulate

a silver chloride product which was visibly precipitated as a white colour, as shown in Figure 6.8. Seven measurements were selected in accordance with the NT Build 492 procedure and as shown in Figures (6.4) and (6.8). The average of the results obtained, therefore, was used in order to determine the non-steady-state chloride migration coefficient, as exhibited in Eq (6.7).
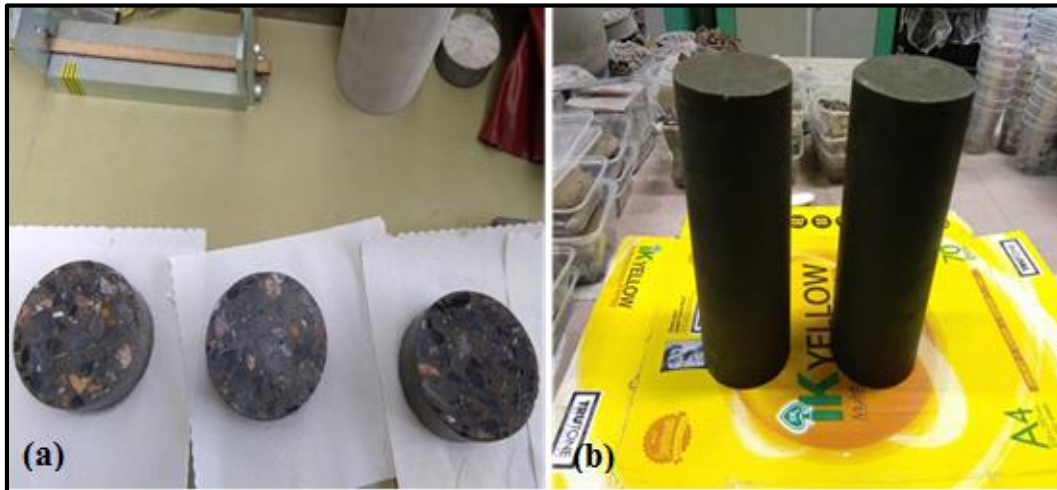
Figure 6.5. (a) Sliced discs, (b) FA-GGBS-HMNS based GPC cylinders

Figure 6.6. Vacuum desiccator system

Figure 6.7. (a) Immersed specimens in saturated $Ca(OH)_2$, (b) RCPT montage
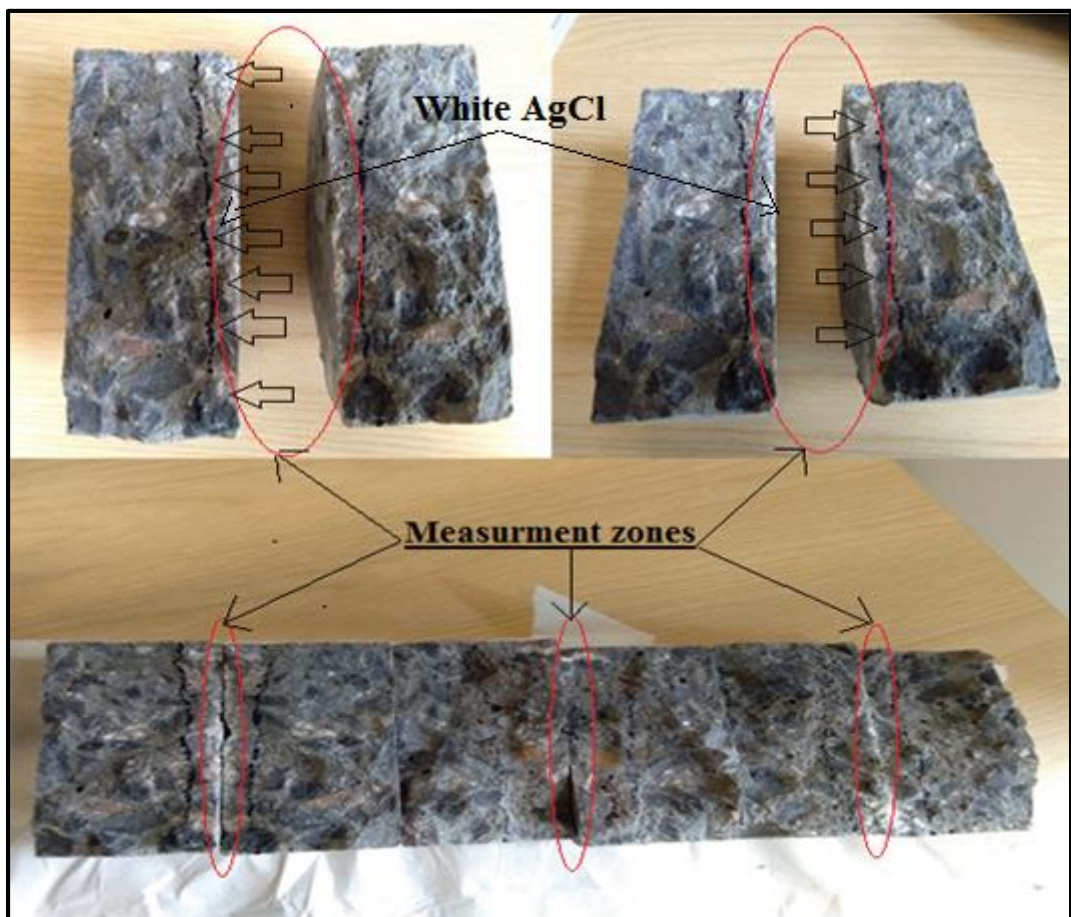
Figure 6.8. Chloride depth measurements from split sections
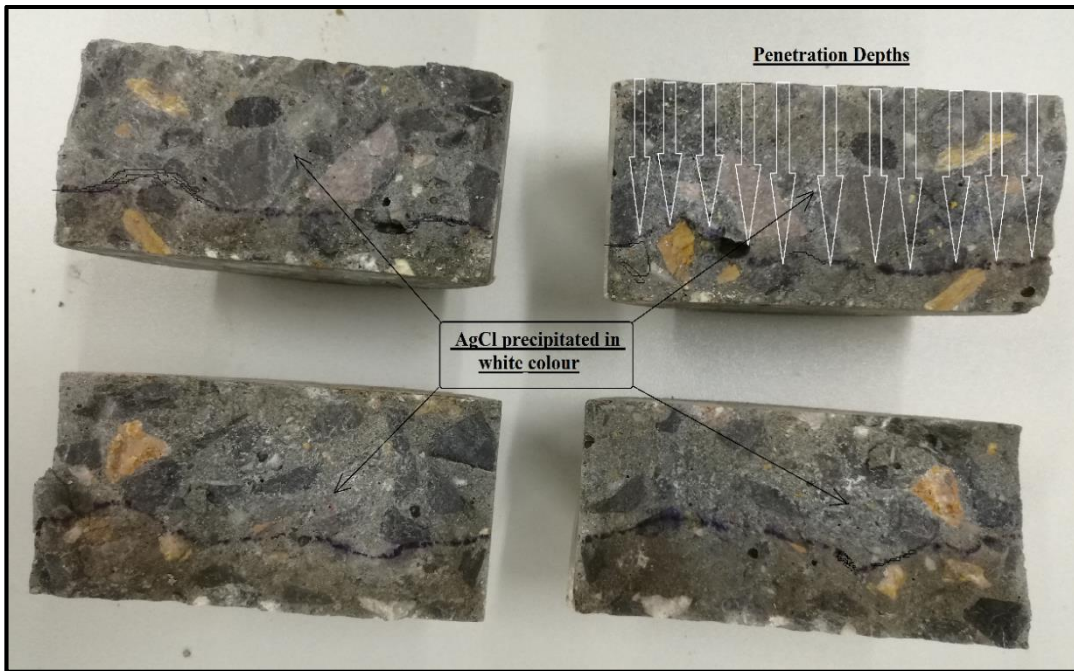
Figure 6. 9. Precipitation of chloride ions as a white colour of AgCl

6.2.1.4. Expression of the Chloride Migration Coefficient

The chloride diffusion coefficient, or the non-steady-state migration coefficient, in the saturated GPC is calculated applying the following formula, as given by the NT Build 492. The calculation is mainly based on the average value of the initial and final temperatures of the electrolyte, the voltage and the average of the measured depths of the penetration of chloride ions.

$$D_{nssm} = \frac{0.0239(273+T)*L}{(U-2)*t}\left(X_d - 0.0238\sqrt{\frac{(273+T)*L*X_d}{U-2}}\right) \qquad \text{Eq (6.7)}$$

where;

D_{nssm} is the non-steady-state migration coefficient [$\times 10^{-12}$ m^2/s],

U is the absolute value of the applied voltage [V],

T is the average value of the initial and final temperatures in the electrolyte solution [°C],

L is the thickness of the specimen [mm],

X_d is the average value of the penetration depths [mm],

t is the test duration [hour].

The non-steady-state migration coefficient (D_{nssm}) is used for estimating the resistivity of the FA-GGBS-HMNS based geopolymer concrete to the chloride ions penetration, in accordance with the criteria illustrated in Table 6.2.

Table 6.2. Estimation criteria for the resistance of concrete to chloride ion penetration (Jozwiak-niedzwiedzka, 2009; Zych, 2014)

Chloride migration coefficient D_{nssm} [m^2/s]	Resistance to chloride ion penetration
$< 2 \times 10^{-12}$	very good
$2 - 8 \times 10^{-12}$	good
$8 - 16 \times 10^{-12}$	acceptable
$> 16 \times 10^{-12}$	unacceptable

6.3. Results and Discussions

6.3.1. Chloride Penetration

The migration of chloride ions was assessed through an accelerated chloride migration test, which is standardized as NordTest method NT Build 492, as detailed in the previous sections. This method is principally based on electrically forcing chloride ions to migrate through concrete specimens, by applying an external electrical potential, as shown in Figure 6.3.

6.3.1.1. Chloride Migration Coefficient

The non-steady-state chloride migration coefficient was calculated by using Eq (6.7), as specified in NordTest protocol and by using specimen discs 50mm thick and 100mm in diameter, sliced from cylindrical FA-GGBS-HMNS based geopolymer concrete cured for 75 and 210 days. Afterwards, colorimetric analysis was applied to measure the penetration depths of chloride ions into the concrete discs. The visible boundary which occurred between the silver nitrate and the chloride ions on the fresh GPC sections provides experimental measurements of the chloride penetration depths. The silver chloride (AgCl) formed can either be seen as a white colour, due to the presence of chloride ions, which is the case shown in Figure 6.9, or can be precipitated as brown silver oxide (Ag_2O), when OH^- ions occur in pore solution, as presented in Eqs. (6.1) and (6.2). In this study, therefore, the penetration depths, with the corresponding chloride migration coefficients, are obtained from the average values of three samples, as presented in Table 6.3.

From a chemical aspect, chloride ions penetrated into concrete specimens could be present in two forms as either bound or free ions. The free chloride is generally water soluble, meaning it moves freely and causes corrosion of reinforcement. However, bound chlorides, which could be physically or chemically bound, typically are

inactive, and do not take part in steel corrosion processes (Ismail *et al.*, 2013). In this study, it is believed that the interaction which occurred between the chloride ions and the matrix of the FA-GGBS-HMNS based GPC has been present in two features: as a chemical reaction with most of the gels formed during the geopolymerization process (C-S-H and A–S–H gels), or taking place on the surface of those gels due to a physical phenomenon known as surface adsorption phenomenon. In this respect, some researchers have reported that during the migration test, the pH of the pore solution in concrete could be changed. This is due to the migration with Cl$^-$ ions of various ions such as OH$^-$, which are extremely hard to distinguish from both physically and chemically bound chlorides in concrete (Glass, Reddy and Buenfeld, 2000; Spiesz, Ballari and Brouwers, 2012).

Figures (6.8) and (6.9) show chloride penetration depths measured at the end of the RCP test, and the precipitated silver chloride as a white colour visibly observable on the splitting surfaces of FA-GGBS-HMNS based GPC. The penetration depths are marked using black lines, as displayed in the figures, where the chloride ingress starts at the top side of each single specimen as shown by the light white arrows. It can be observed that the designed FA-GGBS-HMNS based GPC reveals a maximum average penetration depth of chloride ions, of approximately 11.60 mm and 40.47 mm (Appendix D) for specimens cured at 75 and 210 days respectively. The low penetration depths, for those samples cured at 75 days are believed to be due to the attribution of the dense ternary C-S-H, A-S-H and C-M-S-H gels which formed in this material, as described in the mechanical and microstructural Chapters three and four respectively. The ternary forming gels, therefore, play a significant role and reducing (or even preventing) the penetration of chloride ions into the designed GPC. In this case, the chloride migration coefficient corresponds to the determining depth, exhibiting a good results of 0.66 x 10^{-11} m^2/s, as presented in Table 6.3, which is in fact, very promising results when compared to the criteria shown in Table 6.2. A previous study by Ismail et al. (2013) stated that, an alkali-activated slag mortar with 25% of slag had shown a maximum chloride penetration depth of around 15 mm in comparison to that with 50% of slag.

Nevertheless, full chloride penetration was observed for all the samples tested with an applied voltage of 20V for 24 hours at 210 days of curing. This is assumed to be due to the high energy potential which accelerates the migration process and increases the free movement of chloride ions in GPC. Certainly, those GPC specimens, which have been subjected to a high electrical potential of up to 20V during the RCP test to speed up the migration process, can provide a reasonable description regarding the porosity of the material produced. However, it is noted that the chloride penetration level is confined within the thickness of specimens, when the electrical potential is reduced to 15V, with an average depth of 37.21mm, and with a corresponding chloride migration coefficient of 3.94×10^{-11} m^2/s, as revealed in Table 6.3 for those samples at 210 days of curing. With an increase in D_{nssm} of approximately 83%, the level of chloride penetration changes from good at 75 days to unacceptable at 210 days of curing. This increase in D_{nssm} could be due to the following reasons;

i)   the continuity of geopolymerization reaction, which led to the formation of more porous (N)-A-S-H gel from the unreacted fly ash as a major contributor material with 70% in the geopolymeric mixture. It has been stated in a previous study that the excess of fly ash leads to the creation of highly porous N-A-S-H gel, which in turn affects the resistance to the chloride ions (Ismail *et al.*, 2013, 2014).

ii)   the fineness of the other materials used also has a significant impact on the chloride diffusion coefficient. It can be seen from section 3.2 of Chapter three, that both GGBS and HMNS materials have average (X_{50}) particle sizes of 138 μm and 280 μm respectively. These averages are high when compared to that of FA (17.37 μm). Furthermore, it has been reported that sieving the precursor materials through a 0.125 mm sieve significantly decreases the D_{nssm}, which increases with increasing of fly ash amount (Marks, Glinicki and Gibas, 2015). Other researchers have stated that much finer material can be considered a physical filler in the capillary pores, which can lead to a reduction in the capillary absorption level (Matos and Sousa-Coutinho, 2012).

iii)   the chemical reaction which occurs between silver nitrate and hydroxide ions in the pore solution, where the precipitated white layer can be a mixture of silver chloride and silver oxide, consequently leading to different chloride depths. These differences are mainly dependent on factors such as the nitrate concentration and the pH of the pore solution, which also change due to the migration of various ions other than those of chloride, as schematised in Figure 6.10.

Remarkable outcomes have been noticed from this part of the study. Although FA can improve the engineering properties of the GPC, excessive amounts can lead to an increase in the porosity of the material, due to the formation of porous A-S-H gel. This gel phase dominates the gels structure in the systems, which in turn has a significant effect on chloride permeability. The use of a high electrical potential during the RCP test provides significant information regarding the material's porosity and demonstrates not only the chloride ions, which migrate through the specimens, but also other ions such as OH^-, Na^+, K^+, Ca^{++}, Mg^{++}. The migrated ions precipitate in the pore solution and later react with the sprayed silver nitrate to appear as a browner rather than a whiter colour which normally forms due to the reaction of chloride with silver nitrate. Further, the physical migration of those ions causes a change in the pH environment, in other words the high concentration of the alkaline activator solution and the presence of a considerable amount of FA increase the OH^- ions in the solution, significantly affect the pH of the pore solution, and subsequently influencing the penetration depth level.

Table 6.3. Chloride penetration depth and the corresponding chloride migration coefficients

Specimen	Average Depth [mm]	Temperature [Cº]	Applied voltage U [V]	Chloride migration coefficient D_{nssm} [x10^{-11} m^2/s] at 75 days
1	11.60			0.66
2	7.10			0.55
3	9.40			0.77
Average	9.37	18.2±2	15	0.66
Specimen	Average Depth [mm]	Temperature [Cº]	Applied voltage U [V]	Chloride migration coefficient D_{nssm} [x10^{-11} m^2/s] at 210 days
1	NA		20	NA
2	33.96			3.57
3	40.47			4.31
Average	37.21	20±2	15	3.94

Figure 6.10. A proposal model explains the migration of Cl⁻ and other different ions during RCP test

6.4. Summary

This chapter aimed to evaluate and investigate the effect of combining ternary materials on the durability of FA-GGBS-HMNS based geopolymer concrete. An experimental study on durability has been conducted applying RCPT in accordance with NT Build 492 protocols.

Further, when the specimens were tested at 75 and 210 days of curing, different trends were achieved as earlier discussed. The NT Build 492 procedure is considered a feasible test which accelerates the migration process of chloride ions, during the assessment of the durability of the designed GPC. A lowest chloride diffusion coefficient was found to be for the samples cured at 75 days, as compared to those samples cured at 210 days. This difference is believed to be due to the influence of the following factors:

- The fineness of the precursor materials used, in particular GGBS and HMNS, where, at 138 and 280 μm respectively, the average particle size (X_{50}) was considerably higher than that of FA, which is less than 20 μm.
- The continuity of the geopolymerization process, which takes place between the FA particles, a major material in the mixture, and the activator solution, leading to the formation of more porous A-S-H gel.
- The pH changes that occurred in the pore solution of the mixture, due to the migration of different ions from the system. This migration affects the concentration of the pore solution, then the permeability depths.

In spite of a high alkali concentration (12M), the coefficient of diffusion drastically increased after 210 days of curing. This increase can be related to the excess of OH⁻ released in the mixture, which later took a place in the pore solution as free ions, and then affected the diffusion phenomenon. Therefore, the durability of the manufactured

GPC material can be successfully improved by considering the above stated parameters.

Chapter 7

Thermal Stability of FA-GGBS-HMNS based Geopolymer Paste

7.1. Introduction

This chapter presents the effect of elevated temperatures up to 900ºC on the compressive strength of FA-GGBS-HMNS based geopolymer paste. As widely reported in previous research, geopolymers have excellent fire resistance compared to conventional OPC. Therefore, from this framework, much research has been done on the incorporation of geopolymers, using different by-product materials such as FA, GGBS, Metakaolin, and Rice Husk, etc. However, combining more than two materials to synthesise geopolymers is not yet common, and to date no study of this concept has been found. Currently, most geopolymer materials are synthesized, based on the use of an individual by-products, such as FA, or by using bi-materials, (i.e. by combining two precursor materials, such as FA with GGBS, or Metakaolin with GGBS, at the same time). This study exhibits the successful experimental work of synthesizing geopolymers through a novel synthetic approach, mainly based on combinations of the ternary materials FA, GGBS and HMNS.

The manufactured geopolymer material provides significant improvements in both mechanical and microstructural properties (Chapters three and four). To ensure the feasibility of the proposed mix-design, and expanding its field of application, a thermal resistance test was carried out. The proposed mix design, therefore, was subjected to a series of heat tests, ranging from 200 to 900ºC, to assess its stability and fire resistance.

The author believes that the incorporation of HMNS as a binder in the mix-design could contribute to an improvement in the engineering properties of the geopolymer material produced, in particular, to its compressive strength and microstructure characteristics. This chapter investigates the strength loss of the designed GP paste after exposing it to various elevated temperatures (up to 900ºC).

7.2. Materials and Testing

The chemical composition and morphological structures of the raw materials used in this investigation are shown in Table 3.2 and Figure 3.2 of Chapter three. Class F FA and GGBS were obtained from the Manjung power plant at Perak in Malaysia, and the steel plant in Penang, Malaysia respectively. HMNS was sourced from the steel plant in Shaanxi, China (Mainland). FA is mainly glassy, with the presence of different crystalline phases in the form of quartz and mullite. GGBS is glassy, with considerable crystalline phases, mainly consisting of quartz and calcium carbonate. HMNS is mainly glassy, with significant semi-crystalline phases, and some crystalline presence in the form of protoensatite, albite and forsterite nikeloam. The activator solution is a mix of sodium silicate and sodium hydroxide with a ratio of 2.5. The sodium hydroxide concentration used was 12 M, and prepared 24 hours prior to being used in the experimental work. The technical grades of both alkali solutions are illustrated in Tables 3.4 and 3.5.

7.2.1. Mix Proportion and Manufacturing of Geopolymer Paste

The geopolymer paste was manufactured by mixing class F FA, GGBS and HMNS with the activator solution in a binder-to-liquid ratio of 2.0 as shown in Table 3.6. The ternary raw materials were dry-mixed for 3 minutes, then mixed with the activator solution until a visible homogenous geopolymer paste was achieved. The geopolymer paste, therefore, was transferred into cubic moulds measuring 50mm x 50mm x 50mm and vibrated using a vibration table for 30 seconds, to avoid any formation of air-bubbles due to the high viscosity of the mixture. The cubes of fresh geopolymer paste were then wrapped in a plastic film and kept at a room temperature of 25±2ºC and a relative humidity of 85-90% to be cured before being tested.

7.2.2. Thermal Resistance Testing Method

The thermal resistance of the geopolymer paste was evaluated by measuring the compressive strength changes after exposure of the specimens to high temperatures ranging from 200 to 900℃, this experimental work was conducted in ''Guangdong Provincial Key Laboratory of Durability for Marine Civil Engineering, Shenzhen University''. The diagram in Figure 7.1 displays the thermal scheme of the experiment. Samples selected for the test were heated in an electrical oven (see Figure 7.2a), the temperature, controlled by an auto-temperature regulator, rising by 6 ℃/min to 200℃, as shown in Figure 7.2b. The specimens were held for 2 hours, as presented in Figure 7.3, to ensure that the cubes were well-heated and the heat homogeneously diffused. The specimens were then left in the furnace and naturally cooled to room temperature. This operation was repeated for each of the temperatures 300, 400, 500, 600, 700, 800 and 900℃, and the heating rate was kept the same at 6 ℃/min, with a two hour heating period in the oven. Before and after heating, the compressive strengths of the GP specimens were recorded, using a universal mechanical testing machine, with a compression rate of 0.3 kN/s, as shown in Figure 7.2c.
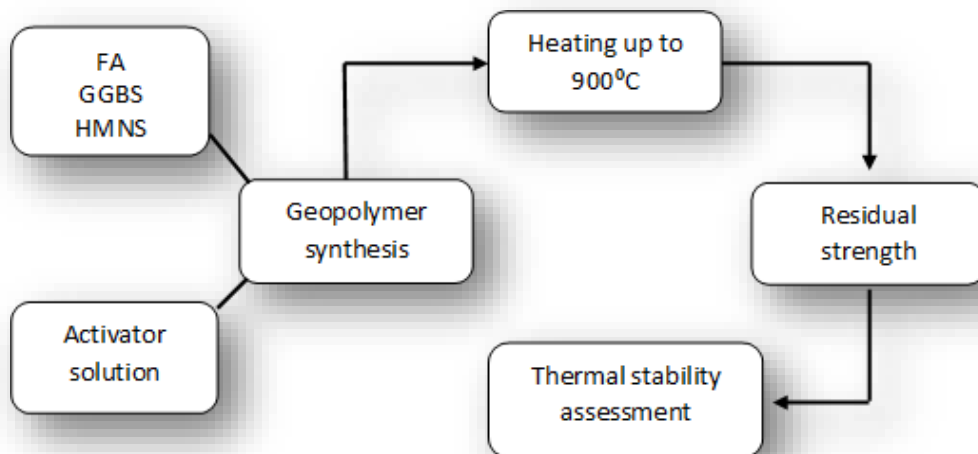
Figure 7.1. Diagram presents the experimental thermal steps

Figure 7.2. (a) Electrical Oven, (b) Auto-temperature regulator, (c) Universal mechanical machine
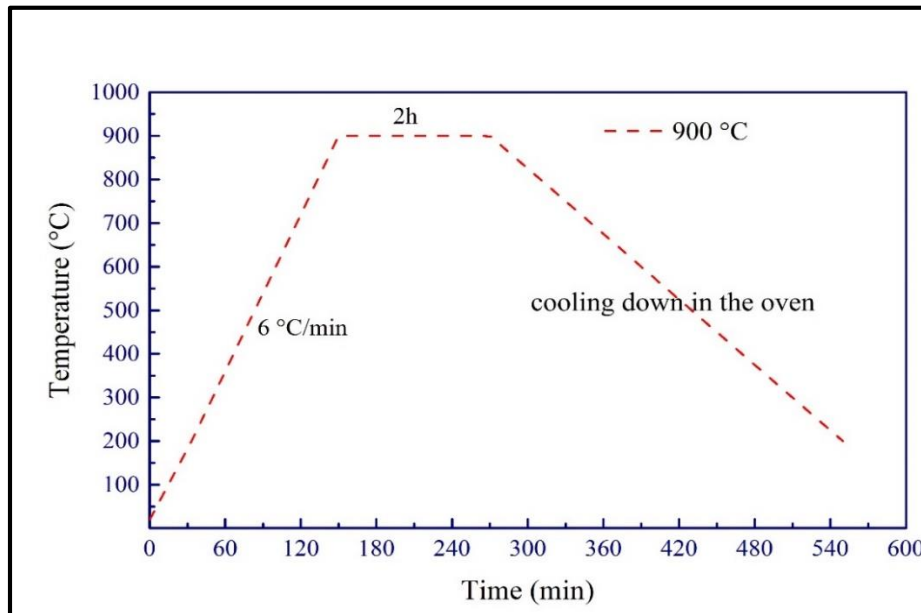
Figure 7.3. The heating curve at different temperatures

7.3. Results and Discussions

7.3.1. Thermal Studies

The effect of high temperatures on the compressive strength of the GP paste after 210 days of curing is presented in Table 7.1. The thermal test was conducted by measuring the compressive strength lost after exposure of the specimens to temperatures ranging from 200 to 900°C. The standard errors and the reduction rates associated with the compressive strengths measured, are also displayed in Table 7.1.

Table 7.1. Residual compressive strength after temperature exposure

Temperature (°C)	Residual compressive strength (MPa)	Standard Error	Reduction rate (%)
ambient (20 °C)	48.40	2.4205	-
200	49.84	2.492	-2.96
300	31.19	1.56	35.54
400	31.05	1.5525	35.84
500	31.94	1.597	34.00
600	22.97	1.1485	52.53
700	21.82	1.091	54.91
800	22.42	1.121	53.66
900	20.56	1.028	57.52

7.3.2. Effect of Temperature on Compressive Strength

Figure 7.4 shows the effect of temperature changes on the compressive strength of the designed GP paste cured after 210 days. It can be seen from the figures that the compressive strength slightly increased with temperature after being heated to 200°C from 48.4 MPa to 49.84 MPa, with a reduction rate of -2.96%. The negative sign

indicates that the heated GP paste specimens gained around 3% of their strength when heated to 200ºC compared to the original strength value measured at ambient temperature. Comparable results have been reported by other researchers which showed that the strength of geopolymers increased when heated to temperatures between 90 to 200ºC (Okoye, Durgaprasad and Singh, 2015; Zhang *et al.*, 2015; Türkmen *et al.*, 2016). The main reason for the increase in the compressive strength of FA-GGBS-HMNS based geopolymer paste at 200ºC is considered in this study to be due to the promotion of a polycondensation phase, occurring between various gels formed when the heat stimulates the unreacted particles to create supplementary across-links.

A remarkable decrease in the strength (approximately 35.5%) seen when the GP samples are exposed to 300ºC. This large strength loss is a consequence of physical and chemical changes and can also be attributed to the decomposition of certain microstructural phases. It has been stated by other researchers that the larger strength loss may be caused by the de-hydroxylation of Ca-containing products, formed in the matrix during geopolymerization (Bernal *et al.*, 2011; Zhang *et al.*, 2015). Afterwards, the strength stabilizes between 300 and 500ºC with a slight increase at 500ºC, where some changes in colour were observed as shown in Table 7.2. The reduction in compressive strength after heating at 500ºC, is fairly due to the decomposition of calcium hydroxides, mostly occurring between 400 and 500ºC (Türkmen *et al.*, 2016). When the samples were subjected to 600ºC, the compressive strength dropped slightly to 22.97 MPa. Some studies have reported that heating to 600ºC significantly reduced the compressive strength due to several factors, such as the length of time spent in heating to elevated temperatures, and the evaporation of the moisture formed during geopolymerization, as revealed by the FTIR analysis in Chapter four (Türkmen *et al.*, 2016). The compressive strength then kept its stability after being subjected to temperatures of 700, 800 and 900ºC, and shows a further reduction at 900ºC associated with colour changes.

However, after the GP paste specimens were heated to 900ºC, their compressive strength achieved the lowest value of 20.56 MPa, with a reduction rate of 57.52%. This decrease in residual compressive strength is mainly attributed to the late evaporation of water molecules, which in turn results in pore pressure, caused by the high steam pressure at the elevated temperature. In other words, the high pressure of the internal-pores increased the pore size, subsequently expanding their connectivity and distribution in the GP matrix. This physical-expansion significantly influenced the residual compressive strength, by reducing its value after temperature exposure. It has been reported in other studies that exposing alkali activated fly ash / slag mixtures to high temperatures (above of 600ºC) results in a considerable degradation of compressive strength. This was explained by the high capillary tension resulting from the growing shrinkage in the geopolymeric system (Fan *et al.*, 2017; Yang *et al.*, 2017). Further, the formation of Na-Al(Mg)-Si-H gel sourced from HMNS, as revealed by the SEM/EDX analysis in section 4.22 of Chapter four, contributes to the enhancement of the thermal stability of the GP matrix. The Na-Al(Mg)-Si-H gel, generally is dense and consists of less morphological porous, when compared to the (N)-A-S-H gel phase which formed from FA. The compactness phase could be the main reason for the thermal stability of GP paste being maintained during the heating process at high temperatures (Yang, Yao and Zhang, 2014; Yang *et al.*, 2017).

A clear comparison of residual compressive strength values can be observed in Figure 7.4. Under most circumstances, the GP paste shows good thermal stability, and up to 900ºC exhibits the highest residual compressive strength, when compared to other mixes, including OPC. Even though the FA-GGBS-HMNS GP showed a sharp decrease in strength at 300ºC, its strength after that remains stable other than slightly decreasing at 600ºC, as previously mentioned.
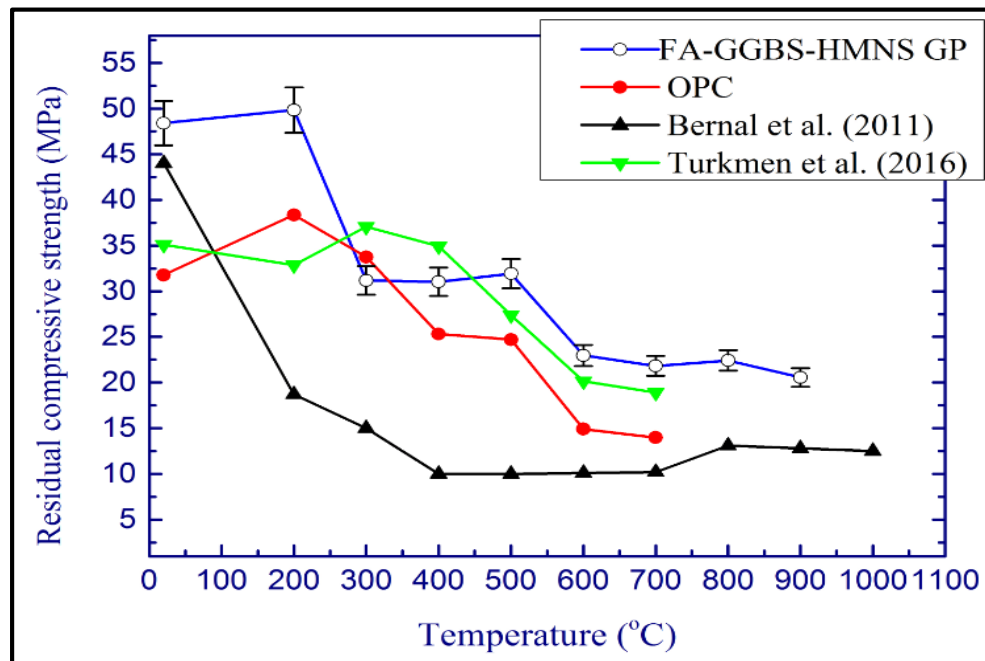
Figure 7.4. Residual compressive strength of the GP paste produced after exposure to high temperatures

7.3.3. Visual and Physical Changes in Paste Specimens

When, during the heating process, specimens were subjected to temperatures above 500ºC, a change in physical appearance was observed. Table 7.2 shows that the GP specimens exhibited remarkable colour changes from the initial grey colour to a clear-orange colour after heating, with a further change to a clear-red colour noticed at 900ºC. These differences of colour and the appearance of cracks are mainly due to the chemical transformation of the content of iron compounds present in the geopolymeric system. The geopolymeric mixture consists approximately 19% of iron oxides (Fe_2O_3), as proven by the X-ray fluorescence (XRF) analysis, shown in Table 3.2, section 3.2.1 of Chapter three (Rickard, Riessen and Walls, 2010; Donatello *et al.*, 2014; Yang *et al.*, 2017).

Visual observation of the heated samples at temperatures beyond of 500 ℃ revealed extensive cracks and micro-fissures, as shown in Table 7.2. The differential between the internal and external temperatures of the samples during the sintering process in the furnace, leads to the formation of cracks, which expand as the samples are further heated. The widening cracks observed on the surfaces of the GP samples could be a reasonable explanation for their thermal expansion. Furthermore, it is believed that the evaporation of water molecules, which in turn causes the formation of micro-capillary, could be the main reason for the formation of cracks in two ways: i) during the heating process, high stresses are created in the internal pores, due to the high steam pressure of the GP matrix, which causes internal-cracks, and then results in micro-capillaries near the surface. ii) again, due to the high pressure on the internal-cracks inside the matrix, the migration of the vapour into the atmosphere will occur, thus, promoting the formation of cracks on the surface (Zheng, Chen and Gbozee, 2016; Yang *et al.*, 2017). Therefore, the exposure of the designed GP paste to different temperature stages, considerably influences the compressive strength, owing to the formation of cracks, which can be linked to the mechanical degradation seen in the samples.

It is considered that the presence of iron oxides (Fe_2O_3) in the geopolymeric system not only have a major effect on the colour changes that occur after the designed GP paste is heated to elevated temperatures, but also plays an important role in strength degradation. These iron oxides have a direct effect on the thermal behaviour of the GP, by changing its morphology and phase composition during the heating process. A previous investigation, carried out on the thermal properties of fly ash-based geopolymer material, showed that part of the amorphous phase of the iron oxides would be transferred to other semi-crystalline phases, such as the hematite. The same study reported that the oxidation of iron oxides could increase the formation of semi-crystalline phases and also cause the formation of cracks, as shown in Eqs (7.1), (7.2) and (7.3). Further, the same authors stated that in geopolymer products, the oxidation of iron oxides can be demonstrated by the mass gain observed by different techniques such as thermal gravimetric analysis (TGA) (Rickard, Riessen and Walls, 2010).

$$2FeO - OH \rightarrow Fe_2O_3 + 2H_2O \qquad\qquad \text{Eq (7. 1)}$$

$$FeO - OH \rightarrow FeO + OH \qquad\qquad \text{Eq (7. 2)}$$

$$2FeO + \tfrac{1}{2}O_2 \rightarrow Fe_2O_3 \qquad\qquad \text{Eq (7. 3)}$$

In this study, the loss on ignition (LOI) results obtained, as tabulated in section 3.2.1 of Chapter three, provide a reasonable explanation that the presence of a considerable amount of iron oxide in the precursor material leads to a gain in mass after exposure to high temperatures above 600ºC. This is indeed the case with HMNS, where the iron oxides constitute of approximately 10% by total mass of the HMNS material, with an associated LOI of -0.3% (see Appendix A). The negative sign indicates that there is a gain in the mass of the material after it is heated at an elevated temperature, the so-called gain on ignition (GOI).

Table 7.2. Change in the visual aspect of GP paste samples after temperature exposure

Heated samples from 500 to 900 ℃, with a visual appearance of cracks and colour changes

7.4. Summary

An experimental study was conducted on the thermo-mechanical behaviours of a designed FA-GGBS-HMNS based geopolymer paste. A thermal stability test was performed by subjecting selected GP paste samples to high temperatures ranging from 200 to 900ºC. Based on the results obtained, the GP paste showed a significant heat resistance, with an increase in compressive strength of 3% at 200ºC. A reduction of strength was observed when the specimens were heated to 300ºC. Thereafter the strength was maintained up to 500ºC, with a slight strength increase at this temperature.

After exposure to a temperature of 900ºC, the FA-GGBS-HMNS based geopolymer paste showed a minimum residual strength of 20.56 MPa with an associated reduction rate of 57.52%. Physical changes and visual changes in colour from the original grey to clear-orange and then to clear-red were observed when the samples were heated beyond 500ºC. Micro-cracks and fractures appeared on the sample surfaces with a visual expansion seen mostly on those samples which were heated at 700, 800 and 900 ºC. The presence of a significant amount of Fe_2O_3 in the geopolymer mixture had an influence on the degradation of compressive strength, due to its reaction with the atmospheric oxygen, which in turn led to thermal expansion of the GP specimens caused by the formation of cracks.

Chapter 8

Conclusions and Recommendations for

Future Research

8.1. Introduction

A high-performance GPC, fabricated using a combination of FA, GGBS and HMNS, is proposed in this research work, due to its significant mechanical and morphological characteristics. The use of such by-products in the FA-GGBS-HMNS–based geopolymer concrete production is considered a feasible solution which also addresses the need to deal with large amounts of industrial waste. To ensure quality and expansion in its field of application, the designed GPC is proposed as an alternative technology, which can be made under ambient conditions. The designed GPC can be classified as a new green and environmentally-friendly concrete, because of its extensive contribution to reducing current financial and environmental problems. These contributions are the main motivations for the research discussed and evaluated in this thesis.

This chapter presents a brief summary of the current research. The thesis comprises seven chapters, an introduction in Chapter one and a literature review in Chapter two. These chapters discuss the thinking behind the study of alkali-activated geopolymer concrete, as an alternative cementitious material to Portland cement, as well as the fundamental processes of OPC and the chemistry of geopolymers. Chapter three

describes and analyses the mechanical properties of the designed FA-GGBS-HMNS-based geopolymer concrete, and the manufacturing procedures, including its fresh and hardened properties. The microstructural characteristics of the manufactured FA-GGBS-HMNS-based geopolymer concrete, including an optical analysis, are examined in Chapter four. The dynamic behaviour of the GPC, and the fundamental procedures of the Split Hopkinson Pressure Bar test (SHPB) are displayed in Chapter five. The long-term properties of the fabricated GPC, which are discussed with regard to durability and thermal stability, are investigated in Chapters six and seven respectively. The significant contribution of this research is shown through the outcomes in Chapters three to seven. Chapter eight provides the exhaustive conclusions of this research work, including contributions and recommendations for future research.

However, it must be noted that, during the experimental work, many attempts were made to fix the optimal portions of each individual slag used. The method was based on the compressive strength results as a control facility, to assess the selected portions of slags, and later used to determine the final mix design. The trial and error method provided successful results in terms of manufacturing of FA-GGBS-HMNS-based geopolymer concrete. Subsequently, a series of tests was performed to examine the effect of different parameters, which might affect the short and long-term properties of the fresh and hardened GPC.

The outcome of this research is summarized in the following sections, including the significant contributions of the research, and recommendations for future research.

1- As the largest worldwide hydraulic binder material, Ordinary Portland cement (OPC) is well-known as a significant greenhouse gas contributor and energy-intensive consumer, with about 40% of its associated emissions being carbon dioxide, as a result of the production processes. However, much research has been done to support the concept of aluminosilicate cementitious binders as an alternative material, known as ''Geopolymer''. This can reduce the production and the use of OPC. Scientific research shows that geopolymers are essentially based

on a combination of alkaline activator solutions and main binder constituents, rich in SiO_2, Al_2O_3 and CaO. From the literature review, the author found that coal-fired fly ash seemed to be the most widely sourced aluminosilicate material, due to its physio-chemical properties (particle size, shape and the content of amorphous oxide elements). Furthermore, sodium hydroxide and sodium silicate are the activator solutions most commonly used in geopolymers, and much more than others, which are potassium and calcium-based.

2- In this study, the geopolymer mixes were synthesised by combining ternary materials of ASTM class F fly ash, ground granulated blast furnace slag (GGBS) and high-magnesium nickel slag (HMNS), which were activated by an alkaline solution prepared by mixing NaOH with Na_2SiO_3 in aqueous phases. The ratios of NaOH to Na_2SiO_3 and of binder to activator solution, were fixed at 2.5 and 2.0 respectively, in accordance with previous research. The selected curing conditions were at room temperatures of 25±2℃ with a relative humidity of 85-90%. In addition, due to its significant influence on the properties of the final product, the percentages of loss on ignition (LOI) were determined for all precursor materials, the results showing that the raw materials consisted of less than 3% LOI. Also, to ensure that the designed geopolymer product could fit engineering requirements, it was necessary to identify through Particle size analysis (PSA) and XRF techniques, the particle distribution, and their chemical composition, for each material, while, the particles' shape and morphology were characterized using SEM analysis.

3- The engineering properties of the manufactured geopolymer proposed in Chapter three, were investigated through a series of mechanical tests, such as compression and splitting tensile tests. A selection procedure, based on the compressive strength tests as a key-controller, was adopted to determine the optimum fractions of the materials used. The manufacturing procedure concentrated on designing a suitable geopolymer paste, as required for this research. Later, a geopolymer concrete was designed using the appropriate geopolymer paste, in accordance with the manufacturing procedure that was proposed in Chapter three. After fixing the

optimum design, the properties of fresh GPC were examined. The findings showed that an initial setting time of around 5 hours was reasonable, with a slightly longer process for the final setting time of approximately 24 hours, believed to be due to the continuity of geopolymerization. Further, a slump test showed a workable FA-GGBS-HMNS-based geopolymer concrete mix, with an average slump of 220mm. The hardening properties were investigated by measuring the compressive strengths and the splitting tensile strengths of the fabricated FA-GGBS-HMNS-based geopolymer paste and concrete. It was found that with a curing regime of ambient conditions, the FA (70%)-GGBS (20%)-HMNS (10%) based GP paste showed a significant development of compressive strength of 60.82MPa over the 55.6MPa for that of FA-GGBS-HMNS-based geopolymer concrete.

4- The microstructural characteristics of the FA-GGBS-HMNS-based GPC were also investigated in this study. It is believed that the strength improvement is mainly related to the different reactions occurring between activators and binders during the geopolymerization process. To examine this, it was necessary to analyse the morphological characteristics by microstructural analysis, using different techniques, such as SEM/EDX, XRD, FTIR and OM. The results showed that the ternary materials used in this study reacted strongly with the activator solutions, in a way that a compact and dense matrix appeared, as shown by SEM/EDX images. Moreover, the XRD patterns revealed that the final FA-GGBS-HMNS-based GP paste/concrete constituted mainly of Quartz (SiO_2), magnesium vanadium molybdenium oxide ($Mg_{2.5}(VMo)O_8$), which is believed to have been sourced from the presence of HMNS and calcium beryllium praseodymium oxide ($CaBePr_2O_5$), which could also have been developed during the reactions of the Ca^{++} cations sourced from the GGBS. It seems that these crystalline phases were the main gels, contributing to an improvement in the mechanical properties, due to their natural strong and rigid crystallinity.

5- The dynamic mechanical behaviour of FA-GGBS-HMNS GP paste under a high-speed impact test was investigated using SHPB system. The results showed a comprehensive concept of the dynamical behaviours of GP paste and revealed that

both the dynamic compressive strength and the DIF increased with loading rates. In addition, the pattern of the energy absorbed was well-fitted in a polynomial distribution with strain rates ranging from 24.1 to 176 s^{-1}. The diameter-to-length ratio of specimens has a significant influence on the dynamic compressive strength and is presented as lateral inertial confinement. Different failure patterns have been observed at different velocities and strain rates. Finally, empirical formulae were proposed to express the dynamical behaviours for FA-GGBS-HMNS GP paste, loaded at different impact velocities and strain rates ($DIF = 0.657 * \log \dot{\varepsilon} - 0.0748$). Due to the lack of such empirical data for geopolymer materials, these formulae can be used to evaluate the performance of other alkali-activated materials under impact loading.

6- To estimate the durability of FA-GGBS-HMNS GP concrete, RCPT has been performed in accordance with NT Build 492 protocols. The findings showed that the chloride diffusion coefficient could be influenced by many factors, such as the fineness of the precursor materials used, the continuity of geopolymerization process, the chemical nature of the gels formed during geopolymerization and also the pH concentration of the mixture.

7- A thermal test at high temperatures up to 900ºC was conducted to evaluate the thermo-mechanical properties of the manufactured FA-GGBS-HMNS GP paste. The results showed that GP paste strength increased when exposed to 200ºC, then gradually decreased. The minimum residual strength maintained after heating to 900ºC was 20.56MPa. Changes in colour and physical features were observed when the specimens were heated to above 500ºC. Overall, the FA-GGBS-HMNS GP paste exhibited good thermal resistance when compared to OPC and other geopolymer materials.

To sum up, the main outcomes of the present research can be listed as follows:

- A novel procedure has been established to manufacture a high performance geopolymer concrete.

- FA-GGBS-HMNS based geopolymer concrete gives high mechanical properties, with 55.6MPa and 4.57MPa of compressive strength and splitting tensile strength respectively.

- A compact and denser microstructure has been shown by the SEM/EDX analysis, with the formation of new crystalline phases mainly consisted of silicate, calcium and magnesium.

- The designed FA-GGBS-HMNS based geopolymer paste is found to be a strain rate-sensitive material when submitted to impact loadings.

- A numerical equation has been proposed to show the strong relationship between the energy absorbed and the strain rate during the impact test and has been given as $W_{ab} = -2*10^{-5}\varepsilon^{\bullet 2} + 0.0065\varepsilon^{\bullet} + 0.3059$ $with$ $R^2 \approx 0.982$

- In respect to the pH of the pore solution and the finesse of the precursor materials, FA-GGBS-HMNS based geopolymer revealed a good resistance to chloride ingress.

- The produced GPC showed very good thermal stability trends at different temperature stages, with a residual compressive strength of 20.56MPa at 900ºC compared to that obtained for OPC at 700ºC of around 15MPa.

8.2. Contributions

The current work provides a new mix design of geopolymer concrete, where, for the first time the combination of ternary materials has been introduced in the production of geopolymers by the author in such as research. For better knowledge and understanding of the performance of a FA-GGBS-HMNS based geopolymer material as an alternative construction product, strongly recommended for the construction industry. Considerable data has been provided through the experimental investigations presented in Chapters three to seven, and has shown significant findings on both engineering and microstructural scales. A fascinating data has been achieved regarding the dynamic behaviours of the produced geopolymer material, which in turn reflects the originality of the research by filling a significant research gap which is the lack and the absence of any data on the dynamical behaviours of geopolymers subjected to high impact loadings. Based on the results achieved in this study for

producing a new mix design for geopolymer material, as a relevant construction material for varied applications, the following contributions can be recorded:

- A simplified manufacturing process has been designed and applied for producing geopolymer material based on by-product materials and activator solutions. The procedure presents clear and simple stages, which can be performed under normal conditions.

- A new design of geopolymer binders has been proposed, based on the use of three precursor by-product materials at the same time, to formulate three-phase gels under ambient conditions. The formulation of three-phase gels shows a potential influence on the enhancement of mechanical and microstructure properties.

- The proposed mix design could be used for different applications. It exhibits significant results at ambient conditions, so reducing its limitations for application.

- Due to the limited prior research into the dynamic behaviour of geopolymer-like materials, this thesis provides significant data, which investigates the effect of high impact loading on geopolymer mechanical behaviours. Based on the dynamic test, empirical formulae have been established for geopolymer paste-like material, which could be a beneficial support for such dynamic test for GP paste-like materials. The data could be a good reference and orientation for future research.

- The produced GPC can be classified as an eco-friendly product, due to its role in reducing the amount of CO_2 emissions, energy consumption and degradation of natural resources.

8.3. Limitations

The present experimental work has shown interesting mechanical and microstructure results which in turn allow this GPC material to be proposed as a sustainable and eco-

friendly product, however, due to the short time and limited facilities, some limitations can be listed as follows:

- Sodium silicate and sodium hydroxide were used as alkaline activators in this study, however, other activators can give different mechanical and microstructure properties.

- The final GPC product can only be used for the area where the sulfate amount is low, due to the lack of the data in such as environments.

- The optimum mix design obtained is negatively affected by the LOI percentage presented in the raw materials.

- The produced GPC is negatively affected by the high NaOH concentration (> 12M).

- The numerical equations given in the dynamical mechanical behaviours chapter is only applicable for geopolymer paste materials not concrete.

- The use of the produced GPC at elevated temperature (more than 1000 ⁰C) should be considered.

8.4. Recommendations for Future Work

This research work has addressed the development of new FA-GGBS-HMNS based geopolymer concrete mix-design and is an investigation of different mechanical and microstructure properties, including durability and thermal stability. However, much experimental data concerning the reaction mechanism of the ternary binders with the activator solution, their long-term properties, and the transitional phases under thermal treatment, need further investigation. Moreover, for a much better understanding of the geopolymer mechanism and its application, additional work should be considered, and this can be summarized as follows:

1. This research has shown that the mechanical and microstructure properties of FA-GGBS-HMNS GPC have been improved. However, further microstructure research on the formation of ternary gel is also needed to demonstrate the reaction mechanism which occur between the chemical activator and the precursors.

2. The mechanical compression test carried out in this research is only a uniaxial test. Other tests, such as bi-and tri-axial tests will be beneficial.

3. The preliminary study of the chloride diffusion has shown that GPC might have better resistance to the migration of chloride ions. Further investigation of chloride migration and its effect on reinforcement should be performed using different comparable methods.

4. To extend its field of application, it would be important to understand geopolymer behaviours, from the aspect of chemical resistivity and the immobilization of contaminants.

5. From the environmental and economic perspective, the use of geopolymer as an alternative material to OPC is well-supported, but the overall cost is still unclear. Further financial and environmental details should be provided to clarify the commercial horizons of geopolymer materials.

6. To explore the influence of high temperatures on the microstructure of the final product, more morphological analysis should be performed.

7. For more understanding the mechanical properties of the produced material, a mechanical testing under low temperatures (freezing-thaw test) should be implemented.

8. Porosity and permeability tests using both gas and water jets should be attempted to explore the material porosity.

9. For more application aspects, more tests on beam, column slabs are required.

10. A corrosion test on the reinforcement should be conducted using different methods.

11. Dynamic behaviours tests on concrete samples should be performed and compared to that of paste samples.

References

ACI 318-08/318R-08 (2008): Building code requirements for structural concrete ACI and commentary. American Concrete Institute, Farmington Hills, MI,USA.

ACI 363R-92 (1997): State-of-the-art report on high- strength concrete, American Concrete Institute, Farmington Hills, MI, USA.

Adam, A. A. (2009) 'Strength and Durability Properties of Alkali Activated Slag and Fly Ash-Based Geopolymer Concrete', *PhD thesis. RMIT University, Australia.*

Ahmari, S., Ren, X., Toufigh,V. and Zhang. L. (2012) 'Production of geopolymeric binder from blended waste concrete powder and fly ash', *Construction and Building Materials*, 35, pp. 718–729.

Ahmari, S. and Zhang, L. (2012) 'Production of eco-friendly bricks from copper mine tailings through geopolymerization', *Construction and Building Materials*, 29,pp. 323–331.

Aliabdo, A. A., Abd Elmoaty, M. A.E. and A. Salam, H. (2016) 'Effect of cement addition , solution resting time and curing characteristics on fly ash based geopolymer concrete performance', *Construction and Building Materials*, 123, pp. 581–593.

Andini, S., Cioffi, R., Colangelo, F., Grieco, T., Montagnaro, F. and Santoro, L. (2007): Coal fly ash as raw material for the manufacture of geopolymer-based products. Waste Management, 28, 426-423.

Anuradha, R., Sreevidya, V., Venkatasubramani, R. and Rangan, B.V. (2012) 'Modified guidelines for geopolymer concrete mix design using Indian standard', 13(3), pp. 353–364.

ASTM C 496/C 496M – 04 (2011): Standard Test Method for Splitting Tensile Strength of Cylindrical Concrete Specimens. American Society for Testing and Materials, USA.

ASTM C191 (2008): Standard test method for normal consistency and setting time of Hydraulic American Society for Testing and Materials, USA.

Aydin, S., Karatay, Ç. and Baradan, B. (2010): The effect of grinding process on mechanical properties and alkali-silica reaction resistance of fly ash incorporated cement mortars. *Powder Technology*, 197(1–2), 68–72.

Bakharev, T. (2006) 'Thermal behaviour of geopolymers prepared using class F fly ash and elevated temperature curing', *Cement and Concrete Research*, 36(6), pp. 1134–1147.

Bakharev, T., Sanjayan, J. G. and Cheng, Y. B. (1999) 'Effect of elevated temperature curing on properties of alkali-activated slag concrete', *Cement and Concrete Research*, 29(10), pp. 1619–1625.

Al Bakri, A. M. M., Kamarudin, H., Khairul Nizar, I., Bnhussain, M., Zarina, Y. and Rafiza, A.R. (2012) 'Correlation between Na 2 SiO 3 / NaOH Ratio and Fly Ash / Alkaline Activator Ratio to the Strength of Geopolymer', *Advanced Materials Research*, 342, pp. 189–193.

Al Bakri, A.M.M., Kamarudin, H., Bnhussain, M., Nizar, I.K., Rafiza, A.R. and Zarina, Y. (2011) 'Microstructure of different NaOH molarity of fly ash- based green polymeric cement', *Journal of Engineering and Technology Research*, 3(2), pp. 44–49.

Barbosa, V. F., MacKenzie, K. J. and Thaumaturgo, C. (2000) 'Synthesis and characterisation of materials based on inorganic polymers of alumina and silica: sodium polysialate polymers', *International Journal of Inorganic Materials*, 2(4), pp. 309–317.

Benhelal, E., Zahedi, G., Shamsaei, E. and Bahadori, A. (2013) 'Global strategies and potentials to curb CO2 emissions in cement industry', *Journal of Cleaner Production*, 51, pp. 142–161.

Bernal, S.A., Rodríguez, E.D., de Gutiérrez, R.M., Gordillo, M. and Provis, J.L. (2011) 'Mechanical and thermal characterisation of geopolymers based on silicate-activated metakaolin / slag blends', *Journal of Materials Science*, 46, pp. 5477–5486.

Bouaissi, A., Li, L.Y., Al Bakri, A. M. M. and Bui, Q.B. (2019) 'Mechanical properties and microstructure analysis of FA-GGBS-HMNS based geopolymer concrete', *Construction and Building Materials*, 210, pp. 198–209.

Cao, S., Yilmaz, E. and Song, W. (2018) 'Dynamic response of cement-tailings matrix composites under SHPB compression load', *Construction and Building Materials*, 186, pp. 892–903.

Chen, X., Wu, S. and Zhou, J. (2013) 'Experimental and modeling study of dynamic mechanical properties of cement paste , mortar and concrete', *Construction and Building Materials*, 47, pp. 419–430.

Chen, Y., Zhang, Y., Chen, T., Zhao, Y. and Bao, S. (2011) 'Preparation of eco-friendly construction bricks from hematite tailings', *Construction and Building Materials*, 25(4), pp. 2107–2111.

Cheng-Yong, H., Yun-Ming, L., Al Bakri, A. M. M. and Hussin, K. (2017) 'Thermal Resistance Variations of Fly Ash Geopolymers : Foaming Responses', *Nature Publishing Group*, pp. 1–11.

Cheng, T. W. and Chiu, J. P. (2003) 'Fire-resistant geopolymer produce by granulated blast furnace slag', *Minerals Engineering*, 16(3), pp. 205–210.

Chindaprasirt, P., Chareerat, T., Hatanaka, S. and Cao, T. (2011) 'High-Strength Geopolymer Using Fine High-Calcium Fly Ash', *Journal of Materials in Civil Engineering*, 23(3), pp. 264–270.

Chindaprasirt, P. and Chalee, W. (2014) 'Effect of sodium hydroxide concentration on chloride penetration and steel corrosion of fly ash-based geopolymer concrete under marine site', *Construction and Building Materials*, 63, pp. 303–310.

Chindaprasirt, P., Chareerat, T. and Sirivivatnanon, V. (2006) 'Workability and strength of coarse high calcium fly ash geopolymer', *Cement & Concrete Composites*, 29(3), pp. 224–229.

Cioffi, R., Maffucci, L. and Santoro, L. (2003) 'Optimization of geopolymer synthesis by calcination and polycondensation of a kaolinitic residue', *Resources, Conservation and Recycling*, 40(1), pp. 27–38.

Collins, F. and Sanjayan, J. G. (1999) 'Effects of ultra-fine materials on workability and strength of concrete containing alkali-activated slag as the binder', Cement and concrete research, 29(3), pp. 459–462.

Das, S., Singh, G., Ahmed, A.A., Saha, S. and Karmakar, S. (2015) 'Ground Granulated Blast Furnace Slag (GGBS) based Concrete Exposed to Artificial Marine Environment(AME) and Sustainable Retrofitting using Glass Fiber Reinforced Polymer (GFRP) sheets', *Procedia - Social and Behavioral Sciences*, 195, pp. 2804–2812.

Davidovits, J. (1989) 'Geopolymers and geopolymeric materials', *Journal of Thermal Analysis and Calorimetry*, 35(2), pp. 429–441.

Davidovits, J. (1994) 'Properties of geopolymer cements', *In First international conference on alkaline cements and concretes*, Kiev State Technical University, Ukraine: Scientific Research Institute on Binders and Materials, 1, pp. 131-149.

Davidovits, J. ed. (2005) '*Geopolymer, green chemistry and sustainable development solutions: proceedings of the world congress geopolymer 2005*', Geopolymer Institute, France.

Davidovits, J., Davidovits, R. and James, C. (1999) '*Geopolymer '99: Second International Conference on Geopolymers'*, Geopolymer Institute, Frence.

Van Deventer, J.S.J., Provis, J.L., Duxson, P. and Lukey, G.C. (2007) 'Reaction mechanisms in the geopolymeric conversion of inorganic waste to useful products', *Journal of Hazardous Materials*, 139, pp. 506–513.

Ding, Y., Dai, J. G. and Shi, C. J. (2016) 'Mechanical properties of alkali-activated concrete: A state-of-the-art review', *Construction and Building Materials*, 127, pp. 68–79.

Donatello, S., Kuenzel, C., Palomo, A. and Fernández-Jiménez, A. (2014) 'High temperature resistance of a very high volume fly ash cement paste', *Cement and Concrete Composites*, 45, pp. 234–242.

Duxson, P., Fernández-Jiménez, A., Provis, J.L., Lukey, G.C., Palomo, A. and van Deventer, J.S. (2007a) 'Geopolymer technology: the current state of the art', *Journal of materials science*, 42(9), pp.2917-2933.

Energy Efficiency and Saving in the Cement Industry | ClimateTechWiki (2017). Available at: http://www.climatetechwiki.org/technology/energy-saving-cement (Accessed: 9 November 2018).

Faisal, M. and Muhammad, K. (2016) 'Synthesis and characterization of geopolymer from bagasse bottom ash , waste of sugar industries and naturally available china clay', *Journal of Cleaner Production*, 129, pp. 491–495.

Fan, F., Liu, Z., Xu, G., Peng, H. and Cai, C.S. (2017) 'Mechanical and thermal properties of fly ash based geopolymers', *Construction and Building Materials*, 160, pp. 66–81.

Feng, K.N., Ruan, D., Pan, Z., Collins, F., Bai, Y., Wang, C.M. and Duan, W.H. (2015) 'Mechanical behavior of geopolymer concrete subjected to high strain rate compressive loadings', *Materials and Structures*, 48(3), pp. 671–681.

Ferdous, M. W., Kayali, O. and Khennane, A. (2013) 'A detailed procedure of mix design for fly ash based geopolymer concrete', In *Fourth Asia-Pacific Conference on FRP in Structures (APFIS 2013),* pp. 11–13.

Fernandez-Jimenez, A., García-Lodeiro, I. and Palomo, A. (2007) 'Durability of alkali-activated fly ash cementitious materials', *Journal of Materials Science*, 42(9), pp. 3055–3065.

Fernández-Jiménez, A. and Palomo, A. (2005) 'Composition and microstructure of alkali activated fly ash binder: Effect of the activator', *Cement and Concrete Research*, 35(10), pp. 1984–1992.

Fernández-Jiménez, A. and Puertas, F. (2003) 'Effect of activator mix on the hydration and strength behaviour of alkali-activated slag cements', *Advances in Cement Research*, 15(3), pp. 129–136.

Fu, Q., Niu, D., Zhang, J., Huang, D., Wang, Y., Hong, M. and Zhang, L. (2018) 'Dynamic compressive mechanical behaviour and modelling of basalt – polypropylene fibre-reinforced concrete', *Archives of Civil and Mechanical Engineering*, 18(3), pp. 914–927.

Gabet, T., Malécot, Y. and Daudeville, L. (2008) 'Triaxial behaviour of concrete under high stresses: Influence of the loading path on compaction and limit states', *Cement and Concrete Research*, 38(3), pp. 403–412.

Gao, Y., Xu, J., Bai, E., Luo, X., Zhu, J. and Nie, L. (2015) 'Static and dynamic mechanical properties of high early strength alkali activated slag concrete', *Ceramics International*, 41(10), pp. 12901–12909.

Glass, G. K., Reddy, B. and Buenfeld, N. R. (2000) 'The participation of bound chloride in passive film breakdown on steel in concrete', *Corrosion Science*, 42(11), pp. 2013–2021.

Görhan, G. and Kürklü, G. (2014) 'The influence of the NaOH solution on the properties of the fly ash-based geopolymer mortar cured at different temperatures', *Composites Part B: Engineering*, 58, pp. 371–377.

Graybeal, B. and Davis, M. (2008) 'Cylinder or Cube : Strength Testing of 80 to 200 MPa (11 . 6 to 29 ksi) Ultra-High-Performance Fiber-Reinforced Concrete', *ACI Materials Journal*, 105(6), pp. 603–609.

Hao, Y., Hao, H., Jiang, G.P. and Zhou, Y. (2013) 'Experimental confirmation of some factors in fl uencing dynamic concrete compressive strengths in high-speed impact tests', *Cement and Concrete Research*, 52, pp. 63–70.

Hardjito, D., Wallah, S.E., Sumajouw, D.M. and Rangan, B.V. (2004) 'Factors Influencing the Compressive Strength of Fly Ash-Based Geopolymer Concrete', *Civil Engineering Dimension*, 6(2), pp. 88–93.

Hardjito, D. (2005) 'Studies on Fly Ash-Based Geopolymer Concrete', *PhD thesis*, Curtin University.

Hardjito, D., Cheak, C. C. and Lee Ing, C. H. (2008) 'Strength and Setting Times of Low Calcium Fly Ash-based Geopolymer Mortar', *Modern Applied Science*, 2(4), pp. 3–11.

He, Z.J. and Song, Y.P. (2010) 'Triaxial strength and failure criterion of plain high-strength and high-performance concrete before and after high temperatures', *Cement and Concrete Research*, 40(1), pp. 171–178.

Hu, S., Wang, H., Zhang, G. and Ding, Q. (2008) 'Bonding and abrasion resistance of geopolymeric repair material made with steel slag', *Cement and Concrete Composites*, 30(3), pp. 239–244.

Ismail, I., Bernal, S.A., Provis, J.L., San Nicolas, R., Brice, D.G., Kilcullen, A.R., Hamdan, S. and van Deventer, J.S. (2013) 'Influence of fly ash on the water and chloride permeability of alkali-activated slag mortars and concretes', *Construction and Building Materials*, 48, pp. 1187–1201.

Ismail, I., Bernal, S.A., Provis, J.L., San Nicolas, R., Hamdan, S. and van Deventer, J.S. (2014) 'Modification of phase evolution in alkali-activated blast furnace slag by the incorporation of fly ash', *Cement and Concrete Composites*, 45, pp. 125–135.

Jayant, D. (2013) '*Mineral Admixtures in Cement and Concrete*. © 2013 by Taylor & Francis Group, LLC, CRC Press.

Jeyageetha, C. and Kumar, S. P. (2016) 'Study of SEM / EDXS and FTIR for Fly Ash to Determine the Chemical Changes of Ash in Marine Environment', *International Journal of Science and Research (IJSR)*, 5(7), pp. 1688–1693.

Jóźwiak-Niedźwiedzka, D. (2009) 'Effect of fluidized bed combustion fly ash on the chloride resistance and scaling resistance of concrete', *Concrete in Aggressive Aqueous Environments, Performance, Testing and Modeling*, 2(05).

Kaiser, M.A. (1998) 'Advancements in the Split Hopkinson Bar Test', *PhD thesis*, University of *Blacksburg, Virginia, USA*.

Ken, P. W., Ramli, M. and Ban, C. C. (2015) 'An overview on the influence of various factors on the properties of geopolymer concrete derived from industrial by-products', *Construction and Building Materials*, 77, pp. 370–395.

Kim, D. J., Sirijaroonchai, K., El-Tawil, S. and Naaman, A.E. (2010) 'Numerical simulation of the Split Hopkinson Pressure Bar test technique for concrete under compression', *International Journal of Impact Engineering*, 37(2), pp. 141–149.

Kim, E. H. (2012) 'Understanding effects of silicon/aluminum ratio and calcium hydroxide on chemical composition, nanostructure and compressive strength for metakaolin geopolymers', *Master thesis.University of Illinois,Urbana.*

Komljenovic, M., Baarevic, Z. and Bradic, V. (2010) 'Mechanical and microstructural properties of alkali-activated fly ash geopolymers', *Journal of Hazardous Materials*, 181(1–3), pp. 35–42.

Komnitsas, K. A. (2011) 'Potential of geopolymer technology towards green buildings and sustainable cities', *Procedia Engineering,* 21, pp. 1023–1032.

Komnitsas, K. and Zaharaki, D. (2007) 'Geopolymerisation: A review and prospects for the minerals industry', *Minerals Engineering*, 20(14), pp. 1261–1277.

Komnitsas, K., Zaharaki, D. and Perdikatsis, V. (2007) 'Geopolymerisation of low calcium ferronickel slags', *Journal of Materials Science*, 42(9), pp. 3073–3082.

Kong, D. L. Y. and Sanjayan, J. G. (2010) 'Effect of elevated temperatures on geopolymer paste , mortar and concrete', *Cement and Concrete Research*, 40(2), pp. 334–339.

Kovalchuk, G., Fernández-Jiménez, A. and Palomo, A. (2007) 'Alkali-activated fly ash: Effect of thermal curing conditions on mechanical and microstructural development - Part II', *Fuel*, 86(3), pp. 315–322.

Kumar, P. and Mcbeath, S. (2015) 'Fire endurance of steel reinforced fly ash geopolymer concrete elements', *Construction and Building Materials*, 90, pp. 91–98.

Kupwade-Patil, K. and Allouche, E. N. (2013) 'Examination of Chloride-Induced Corrosion in Reinforced Geopolymer Concretes', *Journal of Materials in Civil Engineering*, 25(10), pp. 1465–1476.

Lang, S. M. (2012) 'Design of a Split Hopkinson Bar Apparatus for use with Fiber Reinforced Composite Materials', *All Graduate Theses and Dissertations https://digitalcommons.usu.edu/etd/1284.*

Lembo, K., Lokuge, W. and Karunasena, W. (2014) 'Geopolymer Concrete With FRP Confinement', *23rd Australasian Conference on the Mechanics of Structures and Materials (ACMSM23)*, Melbourne, Australia, November 14-16.

Lloyd, N. A. and Rangan, B. V. (2010) 'Geopolymer Concrete with Fly Ash', In *Proceedings of the Second International Conference on Sustainable Construction Materials and Technologies, Italy.* Available at: http://claisse.info/2010papers/k18.pdf (Accessed: 30 May 2017), June 28-30, pp. 1493-1504.

Luo, X., Xu, J.Y., Bai, E.L. and Li, W. (2013) 'Research on the dynamic compressive test of highly fluidized geopolymer concrete', *Construction and Building Materials*, 48, pp. 166–172.

Malhotra, V. M. and Mehta, P. K. (2002) '*High-performance, high-volume fly ash concrete : materials, mixture proportioning, properties, construction practice, and case histories*', Canada.

Mamlouk, M.S. and Zaniewski, J.P. (2011) '*Materials for civil and construction engineers',3rd Ed,* Upper Saddle River, NJ: Pearson Prentice Hall.

Marks, M., Glinicki, M. A. and Gibas, K. (2015) 'Prediction of the chloride resistance of concrete modified with high calcium fly ash using machine learning', *Materials*, 8(12), pp. 8714–8727.

Matos, A. M. and Sousa-Coutinho, J. (2012) 'Durability of mortar using waste glass powder as cement replacement', *Construction and Building Materials*, 36, pp. 205–215.

McNulty, E. (2009) 'Geopolymers : An Environmental Alternative to Carbon Dioxide Producing Ordinary Portland Cement', Department of Chemistry, the Catholic UniversIty of America.

Mehta. K. P. (1986) '*Concrete: Structure, Properties and Materials*. New Jersey. Englewood Cliffs: Prentice-Hall, USA.

Al Bakri, A.M.M., Kamarudin, H., Nizar, I.K., Sandu, A.V., Binhussain, M., Zarina, Y. and Rafiza, A.R. (2013) 'Design , Processing and Characterization of Fly Ash-Based Geopolymers for Lightweight Concrete Application', *Revista de Chimie*, 64(4), pp. 382–387.

Nasvi, M. C. M., Ranjith, P. G. and Sanjayan, J. (2014) 'Effect of different mix compositions on apparent carbon dioxide (CO 2) permeability of geopolymer : Suitability as well cement for CO 2 sequestration wells', *Applied Energy*, 114, pp. 939–948.

Nath, P. and Sarker, P. K. (2014) 'Effect of GGBFS on setting, workability and early strength properties of fly ash geopolymer concrete cured in ambient condition', *Construction and Building Materials*, 66, pp. 163–171.

Nath, P. and Sarker, P. K. (2016) 'Flexural strength and elastic modulus of ambient-cured blended low-calcium fly ash geopolymer concrete', *Construction and Building Materials*, 130, pp. 22–31.

Nath, S. K. and Kumar, S. (2013) 'Influence of iron making slags on strength and microstructure of fly ash geopolymer', *Construction and Building Materials*, 38, pp. 924–930.

Nath, S. K. and Kumar, S. (2013) 'Influence of iron making slags on strength and microstructure of fly ash geopolymer', *Construction and Building Materials*, 38, pp. 924–930.

Neto, A. A. M., Cincotto, M. A. and Repette, W. (2010) 'Mechanical properties, drying and autogenous shrinkage of blast furnace slag activated with hydrated lime and gypsum', *Cement and Concrete Composites*, 32(4), pp. 312–318.

Neupane, K. (2016) 'Fly ash and GGBFS based powder-activated geopolymer binders : A viable sustainable alternative of portland cement in concrete industry', *Mechanics of Materials*, 103, pp. 110–122.

Noushini, A. and Castel, A. (2016) 'The effect of heat-curing on transport properties of low-calcium fly ash-based geopolymer concrete', *Construction and Building Materials*, 112, pp. 464–477.

NT Build 492 (1999) 'Concrete, mortar and cement-based repair materials: Chloride migration coefficient from non-steady-state migration experiments', Nordtest method.

Nuruddin, M.F., Malkawi, A.B., Fauzi, A., Mohammed, B.S. and Almattarneh, H.M. (2016) 'Evolution of geopolymer binders: a review', In *IOP Conference Series: Materials Science and Engineering,* 133(1), pp. 12-52.

Okoye, F. N., Durgaprasad, J. and Singh, N. B. (2015) 'Mechanical properties of alkali activated flyash / Kaolin based geopolymer concrete', *Construction and Building Materials*, 98, pp. 685–691.

Torgal, F.P., Gomes, J.P. and Jalali, S. (2007) 'Tungsten mine waste geopolymeric binder versus ordinary portland cement based concrete: abrasion and acid resistance', In *Alkali Activated Materials-Research, Production and Utilization 3rd Conference*, Agentura Action, pp. 693-702.

Pacheco-Torgal, F., Castro-Gomes, J. and Jalali, S. (2008) 'Alkali-activated binders: A review. Part 1. Historical background, terminology, reaction mechanisms and hydration products', *Construction and Building Materials*, 22(7), pp. 1305–1314.

Palacios, M. and Puertas, F. (2005) 'Effect of superplasticizer and shrinkage-reducing admixtures on alkali-activated slag pastes and mortars', *Cement and Concrete Research*. Pergamon, 35(7), pp. 1358–1367.

Palomo, A., Blanco-Varela, M.T., Granizo, M.L., Puertas, F., Vazquez, T. and Grutzeck, M.W. (1999) 'Chemical stability of cementitious materials based on metakaolin', *Cement and Concrete Research*, 29(7), pp. 997–1004.

Palomo, A., Grutzeck, M. W. and Blanco, M. T. (1999) 'Alkali-activated fly ashes: A cement for the future', *Cement and Concrete Research*, 29(8), pp. 1323–1329.

Panias, D., Giannopoulou, I. P. and Perraki, T. (2007) 'Effect of synthesis parameters on the mechanical properties of fly ash-based geopolymers', *Colloids and Surfaces A: Physicochemical and Engineering Aspects*, 301(1-3), pp. 246–254.

Pavithra, P., Reddy, M.S., Dinakar, P., Rao, B.H., Satpathy, B.K. and Mohanty, A.N. (2016) 'A mix design procedure for geopolymer concrete with fl y ash', *Journal of Cleaner Production*, 133, pp. 117–125.

Phoo-ngernkham, T., Chindaprasirt, P., Sata, V., Pangdaeng, S. and Sinsiri, T. (2013) 'Properties of high calcium fly ash geopolymer pastes with Portland cement as an additive', *International Journal of Minerals, Metallurgy and Materials*, 20(2), pp. 214–220.

Pilehvar, S., Cao, V.D., Szczotok, A.M., Valentini, L., Salvioni, D., Magistri, M., Pamies, R. and Kjøniksen, A.L. (2017) 'Mechanical properties and microscale changes of geopolymer concrete and Portland cement concrete containing micro-

encapsulated phase change materials', *Cement and Concrete Research*, 100, pp. 341–349.

Puertas, F., Martínez-Ramírez, S., Alonso, S. and Vazquez, T. (2000) 'Alkali-activated fly ash/slag cements. Strength behaviour and hydration products', *Cement and Concrete Research*, 30(10), pp. 1625–1632.

Raijiwala, D.B. and Patil, H.S. (2010) 'Geopolymer concrete a green concrete. In *2nd International Conference on Chemical, Biological and Environmental Engineering,* (pp. 202-206). IEEE, Egypt. November 2nd to 4.

Rashad, A. M. (2013) 'Properties of alkali-activated fly ash concrete blended with slag', *Iranian Journal of Materials Science & Engineering*, 10(1), pp. 57–64.

Rashad, A. M. and Zeedan, S. R. (2011) 'The effect of activator concentration on the residual strength of alkali-activated fly ash pastes subjected to thermal load', *Construction and Building Materials*, 25(7), pp. 3098–3107.

Ren, W., Xu, J., Liu, J. and Su, H. (2015) 'Dynamic mechanical properties of geopolymer concrete after water immersion', *Ceramics International*, 41(9), pp. 11852–11860.

Rickard, W. D. A., Riessen, A. Van and Walls, P. (2010) 'Thermal Character of Geopolymers Synthesized from Class F Fly Ash Containing High Concentrations of Iron and a -Quartz', *International Journal of Applied Ceramic Thechnology*, 7(1), pp. 81–88.

Roviello, G., Ricciotti, L., Ferone, C., Colangelo, F. and Tarallo, O. (2015) 'Fire resistant melamine based organic-geopolymer hybrid composites', *Cement and Concrete Composites*, 59, pp. 89–99.

Rovnaník, P. (2010) 'Effect of curing temperature on the development of hard structure of metakaolin-based geopolymer', *Construction and Building Materials*, 24(7), pp. 1176–1183.

Ryu, G.S., Lee, Y.B., Koh, K.T. and Chung, Y.S. (2013) 'The mechanical properties of fly ash-based geopolymer concrete with alkaline activators', *Construction and Building Materials*, 47, pp. 409–418.

Sabitha, D., Dattatreya, J.K., Sakthivel, N., Bhuvaneshwari, M. and Sathik, S.J. (2012) 'Reactivity, workability and strength of potassium versus sodium-activated high volume fly ash-based geopolymers', *Current Science(Bangalore)*, 103(11), pp.1320-1327.

Sathia, R., Babu, K.G. and Santhanam, M. (2008) 'Durability study of low calcium fly ash geopolymer concrete', In *Proceedings of the 3rd ACF International Conference-ACF/VCA,* November.

Shang, H.S. (2013) 'Triaxial T-C-C behavior of air-entrained concrete after freeze-thaw cycles', *Cold Regions Science and Technology*, 89, pp. 1–6.

Shi, L., Wang, L., Song, Y. and Shen, L. (2014) 'Dynamic multiaxial strength and failure criterion of dam concrete', *Construction and Building Materials*, 66, pp. 181–191.

Shinde, B. H. and Kadam, K. S. (2016) 'Properties of Fly Ash Based Geopolymer Mortar with Ambient Curing', *International Journal of Engineering Research*, 5, pp.203-206.

Silo Transport '*Fly ash, How is fly ash produced?',* Available at: https://www.silotransport.cz/3 (Accessed: 9 November 2018).

Singh, B., Ishwarya, G., Gupta, M. and Bhattacharyya, S.K. (2015) 'Geopolymer concrete : A review of some recent developments', *Construction and Building Materials*, 85, pp. 78–90.

Sofi, M., Van Deventer, J.S.J., Mendis, P.A. and Lukey, G.C. (2007) 'Engineering properties of inorganic polymer concretes (IPCs)', *Cement and Concrete Research*, 37(2), pp. 251–257.

Somna, K., Jaturapitakkul, C., Kajitvichyanukul, P. and Chindaprasirt, P. (2011) 'NaOH-activated ground fly ash geopolymer cured at ambient temperature', *Fuel*, 90(6), pp. 2118–2124.

Song, S. and Jennings, H. M. (1999) 'Pore solution chemistry of alkali-activated ground granulated blast-furnace slag', *Cement and Concrete Research*, 29(2), pp. 159–170.

Spiesz, P., Ballari, M. M. and Brouwers, H. J. H. (2012) 'RCM: A new model accounting for the non-linear chloride binding isotherm and the non-equilibrium conditions between the free- and bound-chloride concentrations', *Construction and Building Materials*, 27(1), pp. 293–304.

Su, H. and Xu, J. (2013) 'Dynamic compressive behavior of ceramic fiber reinforced concrete under impact load', *Construction and Building Materials*, 45, pp. 306–313.

Sujatha, T., Kannapiran, K. and Nagan, S. (2012) 'Strength assessment of heat cured geopolymer concrete slender column', *Asian Journal of Civil Engineering (Building and Housing)*, 13(5), pp.635-646.

Sukmak, P., Horpibulsuk, S., Shen, S.L., Chindaprasirt, P. and Suksiripattanapong, C. (2013) 'Factors influencing strength development in clay–fly ash geopolymer', Construction *and Building Materials*, 47, pp. 1125–1136.

Suwan, T. (2016) 'Development of Self-cured Geopolymer Cement', *PhD thesis. Brunel University London. UK.*

Swamy, R. N. (1992) 'The Alkali-Silica Reaction in Concrete'. 1st ed, UK: CRC Press.

Tatzber, M., Stemmer, M., Spiegel, H., Katzlberger, C., Haberhauer, G., Mentler, A. and Gerzabek, M.H. (2007) 'FTIR-spectroscopic characterization of humic acids and humin fractions obtained by advanced NaOH, Na4P2O7, and Na 2CO3 extraction procedures', *Journal of Plant Nutrition and Soil Science*, 170(4), pp. 522–529.

Tedesco, J.W., Powell, J.C., Ross, C.A. and Hughes, M.L. (1997) 'A strain-rate-dependent concrete material model for ADINA', *Computers & Structures*, 64(5-6), pp.1053-1067.

Temuujin, J., Williams, R. P. and van Riessen, A. (2009) 'Effect of mechanical activation of fly ash on the properties of geopolymer cured at ambient temperature', *Journal of Materials Processing Technology*, 209(12–13), pp. 5276–5280.

Thomas, R. V. and Nair, D. G. (2015) 'Fly ash as a Fine Aggregate Replacement in Concrete Building Blocks', *International Journal of Engineering and Advanced Research Technology*, 1(2), pp. 47–51.

Topark-ngarm, P., Chindaprasirt, P. and Sata, V. (2014) 'Setting Time , Strength , and Bond of High-Calcium Fly Ash Geopolymer Concrete', *The Journal of Materials in Civil Engineering*, 27(7), pp. 1–7.

Topçu, I. B., Toprak, M. U. and Uygunoğlu, T. (2014) 'Durability and microstructure characteristics of alkali activated coal bottom ash geopolymer cement', *Journal of Cleaner Production*, 81, pp. 211–217.

Türkmen, İ., Karakoç, M.B., Kantarcı, F., Maraş, M.M. and Demirboğa, R. (2016) 'Fire resistance of geopolymer concrete produced from Elazığ ferrochrome slag', *Fire and Materials*, 40(6), pp.836-847.

Vásquez, A., Cárdenas, V., Robayo, R.A. and de Gutiérrez, R.M. (2016) 'Geopolymer based on concrete demolition waste', *Advanced Powder Technology*, 27(4), pp.1173-1179.

Wallah, S. E. and Rangan, B. V. (2006) 'Low-calcium Fly ash-based Geopolymer Concrete : Long-term Properties', *Research Report GC2*. Curtin University of Technology, Perth, Australia.

Xin, L., Jin-yu, X., Weimin, L. and Erlei, B. (2014) 'Effect of alkali-activator types on the dynamic compressive deformation behavior of geopolymer concrete', *Materials Letters*, 124, pp. 310–312.

Xu, H. and Van Deventer, J. S. J. (2000) 'The geopolymerisation of alumino-silicate minerals', *International Journal of Mineral Processing*, 59(3), pp. 247–266.

Xu, H. and Van Deventer, J. S. J. (2002) 'Geopolymerisation of multiple minerals', *Minerals Engineering*, 15(12), pp. 1131–1139.

Yahya, Z., Abdullah, M.M.A.B., Hussin, K., Ismail, K.N., Sandu, A.V., Vizureanu, P. and Razak, R.A. (2013) 'Chemical and Physical Characterization of Boiler Ash from Palm Oil Industry Waste for Geopolymer Composite', *Revista de Chimie*, 64(12), pp. 32–34.

Yaman, I., Aktan, H. and Hearn, N. (2002) 'Active and Non-active Porosity in Concrete Part II: Evaluation of Existing Models', *Materials and Structures*, 35(2), pp. 110–116.

Yang, G., Chen, X., Xuan, W. and Chen, Y. (2018) 'Dynamic compressive and splitting tensile properties of concrete containing recycled tyre rubber under high strain rates', *Sādhanā*, 43(11), pp. 165–178.

Yang, T., Wu, Q., Zhu, H. and Zhang, Z. (2017) 'Geopolymer with improved thermal stability by incorporating high-magnesium nickel slag', *Construction and Building Materials*, 155, pp. 475–484.

Yang, T., Yao, X. and Zhang, Z. (2014) 'Geopolymer prepared with high-magnesium nickel slag: Characterization of properties and microstructure', *Construction and Building Materials*, 59, pp. 188–194.

Yao, W., Xia, K., Liu, Y., Shi, Y. and Peterson, K. (2019) 'Dependences of dynamic compressive and tensile strengths of four alkali-activated mortars on the loading rate and curing time', *Construction and Building Materials*, 202, pp. 891–903.

Liu, M.Y.J., Alengaram, U.J., Jumaat, M.Z. and Mo, K.H. (2014) 'Evaluation of thermal conductivity , mechanical and transport properties of lightweight aggregate foamed geopolymer concrete', *Energy & Buildings*, 72, pp. 238–245.

Liew, Y.M., Heah, C.Y., Abdullah, M.M.A.B. and Kamarudin, H. (2016) 'Progress in Materials Science Structure and properties of clay-based geopolymer cements : A review', *Progress in Materials Science*, 83, pp. 595–629.

Yunsheng, Z., Wei, S., Qianli, C. and Lin, C. (2007) 'Synthesis and heavy metal immobilization behaviors of slag based geopolymer', *Journal of Hazardous Materials*, 143, pp. 206–213.

Zhang, M., Wu, H.J., Li, Q.M. and Huang, F.L. (2009) 'Further investigation on the dynamic compressive strength enhancement of concrete-like materials based on split Hopkinson pressure bar tests . Part I : Experiments', *International Journal of Impact Engineering*, 36(12), pp. 1327–1334.

Zhang, Z., Provis, J.L., Reid, A. and Wang, H. (2015) 'Mechanical , thermal insulation , thermal resistance and acoustic absorption properties of geopolymer foam concrete', *Cement and Concrete Composites*, 62, pp. 97–105.

Zhang, Z., Zhu, Y., Yang, T., Li, L., Zhu, H. and Wang, H. (2017) 'Conversion of local industrial wastes into greener cement through geopolymer technology : A case study of high-magnesium nickel slag', *Journal of Cleaner Production*, 141, pp. 463–471.

Zheng, K., Chen, L. and Gbozee, M. (2016) 'Thermal stability of geopolymers used as supporting materials for TiO 2 film coating through sol-gel process : Feasibility and improvement', *Construction and Building Materials*, 125, pp. 1114–1126.

Zuhua, Z., Xiao, Y., Huajun, Z. and Yue, C. (2009) 'Role of water in the synthesis of calcined kaolin-based geopolymer', *Applied Clay Science*, 43(2), pp. 218–223.

Zych, T. (2014) 'Test methods of concrete resistance to chloride ingress', *Czasopismo Techniczne*, 21, pp. 117–139.

Appendices

Appendix A
A.1. Calculation of LOI

Loss on ignition (LOI) (%) was carried out following CoRiF standard procedures by igniting samples in triplicate at 1050 °C for 60 minutes in a muffle furnace. Replicates are denoted by a number (1, 2 or 3) after the sample code. A Quality Control (QC) sample of known LOI was included in the sample batch. The following formula was applied to calculate the LOI % of the precursor material and tabulated in Table A.1.

$$LOI\% = \frac{(Crucible + dry\ sample) - (Crucible + ignited\ sample)}{(Crucible + dry\ sample) - (Crucible)} * 100 \qquad \text{Eq (A.1)}$$

Table A.1.Calculation of LOI of precursor materials

Sample Code	Crucible (g)	Crucible + dry sample (g)	Crucible + ignited sample (g)	LOI %	LOI% Average
F1	12.5224	13.742	13.7053	3.009183339	
F2	12.3442	13.5837	13.5462	3.025413473	3.046418
F3	13.7376	14.5364	14.5116	3.104656985	
G1	13.177	14.5087	14.4586	3.762108583	
G2	13.288	14.2056	14.1729	3.563644289	3.766214
G3	14.1888	15.1478	15.1097	3.972888425	
H1	12.3542	13.9556	13.9595	-0.243536905	
H2	13.5017	14.5836	14.5868	-0.29577595	-0.3015
H3	14.2994	15.6138	15.6186	-0.365185636	
QC	12.6845	13.4463	13.3734	9.569440798	9.569440798

Appendix B

B.1. Microstructure additional data
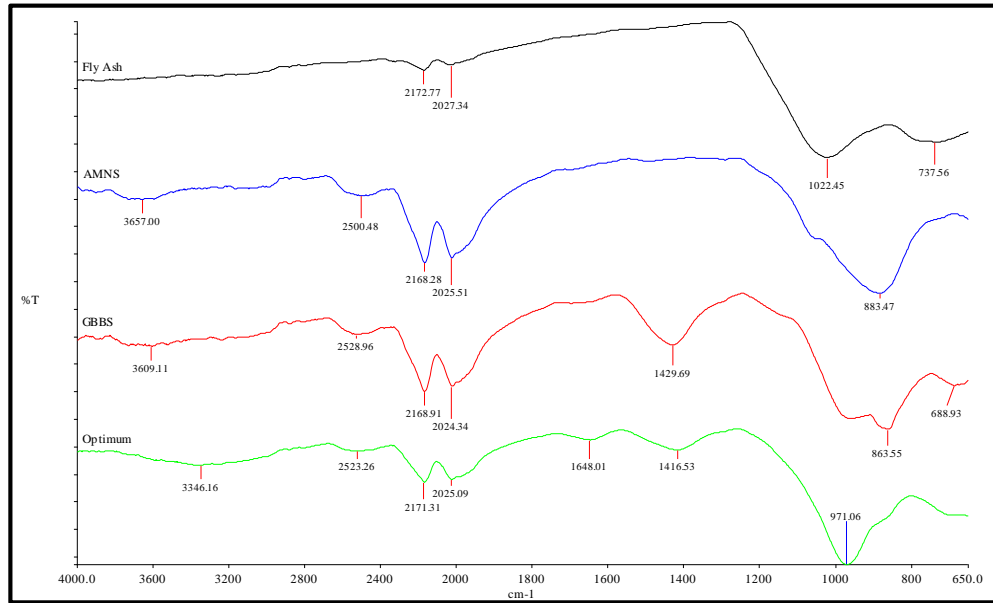
Figure B.1. FTIR results of raw material and GP paste
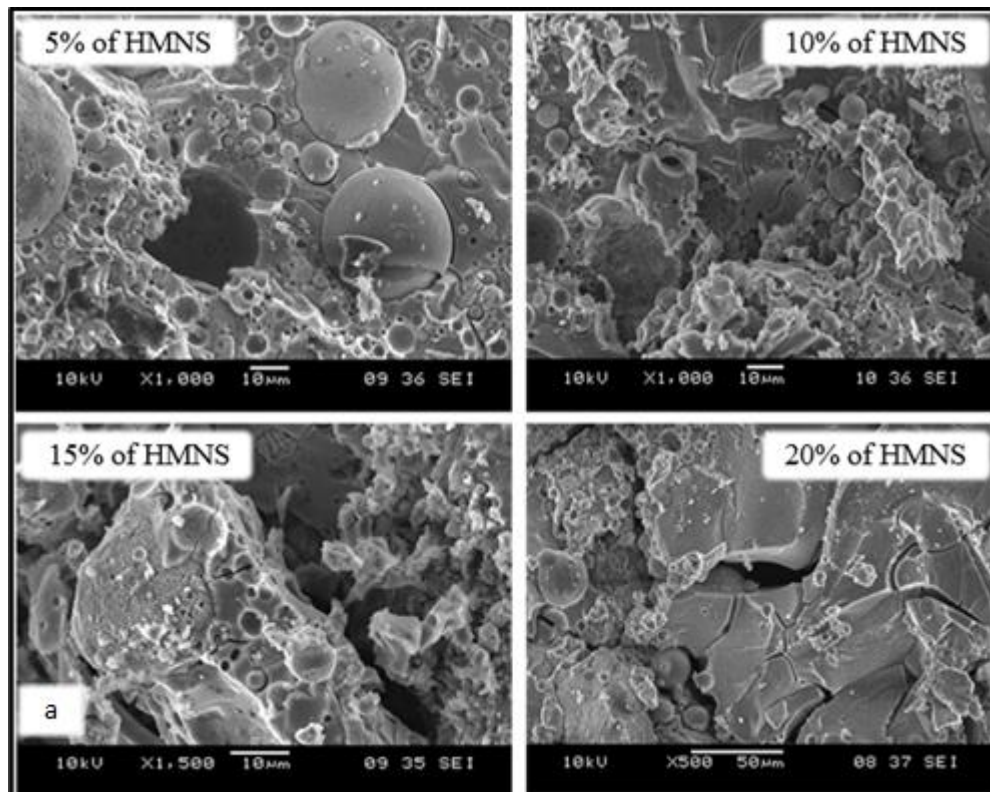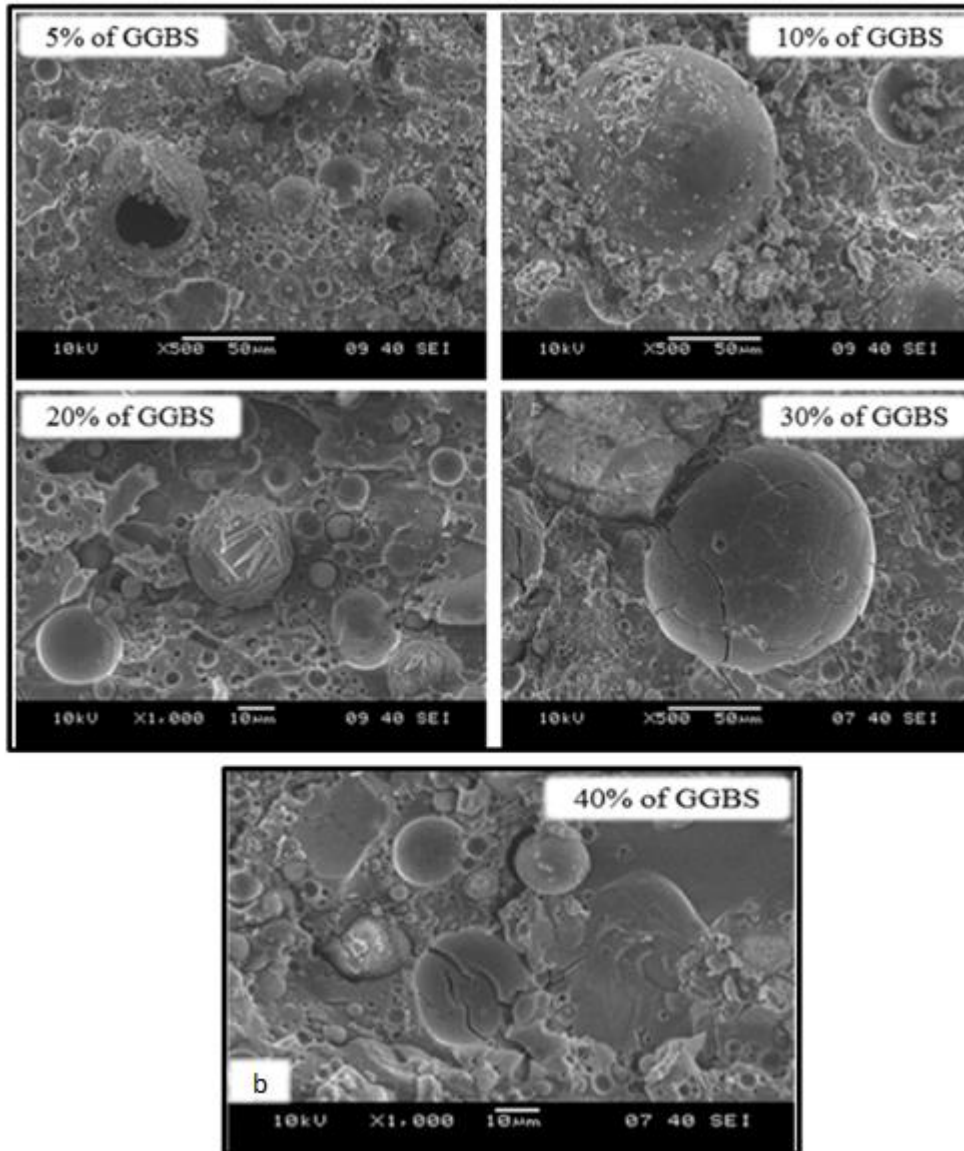
Figure B. 2. SEM images by percentage of HMNS and GGBS

Appendix C

C.1. Calculation of Different Dynamic Mechanical Properties of FA-GGBS-HMNS based GP Paste

A- Quasi a static compressive strength for cubic samples- calculation of loading rate-

In accordance to IS-516 standard, the rate of loading is 140 kg/squar.cm/min

As known: 1kg = 9.81N

Then,

$$\frac{140*9.81}{1000} = 1.373 \, \text{kN}$$

- For samples size of 5*5*5 cm^3

Surface area = 5*5

$\qquad$ =25 cm^2

- Rate of loading = 1.373*25/60

$\qquad$ = 0.57 kN/s

The approximate static compressive strength is 55.85MPa,

B- In order to calculate the static compressive strength for cylindrical samples the formula Eq (C.1) is applied;

$$Compressive\ strength\ of\ cylinder = 0.96*Compressive\ strength\ of\ cube \qquad \text{Eq (C.1)}$$

Then, the cylindrical compressive strength = 0.96*55.85

$\qquad\qquad\qquad\qquad$ = 53.62 MPa

Then the static compressive strength which is used in this study is 53.62 MPa

Table C.1. Dynamic increase factor index

Dynamic peak stress (MPa)	Log strain rate (1/s)	Tedesco et al.(1997)	FA-GGBS-HMNS GP paste	Chen et al.(2013)
54.4	1.38202	1.05933	1.01451	0.96527
55.4	1.51983	1.05947	1.03316	0.97905
64.3	1.5302	1.05948	1.19914	0.98009
66.6	1.91908	1.16566	1.24203	1.01897
56.5	2.13033	1.32579	1.05368	1.0401
48.5	2.08991	1.29515	0.90448	1.03606
91	2.20952	1.38581	1.69707	1.04802
42.4	1.58883	1.05953	0.79072	0.98595
44.8	1.57287	1.05952	0.83548	0.98435
50.1	1.56703	1.05951	0.93432	0.98377
53.5	1.88024	1.13622	0.99773	1.01509
61.4	1.73957	1.05968	1.14506	1.00102
94.6	2.17319	1.35828	1.76421	1.04438
47	1.70927	1.05965	0.87651	0.99799
48.2	1.58995	1.05953	0.89889	0.98606
46	1.62737	1.05957	0.85786	0.9898
78.5	1.98091	1.21253	1.46396	1.02516
68.1	2.24551	1.4131	1.27001	1.05162

Table C.2. Energy absorption of FA-GGBS-HMNS GP paste

Strain rate average (1/s)	Strain energy (J)	Incident energy (J)	Transmitted energy (J)	(incident-transmitted)/incident energy (J)
24.1	63.52683	202.24543	103.38625	0.48881
33.1	59.19274	219.24402	109.59816	0.50011
33.9	89.18365	271.03567	131.78263	0.51378
83	163.47335	417.19029	123.32615	0.70439
135	205.27569	474.83586	85.14038	0.8207
123	150.28527	413.25917	68.85151	0.83339
162	468.16633	865.46207	161.91622	0.81291
38.8	71.90314	272.01825	125.82384	0.53744
37.4	67.19458	274.75376	137.30999	0.50024
36.9	67.33306	289.2024	153.60857	0.46885
75.9	172.94082	461.95296	147.84607	0.67995
54.9	138.84981	428.56211	192.36419	0.55114
144	132.47823	466.89345	65.64869	0.85939
149	564.55993	1160.96989	284.24509	0.75517
51.2	84.83718	303.0121	116.43124	0.61575
38.9	90.61442	298.98394	139.88565	0.53213
42.4	77.55653	282.20201	129.65345	0.54057
95.7	273.59021	622.95005	186.65011	0.70038
176	393.69302	872.64135	180.9335	0.79266

Table C.3. Impact test record by group

Group a	Diameter (mm)	Thickness (mm)	Speed (m/s)	Average strain rate (1/s)	Peak-stress (MPa)
a-2m-01	32.72	18.70	2.35	24.1	54.4
a-2m-02	33.54	18.76	2.42	33.1	55.4
a-2m-03	33.64	18.06	2.62	33.9	64.3
a-4m-01	33.32	19.58	4.48	83	66.6
a-4m-02	32.56	17.76	4.56	135	56.5
a-4m-03	33.64	19.32	4.36	123	48.5
a-6m-01	33.10	19.28	/	/	/
a-6m-02	33.54	17.86	6.08	162	91
a-6m-03	32.96	18.30	/	/	/

Group b	Diameter (mm)	Thickness (mm)	Speed (m/s)	Average strain rate (1/s)	Peak-stress (MPa)
b-2m-01	36.10	21.08	2.42	51.2	47
b-2m-02	36.32	18.46	2.35	38.9	48.2
b-2m-03	36.18	18.68	2.57	42.4	46
b-4m-01	36.12	18.02	4.36	95.7	78.5
b-4m-02	36.48	17.66	/	/	/
b-4m-03	36.28	18.24	/	/	/
b-6m-01	36.38	17.74	6.21	176	68.1
b-6m-02	36.50	18.86	/	/	/
b-6m-03	36.72	17.34	/	/	/

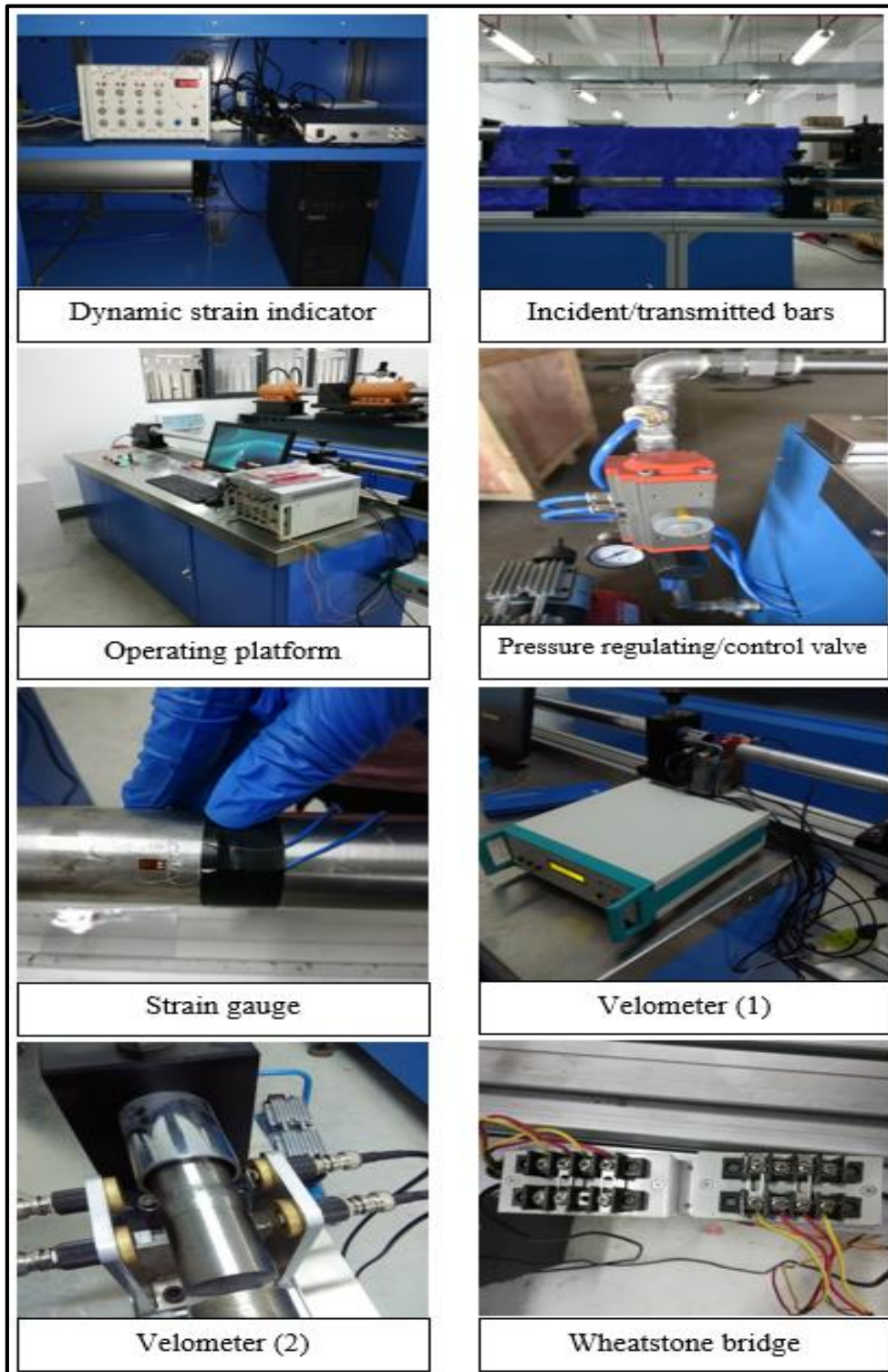| Group c	Diameter (mm)	Thickness (mm)	Speed (m/s)	Average strain rate (1/s)	Peak-stress (MPa)
c-2m-01	37.66	18.68	2.44	38.8	42.4
c-2m-02	37.58	18.42	2.78	37.4	44.8
c-2m-03	37.46	18.22	2.57	36.9	50.1
c-4m-01	37.20	18.60	4.13	75.9	53.5
c-4m-02	37.86	17.12	4.22	54.9	61.4
c-4m-03	37.70	18.18	4.65	144	38.5
c-6m-01	38.20	19.82	6.02	149	94.6
c-6m-02	37.54	18.42	/	/	/
c-6m-03	37.90	17.98	/	/	/

Figure C.1. SHPB system set up

Appendix D

D.1. Chloride Depth Measurements

Table D.1. RCP test results after 75 days of curing

No	Sample 1	Sample 2	Sample 3	Temp (°C)	duration (h)	Voltage (V)	Current (A)
1	12	6	8				
2	18	5	10				
3	14	3	8				
4	13	7	9				
5	7	8	6				
6	5	7	8	18.2±2	24	15	0.37
7	7	7	11				
8	12	8	9				
9	15	9	13				
10	13	11	12				
Average depth (mm)	11.60	7.10	9.40				

Table D.2. RCP test results after 210 days of curing

No	Sample 1	Sample 2	Sample 3	Temp (°C)	duration (h)	Voltage (V)	Current (A)
1		30	41				
2		38.2	40				
3		34.5	41				
4		37.5	38.5				
5		34.9	39				
6		33	41.5				
7	N/A	29	42.5	20±2	24	15	0.23
8		34.5	42.2				
9		37	43				
10		31	36				
Average depth (mm)	N/A	33.96	40.47				

UNDER PUBLICATION

A corresponding author for a review paper titled '' Alternative materials of rapid tooling in injection moulding using Geopolymer materials'', under submission process.

A paper titled ''Slant shear bonding strength of FA-based geopolymer paste as a repair material when applied on OPC substrate'' under submission process.